The role of activity in remodelling area-specific neocortical circuits during development

Jacqueline Ann Stacey
Merton College



Supervisors:
Professor Simon Butt, Professor Zoltán Molnár

Department of Physiology, Anatomy and Genetics
University of Oxford

Doctor of Philosophy

September 2018

Jacqueline Ann Stacey
Merton College

Doctor of Philosophy
September 2018

The role of activity in remodelling area-specific neocortical circuits during development

Abstract

How sensory activity contributes to the development of the brain has been a long-standing question in neuroscience (Katz & Shatz, 1996). A recent study by Marques-Smith et al. (2016) showed that a transient translaminar cortical circuit exists in the primary somatosensory barrel field (S1BF). This connection consists of a reciprocal connection between L5b somatostatin Lpar1-EGFP interneurons onto layer 4 spiny stellate neurons. This transient L5b-L4 connection was observed to be modulated by perturbations of sensory input and appeared to be required for correct integration of thalamic afferents into layer 4 of the adult mouse (Marques-Smith et al., 2016). This circuit was, therefore, an ideal candidate to examine the role of sensory activity on circuit refinement.

In this thesis I used laser scanning photo stimulation (LSPS) to map the developing L5b-L4 cortical circuit in the Celsr3|Dlx5/6 mouse line, devoid of thalamocortical and corticothalamic connections, to investigate the role of sensory information during circuit development (Zhou et al., 2008). The presence and development of the L5b-L4 reciprocal circuit was found to occur independently of thalamic connections.

It was hypothesised that the L5b-L4 circuit may exist as a ubiquitous developmental mechanism in other sensory areas, therefore I mapped developing cortical circuitry in the primary visual cortex (V1) of mice. In V1, the L5b-L4 connection was not present in either WT or Celsr3|Dlx5/6 mice, suggesting that intrinsic cortical properties have a central role in neonatal circuit development.

Due to S1BF and V1 circuitry differences, Lpar1-eGFP interneuron distributions and thalamic innervation were compared between the two regions. Both density and distribution of Lpar1-eGFP and SST+ cells differed between S1BF and V1. No timing differences in thalamic innervation were observed, however the cell types receiving direct thalamic input into layer 4 differed between S1BF and V1.

These findings suggest that although sensory-evoked activity can remodel features such as barrels and ODCs, some aspects of initial cortical circuit formation in the first 2-3 weeks of a mouse's life does not require thalamic-driven input.

Statement of Authorship

This thesis is submitted to the Department of Physiology, Anatomy and Genetics, University of Oxford, in fulfilment of the requirements for the degree of Doctor of Philosophy. This thesis is entirely my own work, and except where otherwise stated, describes my own research.

Jacqueline Stacey, Merton College

Funding

The work described in this thesis was funded by the Wellcome Trust.

Acknowledgements

This thesis, although only listing one author on the title page, is a product of many wonderful people who have guided, supported and sometimes dragged me through the process of completing a PhD.

Firstly, I would like to thank my supervisors, Professor Simon Butt and Professor Zoltán Molnár. Thank you to Simon for making this thesis possible, for accepting me into your lab back in the days of the Masters degree and for guiding me every step of the way to the completion of this thesis. Thank you to Zoltán for always being available to chat about my results and to look down microscopes with me and, most importantly, for helping me see the bigger picture in the research I was doing. Secondly, thank you to my fellow Butt lab PhD students and friends, Yayoi and Cristiana. Sharing my PhD days, lab work and Will's Deli lunches with you has been a wonderful experience. Thank you also to Butt lab alumni Andre and Dan. Andre - thank you for teaching me to patch and for your PhD wisdom. Dan, thank you for your calming post-doc aura and for getting me up and running in my first year. Thank you to the Molnár lab and in particular, Anna, Kris, and Wei-zhi for always having the time to answer my questions.

During my time in Oxford, I met many incredible people and forged the strongest friendships I have ever made. In particular, I would like to thank Helen, Magda and Anne for all the 'study sessions' where we mostly ate cake, the fabulous dinners, gorgeous balls, and the long brunches over which we would share our lives with all their excitements and challenges. Thank you to Yves and Lydia, two of the most genuinely lovely people I have ever met, for all the laughter, brunches and that beach holiday. Thank you to Owen, for all the gym gainz, hilarious gossip and for never failing to make me laugh out loud even at the end of a long week in the lab.

My family in Australia, my mother Carolyn and father Conrad and brothers Adam and Karl, although far away, have always been at the other end of a Skype call when I needed to chat about the PhD, life, or just wanted to wave at my dog. I am forever grateful for their never ending support, love and laughs.

Finally, I want to thank my amazing husband, Will, without whom I would never have made the trip across to the northern hemisphere and discovered the wonders of Oxford. I truly cannot put into words the impact his support has had on me during the last 4 years. I will let the fact that we were married in my last year of the PhD speak for itself.

Contents

1 Introduction **1**

1.1 The role of sensory information in the development of cortical circuitry 2

1.1.1 The role of spontaneous, thalamic-driven activity in cortical development 2

1.1.2 The role of sensory-evoked information in V1 development . . 5

1.1.3 The role of sensory evoked information in S1 development . . 7

1.1.4 Reassigning sensory cortex identity through sensory activity . 9

1.1.5 The missing link - how are cortical circuits changed by sensory activity? 12

1.1.6 Transient circuits 15

1.1.7 A transient, translaminar L5b-L4 loop modified by sensory activity 18

1.2 Thesis objectives 20

1.2.1 Transient cortical circuits in a sensory naïve mouse - Chapter 3 22

1.2.2 Transient cortical circuits in the developing mouse primary visual cortex - Chapter 4 23

1.2.3 Thalamocortical input into neonatal V1 and S1BF - Chapter 5 25

2 Methods **27**

2.1 Mouselines 27

2.1.1 Genotyping 29
2.2 Slice Preparation 31
2.3 Whole-cell patch-clamp electrophysiology 32
2.4 Intrinsic properties of recorded neurons 33
2.5 Laser scanning photostimulation - glutamate uncaging 34
2.6 Laser scanning photostimulation - ATP uncaging 37
2.7 Analysis of LSPS data 38
2.8 Optogenetic stimulation of thalamocortical afferents 38
2.9 Optogenetic stimulation analysis 39
2.10 Statistics 40
2.11 Histochemistry 40
2.11.1 Slice preparation 40
2.11.2 Antibody staining 41
2.11.3 Morphological reconstruction of biocytin filled neurons 41
2.11.4 DiI tracing 42

3 Thalamic input is not required for the development of the L5b-L4 GABAergic connection 43

3.1 Characterisation of Celsr3|Dlx5/6 mouse line 45
3.1.1 Whole Brain DiI tracing of reciprocal thalamocortical connectivity in Celsr3|Dlx5/6 mice 45
3.1.2 Anatomy and cell morphologies of Celsr3|Dlx5/6 layer 4 spiny stellate cells 46
3.1.3 Intrinsic firing properties of Celsr3|Dlx5/6 L4 spiny stellate cells 48
3.2 *In vitro* electrophysiology 50
3.2.1 GABAergic input onto L4 excitatory cells in S1 50
3.2.2 Spontaneous GABAergic activity in layer 4 56

3.3 Discussion 56

4 The L5b-L4 transient circuit is not observed in the primary visual cortex 63

4.1 Characterisation of V1 64

4.1.1 Targeting layer 4 in V1 65

4.2 *In vitro* electrophysiology in V1 65

4.2.1 GABAergic input onto L4 excitatory cells. 65

4.2.2 SST-specific GABAergic input onto excitatory cells in V1. . . 68

4.2.3 Alternative slice angles 71

4.2.4 GABAergic input onto excitatory cells in all layers 74

4.2.5 Glutamatergic input onto L5b SST+ cells in V1 74

4.2.6 GABAergic input onto V1 L4 excitatory cells in the Celsr3|Dlx5/6 mouse 78

4.3 Discussion 79

5 Thalamic innervation in V1 and S1BF during neonatal development 87

5.1 Properties of layer 5 Lpar1-EGFP in S1BF and V1 90

5.1.1 Intrinsic electrophysiological properties of Lpar1-EGFP GABAergic cells in S1BF and V1 are not different 90

5.1.2 Lpar1-EGFP GABAergic layer 5 cells in S1BF have more extensive axonal arborisation than Lpar1-EGFP GABAergic layer 5 cells in V1 90

5.1.3 The density and distribution of SST+ve and Lpar1-EGFP cells differs between S1BF and V1 91

5.2 Characterisation of Olig3|Ai32 96

5.2.1 Characterisation of channelrhodopsin-2 response 97

5.3 Functional thalamocortical synapses during neonatal development in S1 and V1 . . . 107
5.3.1 Discussion . . . 112

6 Discussion **119**

6.1 Summary of contributions . . . 119
6.2 Implications . . . 122
6.3 Future work . . . 126
6.4 Concluding Remarks . . . 128

References **131**

A Abbreviations **149**

List of Figures

1.1 Dynamics of the L5b-L4 transient translaminar connection in the neonatal somatosensory cortex 19

1.2 Thalamocortical connections in Celsr3 conditional mutants 24

2.1 Genotyping for *Celsr3*$^{fl/fl}$ and *Dlx5/6*$^{Cre/+}$ 29

2.2 Genotyping for *Olig3*$^{cre/+}$ and Ai32(EYFP) 30

2.3 Current input protocols used to calculate electrophysiological parameters 35

2.4 Steps in LSPS methodology 37

3.1 Anatomical verification of a defective internal capsule in Celsr3|Dlx5/6 mice 47

3.2 Morphological analysis of apical dendrite length in WT and Celsr3|Dlx5/6 spiny stellate cells 49

3.3 Raw IPSC data and connectivity mapping variability for the L5b-L4 circuit 52

3.4 Heat maps of GABAergic input onto WT and Celsr3|Dlx5/6 layer 4 S1BF excitatory cells 53

3.5 Percentage of total GABAergic input that originates from each cortical layer for WT and Celsr3|Dlx5/6 layer 4 spiny stellate cells . . . 55

3.6 Total GABAergic input that originates from each cortical layer for WT and Celsr3|Dlx5/6 layer 4 spiny stellate cells 57
3.7 Frequency and amplitude of spontaneous GABAergic events (sIPSCs) in WT and Celsr3|Dlx5/6 mice 58

4.1 V1 and S1BF DAPI staining on P10 coronal sections and Brn2 and Ctip2 staining on P8 sagittal sections 66
4.2 Layer identification in V1 using the Rpb4 Cre; Ai14 mice 67
4.3 Averaged heat maps of global GABAergic input onto layer 4 excitatory neurons in V1 69
4.4 V1 and S1BF have significantly different early GABAergic input profiles onto L4. 70
4.5 SST-specific GABAergic input onto layer 4 in V1 72
4.6 GABAergic input onto layer 4 in V1 for sagittal and visual-thalamocortical slice preparations 73
4.7 GABAergic input onto each cortical layer from P5-P24. 75
4.8 Averaged heat maps of GABAergic input onto layer 2/3 in V1 76
4.9 Glutamatergic input onto L5b SST+ cells in V1 77
4.10 GABAergic input onto V1 layer 4 in Celsr3|Dlx5/6 mice 79
4.11 Layer contributions to GABAergic input onto V1 L4 for Celsr3|Dlx5/6 and WT 80
4.12 Layer contributions for GABAergic input onto V1 and S1BF layer 4 for Celsr3|Dlx5/6 mice 81

5.1 Morphologies of Lpar1-EGFP cells in S1BF and V1 92
5.2 Anti-GFP and anti-RFP immunohistochemistry showing the distribution and density of Lpar1-EGFP (green) and SST+ve (red) cells in V1 and S1BF of a P21 mouse 94

5.3 Cell counts for Lpar1-EGFP and SST+ve cells in S1BF and V1 . . . 95
5.4 Characterisation of EYFP cortical expression in the Olig3|Ai32 mouse 98
5.5 Characterisation of of ChR2 expressing thalamic cell response in neonatal Olig3|Ai32 mice 101
5.6 Application of TTX inhibits action potential firing in cortical cells . . 102
5.7 The addition of TTX and 4-AP greatly reduces response amplitudes and eliminates evoked-responses in cells younger than P17 104
5.8 Strength and duration of blue light stimulation alters evoked response latency with and without TTX 106
5.9 The standard error of the latency of evoked responses plotted with respect to mean response latency 108
5.10 Amplitude of evoked excitatory responses in S1BF and V1 after optogenetic stimulation of thalamic afferents with respect to age 110
5.11 The percentage of cells that appeared to receive monosynaptic input from the thalamus 111

6.1 Summary of early postnatal circuit differences between S1BF and V1 120

List of Tables

3.1 Intrinsic electrophysiological properties of WT and Celsr3|Dlx5/6 L4 Excitatory Neurons (P7-P10) 50

5.1 Intrinsic electrophysiological properties of Lpar1-EGFP GABAergic neurons in S1BF L5b and V1 L5b (P8-P9) 91

Chapter 1

Introduction

The human brain undergoes a fourfold increase in volume from birth to the teenage years, particularly during the first years after birth when the volume and cognitive function of the brain increases considerably. At the cellular level the growth of contacts between neurons, synaptogenesis, continues to take place at a high rate during the first year of life with the number of synapses peaking by 8 months of age at 150% of adult numbers (Johnson, 2001; Huttenlocher, de Courten, Garey, & Van der Loos, 1982). Not only does synaptogenesis occur rapidly after birth, but the majority of myelination appears postnatally. (Yakovlev, 1967). This extended postnatal developmental window allows for sensory information to play a role in shaping the final adult circuitry. However, the degree to which sensory information shapes brain circuits in early life and its interaction with more 'hardwired' intrinsic genetic factors remains elusive.

In the following section, the current knowledge surrounding the role of both spontaneous and sensory-evoked activity in cortical development will be reviewed with particular focus on primary somatosensory and visual cortices. Following on from this, the gaps in our understanding of sensory-driven cortical development will be highlighted to frame the motivation for this thesis. Finally, the three main aims

of this thesis are outlined, corresponding to the three primary results chapters, and summarise the experimental approaches undertaken to address these aims.

1.1 The role of sensory information in the development of cortical circuitry

The role of sensory information such as sight, touch, and sound in the development of neuronal circuits remains a fundamental question in neuroscience since the pioneering work of Hubel and Wiesel. How do primary sensory areas become specialised processors for their given input?

It has long been thought that two distinct waves of electrical activity play a vital role in shaping early sensory areas. The first wave, spontaneous activity, provides a 'best guess' when shaping circuitry, while the second wave, incoming sensory experience, refines and solidifies sensory-specific connections (Katz & Shatz, 1996; Hubel & Wiesel, 1970; Hubel, Wiesel, & LeVay, 1977; Le Vay, Wiesel, & Hubel, 1980; Blakemore & Cooper, 1970).

1.1.1 The role of spontaneous, thalamic-driven activity in cortical development

Upon reaching the cortex, neurons experience and participate in oscillatory and patterned waves of spontaneous activity which are believed to help shape area-specific circuitry. These oscillations have been shown to be grossly similar across the retina, spinal cord, hippocampus, cochlea and cerebellum (Blankenship & Feller, 2010). Although such spontaneous electrical activity is not considered to be driven by behaviourally relevant external stimuli, many of these activity waves originate from sensory organs or thalamic nuclei (Yang et al., 2012; Khazipov et al., 2004;

Luhmann & Khazipov, 2018; Khazipov & Milh, 2017; Galli & Maffei, 1988; Maffei & Galli-Resta, 1990).

In the mouse somatosensory cortex, thalamic afferents reach the subplate at embryonic day (E)18 and innervate layer 4 of the neocortex shortly after birth (Yang et al., 2018; López-Bendito et al., 2006; López-Bendito & Molnár, 2003; Catalano, Robertson, & Killackey, 1991). Coinciding with thalamic innervation of the cortex, spindle bursts and early gamma oscillations (EGOs) are observed in the rat at approximately two days after birth (Khazipov & Milh, 2017; Minlebaev, Colonnese, Tsintsadze, Sirota, & Khazipov, 2011; Mitrukhina, Suchkov, Khazipov, & Minlebaev, 2014; Yang et al., 2012). Spindle bursts are defined as local network oscillations at 5-25 Hz and last from 0.5 to 3 seconds. EGOs often co-occur with spindle bursts, but are independent and can be recognised by oscillations of 30-50 Hz for a duration of 100-300 ms (Khazipov et al., 2004; Minlebaev, Ben-Ari, & Khazipov, 2007; Yang, Hanganu-Opatz, Sun, & Luhmann, 2009). It is believed that both oscillations act to synchronize local columnar networks (Hanganu-Opatz, 2010; Khazipov & Milh, 2017; Luhmann & Khazipov, 2018).

Although both EGOs and spindle bursts are internally generated and persist in the deafferented rodent, spontaneous motor movement and retinal waves can trigger these oscillations in primary somatosensory (S1) and primary visual (V1) cortices (Khazipov et al., 2004; Hanganu, Staiger, Ben-Ari, & Khazipov, 2007; Akhmetshina, Nasretdinov, Zakharov, Valeeva, & Khazipov, 2016; Yang et al., 2009; Khazipov et al., 2004; Akhmetshina et al., 2016; Hanganu, Ben-Ari, & Khazipov, 2006; Colonnese & Khazipov, 2010).

1.1.1.1 The role of retinal waves in cortical development

Not only can retinal waves act as triggers for oscillatory activity, but their contribution to visual cortex development has been extensively studied in its own right.

1.1 The role of sensory information in the development of cortical circuitry

Retinal waves are topographically-patterned waves of activity that sweep across the retina of each eye, propagating to the thalamus and visual cortices (Ackman, Burbridge, & Crair, 2012; Galli & Maffei, 1988; Maffei & Galli-Resta, 1990; Sernagor & Grzywacz, 1999).

In mice, retinal waves begin to occur from postnatal day (P)0 during the 'pre critical period' (P0-P20), and after eye opening (P12) are observed alongside visual stimulus-evoked responses (Feller & Scanziani, 2005; Crowley & Katz, 2000). These waves are transmitted through the thalamus (Mooney, Penn, Gallego, & Shatz, 1996) and are thought to provide eye-specific topographic input that aids in segregation of ocular dominance columns (ODCs) in the thalamus and visual cortex (Grubb & Thompson, 2004; R. O. Wong, 1999).

The appearance of ODCs has often been used as a yardstick by which to measure visual cortex development since their visually-driven plasticity was described by Hubel and Wiesel (Hubel & Wiesel, 1970). Although ODCs appear in rats (Laing, Turecek, Takahata, & Olavarria, 2014), mice do not have ocular dominance columns, but instead a 'salt and pepper' organisation of V1 (Ohtsuki et al., 2012) allowing eye-specific segregation but not ODCs to be measured.

When the subplate is ablated in P6-P9 cats, the maturation of thalamocortical synapses is prevented and the cortex is effectively decoupled from its inputs. In these animals, ocular dominance columns do not form and synapse maturation, visual map formation, and orientation selectivity are all affected (Allendoerfer & Shatz, 1994; Kanold, Kara, Reid, & Shatz, 2003; Kanold & Luhmann, 2010; Ghosh & Shatz, 1992). These results differ from more recent findings showing that orientation selectivity is largely independent of neural activity, both spontaneous and evoked (Hagihara, Murakami, Yoshida, Tagawa, & Ohki, 2015). It is important to note that Hagihara et al. (2015) used genetic silencing of cortical activity to investigate the effect of neuronal activity, as opposed to subplate ablation; both of which may have

consequences beyond removal of thalamic input. Subplate ablation also removes a cortical cell layer from the developing circuit while genetic silencing of cortical activity modifies cortically generated spontaneous activity alongside retinal waves and sensory-evoked activity. In order to more accurately isolate the role of retinal waves, a more refined approach is needed.

Whether retinal waves or other peripherally generated neuronal activity is permissive or instructive for the development of ocular dominance columns is not clear from these results. To answer this question, Xu et al. (2011) manipulated the pattern but not the overall activity level of retinal waves through transgenic expression of 2-nicotinic acetylcholine receptors in retinal ganglion cells of mice (H. Xu et al., 2011; Sernagor & Grzywacz, 1999). Mice with disrupted retinal wave patterns showed profoundly disturbed eye-specific segregation, thus demonstrating that retinal waves are instructive in the formation of ocular dominance columns. In a follow up study, Xu et al. (2015) determined that spatial patterns of retinal waves were also instructive to the development of retinotopy (H.-P. Xu et al., 2015).

These studies show that during the pre-critical period, patterned retinal waves appear necessary and instructive for the formation of ODCs and retinotopy in the visual cortex. Retinal waves also appear to be required for other characteristics of the visual cortex, such as orientation selectivity.

1.1.2 The role of sensory-evoked information in V1 development

It is well known that disrupting incoming sensory information during development can alter the formation of gross morphological structures in the primary sensory cortices (Morishita & Hensch, 2008; Van der Loos & Woolsey, 1973). In pioneering experiments, Hubel and Wiesel showed that monocular deprivation led to disrup-

tion of ocular dominance columns in the primary visual cortex of cats (Hubel & Wiesel, 1962; Wiesel, Hubel, et al., 1963; Hubel & Wiesel, 1970; Wiesel & Hubel, 1965). During the mouse V1 critical period (P19-P32), transient eye closure is able to cause ocular dominance shifts driven by loss of responsiveness of cortical neurons to the deprived eye (Gordon & Stryker, 1996). Experiments in the cat visual cortex have also demonstrated that while cortical maps for orientation selectivity and ocular dominance develop in the absence of visual experience, visually evoked activity is required to develop strong ipsilateral connections and maintain both cortical maps in the long term. Continued deprivation of sight caused deterioration of responses (Crair, Gillespie, & Stryker, 1998). The role of visual experience in the development of the visual system begins even before eye opening (Akerman, Smyth, & Thompson, 2002; Krug, Akerman, & Thompson, 2001). In ferrets, dark-rearing results in increased convergence of On- and Off-center responses in dLGN neurons, while exposure to naturalistic stimuli before eye-opening promotes On-Off response segregation (Akerman et al., 2002).

Although ocular dominance within the cortex can be drastically re-shaped by sensory deprivation, sensory-evoked input is not required for initial ODC formation. In the ferret, ocular dominance columns are present during the pre-critical period and well before visual stimulus-evoked responses (Crowley & Katz, 2000). Similar to orientation selectivity, direction selectivity develops normally in dark reared mice, independently of visual experience (Rochefort et al., 2011). Additionally, genetic silencing of cortical activity and, thereby, suppression of both spontaneous and sensory-evoked activity does not affect formation and maturation of orientation selectivity (Hagihara et al., 2015). In the ferret, neither monocular nor binocular deprivation between P0 and P15 (pre-critial period) had any effect on axon clustering in ODCs (Crowley & Katz, 1999, 2000).

A hallmark of a maturing cortex is the switch in neuronal activity from highly

correlated, mostly slow wave oscillations, to sparse, decorrelated activity. In a healthy mouse visual cortex, this switch coincides with eye opening (Kerr, Greenberg, & Helmchen, 2005; Rochefort et al., 2009). Using 2-photon imaging, Rochefort et al. (2009) was able to determine that this change occurred independently of visually evoked activity. This suggests that this 'sparsification' of electrical activity is needed for a change in role once eyes open and that change in role is not caused by eye opening (Rochefort et al., 2009). Interestingly, the same observation had been made in the somatosensory cortex, with a slight temporal shift to accommodate the earlier critical period (Golshani et al., 2009).

These studies suggest that the formation of ODC, direction and orientation selectivity do not require visually evoked activity, but that the balance of eye-specific segregation in the mature visual cortex can be heavily influenced by visually evoked activity during a critical developmental window and that visual experience is required to maintain mature circuitry (Crair et al., 1998). Other developmental milestones, such as sparsification, coincide with sensory experience in both S1BF and V1 but are not driven by it. This highlights the existence of developmental programs which occur independently of thalamic input (Colonnese et al., 2010).

1.1.3 The role of sensory evoked information in S1 development

In the rodent somatosensory cortex, the appearance of the barrel field is often used to assess how perturbations in sensory activity affect cortical development (Simons & Land, 1987; Van der Loos & Woolsey, 1973; Buonomano & Merzenich, 1998). For example, removal of whisker-evoked sensory information via infraorbital nerve (ION) lesions or vibrissae pad injury results in the total absence of barrels in S1 (H. Li et al., 2013; Erzurumlu & Gaspar, 2012; Feldman & Brecht, 2005). When

glutamatergic synaptic transmission from thalamic afferents is eliminated, barrel formation in S1BF is prevented (H. Li et al., 2013). Additionally, mice that lack metabotropic glutamate receptor 5 (mGluR5), or its downstream receptor-activated G-protein-coupled phosphodiesterase Plcβ1, show segregation and patterning of thalamic innervation but no cytoarchitectural rearrangement of L4 cells into barrels. This further supports the argument that glutamatergic signalling is required for barrel formation (Hannan et al., 2001). These knock-out mice, along with other genetic manipulations, show that the periphery-related patterning of thalamocortical axons and barrel patterning of layer 4 cells (cytoarchitecture) can be disassociated and that the two features are achieved through different mechanisms (Hannan et al., 2001; Iwasato et al., 2000; López-Bendito & Molnár, 2003).

Whisker trimming is another intervention that has demonstrated a wide range of effects on S1BF connectivity and barrel development. Trimming all whiskers from P0 to P3 but leaving the neuronal pathways intact causes adult rats to show poor gap crossing behaviour (Lee, Chen, Chuang, & Wang, 2009). Whisker trimming for a longer period of time (40-45 days from P0) led to enlarged excitatory and weakened inhibitory receptive fields in layer 4 neurons (Shoykhet, Land, & Simons, 2005). Therefore, even with intact neuronal sensory pathways, the absence of whisker information caused adult mice to exhibit poorly developed somatosensation. When subsets of whiskers are removed, the effect on connectivity is more apparent. Removing all but a single whisker at P0 causes expansion of the cortical area stimulated by that whisker and reduction in all others (Fox, 1992, 2002). Therefore, similar to V1, it is clear that manipulations of sensory activity, such as whisker trimming, during the critical period in S1 can shrink or expand sensory-specific receptive fields in each cortex.

As with V1, S1BF has a clearly defined critical period during which perturbations of sensory input have the most profound effect. The S1BF critical period, accounting

for all layers, lasts from approximately P3 to P14. Different layers have clearly defined critical periods, with plasticity of barrel formation in layer 4 ending days earlier than layer 2/3 and 5 plasticity (Stern, Maravall, & Svoboda, 2001; Hensch, 2005; Rebsam, Seif, & Gaspar, 2005). The critical period in mouse somatosensory barrel cortex lasts from appropriately P5-P8 (Anastasiades et al., 2016; Fox, 1992; Hensch, 2005)

These results from S1BF suggest that sensory activity plays a large role in refining early somatosensory cortex cytoarchitecture. Thalamic input in S1BF has roles both in establishing initial barrel cytoarchitecture and remodelling functional connectivity during the critical period.

1.1.4 Reassigning sensory cortex identity through sensory activity

Not only are the recognisable hallmarks of primary sensory areas, such as barrels or ODCs, often poorly defined when sensory input is disrupted, but these areas can be resized or reassigned as a different, and in some cases novel, cortical area by manipulating sensory-evoked activity.

Anecdotal evidence has, for a long time, suggested that sensory deprivation in one area can heighten other senses. This observation is also supported by experimental evidence. Congenitally blind humans have been reported to activate their visual cortex for other sensory tasks such as braille reading (Sadato et al., 1996). Such cross-modal plasticity co-opting V1 for other senses, namely auditory and somatic inputs, has also been demonstrated experimentally in opossums, *Monodelphis domestica*, that were bilaterally enucleated before thalamic axons reached the cortex (Kahn & Krubitzer, 2002).

Surgically re-routing sensory information into other thalamic nuclei results in a

similar reassignment of cortical identity. In the neonatal ferret, retinal projections surgically rerouted into the auditory pathway at birth have resulted in a two dimensional retinoptic map, orientation, spatial and velocity tuning, as well as the ability to distinguish gratings; albeit with reduced acuity (Roe, Pallas, Hahm, & Sur, 1990; Roe, Pallas, Kwon, & Sur, 1992; Sharma, Angelucci, & Sur, 2000; Von Melchner, Pallas, & Sur, 2000).

More refined approaches to re-wiring show the deafferented cortex taking on functions of neighbouring cortical areas. Removing a small amount of retina from adult cats causes the deafferented cortex to become responsive to the retinal area neighbouring the lesion (Kaas et al., 1990). While in the somatosensory cortex, the barrel field region takes on characteristics of secondary somatosensory regions in the absence of lemniscal input after genetic ablation of the thalamic VPM nucleus at birth (Pouchelon et al., 2014). Disrupting sensory input can also alter cortical area boundaries. When sensory input into mouse V1 was ablated genetically by E15.5, cortical markers could no longer define the boundary between V1 and higher order visual processing areas (Chou et al., 2013). Entirely novel cortical areas have also been induced by reducing thalamic input into V1 (Rakic, Suner, & Williams, 1991).

More complex transplant studies have also shown the ability of embryonic cortex to take on characteristics of the host region. Transplanting E17 or E18 rat visual cortex into parietal cortex of newborn rats resulted in barrels forming in the transplanted visual cortex that resembled the pattern of the normal barrel field (Schlaggar & O'Leary, 1991). More recent transplant studies have demonstrated that the effect thalamic afferents exert on cortical identity can be time-dependent. When rat E12 occipital lobe is transplanted into newborn frontal cortex, the transplanted cortex can form connections with the spinal cord. When the same transplant is done at E14, the transplanted occipital lobe forms normal tectal projections (Pinaudeau, Gaillard, & Roger, 2000). Transplanting E16 parietal to occipital cortex of a newborn

rat successfully attracts TC axons appropriate for S1BF, but cannot form barrels (Gaillard & Roger, 2000). The importance of timing in sensory manipulations is also apparent in Dehay et al. (1996). Bilateral enucleations in fetal monkeys from E59 to E110 showed the time-critical effect retinal input deprivation has on the size and identity of neocortex (Dehay, Giroud, Berland, Killackey, & Kennedy, 1996).

The lack or reduced reassignment of cortical identity after an early time point is thought to be due to the intrinsic factors which specify cortical arealization. Expression gradients of molecules such as FGF8, EMX2 and WNT signalling have long been known to pattern the cortex and specify area sizes (Rash & Grove, 2006). For example, manipulating FGF8 (fibroblast growth factor 8) expression can induce a duplicate, mirror-reversed barrel field (Fukuchi-Shimogori & Grove, 2001). This ectopic barrel field suggests a complex interplay between thalamocortical projections and cortical gradients.

Although early re-wiring of thalamic afferents is able to alter region identity and function, in the absence of thalamic input region-specific gene expression (Cadherin-6, EphA-7, Id-2, and RZR-beta) develops normally (Miyashita-Lin, Hevner, Wassarman, Martinez, & Rubenstein, 1999). Therefore, specification of area identity requires intrinsic molecular signals followed by spatial and temporal signals from thalamic afferents.

These results show that the ability of sensory input to change the identity of a cortical region points to a major role for sensory-evoked information in instructing sensory-specific circuit formation. The extent of this ability, however, appears to be temporally restricted. Certain identity reassignment, such as the development of area appropriate subcerebral projections seems only possible when embryonic tissue is transplanted into a newborn cortex. After this time, the partial identity of cortical areas appears to be established, likely by intrinsic factors. Even after early cortical identity has been established, the data from neonatal and newborn manipulations

shows that the neocortex at this stage can still be moulded by thalamic input to transform, albeit incompletely, into neighbouring, novel or different modality cortices. These thalamic-driven cortical identity reassignments at varying time points with a range of plasticity outcomes suggests that cortical area identity involves a complex interplay between both intrinsic genetic programs and incoming sensory information.

1.1.5 The missing link - how are cortical circuits changed by sensory activity?

It is clear from these studies that activity has a role to play in refining sensory-specific processing centres on a macroscopic level. Changes on the scale of barrels and columns hint at underlying circuit remodelling, but thus far, the precise circuit changes remain elusive.

The 'canonical cortical circuit' consists of thalamic input onto layer (L)4 which then propagates to supragranular layers before being sent to infragranular layers and onto subcortical structures. It is ubiquitous in all primary sensory cortices and is considered to be the foundation of information processing across the neocortex (Douglas & Martin, 2004; Dhruv, 2015). Additionally, it has been known since Ramon y Cajal's meticulous observations that the same cell types and layer lamination is a common neocortex feature (Cajal, 1911). However, the functional differences between primary sensory areas strongly imply that the circuitry in these areas must be a unique variation on the canonical circuit in order to specialise. Indeed, when comparing primary sensory areas, layer 4, in particular, varies markedly in thickness and the layer 4 spiny stellate cells present in abundance in S1BF are not found in rodent V1 or A1 (Harris & Shepherd, 2015; Douglas & Martin, 2004; Peters & Kara, 1985; Nassi & Callaway, 2009). Moreover, advances in our ability

to interrogate neural circuits has resulted in the identification of many connections outside the canonical view of cortical circuitry and the knowledge of inhibitory circuitry, overlooked by the canonical circuit, has been expanding rapidly (Pluta et al., 2015; Constantinople & Bruno, 2013; Armstrong-James, Fox, & Das-Gupta, 1992; Malpeli, 1983; Butt, Stacey, Teramoto, & Vagnoni, 2017).

The balance of intrinsic and extrinsic factors in circuit specialisation and to what extent there exists a 'blank slate' cortex common across all sensory areas prior to sensory input is not yet known. It is unclear how sensory activity interacts with the innate cortical wiring and how much of an impact sensory-specific information has on remodelling a sensory-naïve cortex at the level of neuronal circuits.

Our current knowledge of activity driven circuit changes is limited. Chittajallu & Isaac (2010), demonstrated that sensory experience drove the development of feed-forward inhibition onto L4 of S1BF by both strengthening thalamocortical input onto L4 feed forward interneurons and down-regulating thalamocortical excitatory post-synaptic potentials (EPSPs) in L4 spiny stellates (Chittajallu & Isaac, 2010). Shepherd et al. (2003) used LSPS in the rat barrel cortex to investigate underlying causes of receptive field changes in L2/3 neurons. They found that L2/3 pyramidal neurons above the barrels receive L4 input while cells above the septa do not. When the whiskers are trimmed, depriving S1BF of sensory information, septa L2/3 neurons receive L4 input and barrel L2/3 neurons do not, suggesting sensory-dependent, competitive interactions between barrel and septal circuits (Shepherd, Pologruto, & Svoboda, 2003). Further evidence of an activity-dependent competitive interaction between septal and barrel circuitry is observed in the rearrangement of of subplate neurites in S1BF L4 (Piñon, Jethwa, Jacobs, Campagnoni, & Molnár, 2009). Aside from a handful of studies, our understanding of activity-driven circuit changes is indirectly informed through changes observed on the cellular level. Thalamic input has been shown to influence neuronal migration, survival, differentiation, synapse

formation, and cell morphology.

In early mouse cortical development, thalamic axons have been shown to release diffusable factors that promote cortical cell proliferation (Dehay, Savatier, Cortay, & Kennedy, 2001), regulate subplate survival (Cooke, Grant, McLauchlan, Lotto, & Price, 1999), and enhance radial migration (Edgar & Price, 2001). In the tectum of *Xenopus laevis* tadpoles, visual experience is permissive in activating NMDA receptors and enabling sensory-evoked spikes (van Rheede, Richards, & Akerman, 2015), thereby facilitating inclusion of these neurons in circuit activity.

Sensory activity has also been demonstrated to influence neuronal morphologies in both S1BF and V1. In the visual cortex of kittens, lesioning the lateral geniculate nucleus (LGN) results in fewer and more immature corticocortical projections (Carić & Price, 1999). Many other studies have reported structural changes in spine growth in the visual cortex following monocular deprivation (Hofer, Mrsic-Flogel, Bonhoeffer, & Hübener, 2009; Keck et al., 2008; Valverde, 1967) and shown that neurons with similar visual responses connect preferentially to each other after the onset of sensory information (Ko et al., 2013). Rapid remodelling of V1 cortical axons is also triggered by monocular deprivation (Katz & Shatz, 1996; Antonini & Stryker, 1993). When the effect of dark-rearing and whisker trimming was directly compared, it appeared that sensory experience plays a greater role in S1BF presynaptic development. While whisker deprivation blocked the developmental decrease in release probability in S1BF, dark-rearing did not affect maturation of short-term plasticity in V1 (Cheetham & Fox, 2011).

In the mouse somatosensory cortex, sensory input has been shown to be critical for both the balance of local and long range connections, and integration of Reelin expressing interneurons into cortical circuits through maturation of axonal and dendritic arbours (García, Priya, Tuncdemir, Fishell, & Karayannis, 2015). Maturation of parvalbumin (PV) positive interneurons (INs) in S1BF is also affected by sensory

input modifications. Whisker removal, until the second postnatal week, results in a reduction in perisomatic basket synaptic structures in S1BF PV INs, making these cells appear similar to immature PV cells or V1 PV cells (Wamsley & Fishell, 2017; Chattopadhyaya et al., 2004). PV INs in layer 4 also show barrel-specific projections and morphology (Koelbl, Helmstaedter, Lübke, & Feldmeyer, 2013) and sensory activity is believed to be permissive for PV cell maturation (Daw, Ashby, & Isaac, 2007; Morales, Choi, & Kirkwood, 2002; Hensch, 2005). The activity-dependent expression of Etv1/Er81 has also been shown to modulate PV+ cell properties (Dehorter et al., 2015). Somatostatin (SST) positive INs are also affected by activity-regulated transcription, in particular Satb1 expression. If Satb1 expression is elevated, SST INs mature too quickly (Tuncdemir et al., 2016). The interaction of sensory input and the intrinsic genetic make up of cortical cell types points to a complex interplay between the two factors. Indeed, there are thousands of distinct chromatin and methylation signatures in VIP, SST, PV, and excitatory cells which may respond differently to sensory activity (Mo et al., 2015). In long-distance projection neurons, modulation of epigenetic mechanisms appears to define neuronal subclasses (Harb et al., 2016).

These results show that sensory-dependant changes occur on the level of cell morphologies, synapses and receptors. However, few studies have mapped specific circuit changes spanning the critical period.

1.1.6 Transient circuits

Likely targets for cortical circuit remodelling by sensory information are transient cell populations and circuits found in the neonatal cortex. Indeed, it is well established that transient connections and populations are fundamental for integration of cortico-thalamic input and correct cortical wiring. These include the early thalamus-subplate connection (Allendoerfer & Shatz, 1994; Kanold, 2004; Kanold

& Luhmann, 2010; Hoerder-Suabedissen & Molnár, 2015; Wang et al., 2010) and Cajal retzius cells (Tissir & Goffinet, 2003; Kirischuk, Luhmann, & Kilb, 2014).

Subplate cells are a transient cell population that receives direct inputs from the thalamus, cortical plate and subplate during the first postnatal days, positioning them as an excellent candidate for processing and integrating cortical and subcortical information (Hanganu, Kilb, & Luhmann, 2002). Not only are subplate neurons able to act as a transient relay for thalamic input, but through their gap junction coupling are able to amplify local columnar oscillations (Dupont, Hanganu, Kilb, Hirsch, & Luhmann, 2006; Hanganu, Okabe, Lessmann, & Luhmann, 2008; Luhmann, Kilb, & Hanganu-Opatz, 2009). During the critical period in mouse S1BF, subplate cells undergo significant morphological changes. At P2, the primary dendrite extends to the marginal zone, but by P7 dendrites end in or below layer 4 (Hoerder-Suabedissen & Molnár, 2012b). At the same time that these morphological changes are occurring, subplate neurites also undergo activity-dependent rearrangement of their position within layer 4. At P6, neurites are localised within the barrel, but by P14 are found predominately in the septa and layer 5a (Piñon et al., 2009). Mapping of subplate connections in the neonatal mouse auditory cortex revealed two classes of subplate neuron connectivity. The first group of subplate cell receives input from deep cortical layers. The second group receives input from deep and superficial layers, starting from the second postnatal week (Viswanathan, Bandyopadhyay, Kao, & Kanold, 2012). Therefore, subplate cells both receive input from and target cortical layers, particularly layer 4, and function as an early relay between thalamus and layer 4 (Zhao, Kao, & Kanold, 2009). These results suggests that subplate cells participate in transient activity-dependent circuits during S1BF critical period.

Recently, a number of transient interneuron circuits have been identified (Butt et al., 2017). The function of transient GABAergic IN circuits is of particular interest given the very early and specialised roles that GABAergic signalling plays in cortical

circuit development (Ben-Ari, Khalilov, Represa, & Gozlan, 2004; Butt et al., 2017; Ben-Ari, Cherubini, Corradetti, & Gaiarsa, 1989; Ben-Ari, 2002). From as early as E18, the first spontaneous inhibitory postsynaptic currents can be recorded (Owens, Liu, & Kriegstein, 1999), and during early postnatal development GABA is able to depolarize immature neurons (Ben-Ari, 2002; Mueller, Taube, & Schwartzkroin, 1984). This is thought to promote synaptogenesis as well as regulate the balance of excitation and inhibition (Akerman & Cline, 2006, 2007; Ge et al., 2006).

Guan et al. (2017) identified a transient connection in V1 in which SST mediated inhibition onto L2/3 was decreased, while fast-spiking (FS) IN mediated inhibition onto L2/3 was increased as a result of eye-opening. These connectivity changes could be prevented by dark-rearing and indicates that eye opening can differentially regulate GABAergic circuits (Guan et al., 2017).

Two transient cortical connections involving both SST and PV interneurons were reported by Anastasiades et al. (2016). The two transient connections reported were excitatory input from L2/3 onto L4 PV interneurons, and a GABAergic input from SST L5/6 INs onto L4 excitatory cell. Both these connections were observed between P5 and P8, before the end of the critical period, and disappeared from P9 onwards. Layer 2/3 excitatory cells began to receive L5/6 GABAergic input after P8, suggesting that L5/6 INs may extend their axons into supragranular layers during this time (Anastasiades et al., 2016).

The nature and function of the L5/6 GABAergic input onto L4 before P8 was investigated further by Marques-Smith et al. (2016), who showed that the GABAergic input onto L4 was part of a transient translaminar circuit that was both reshaped by thalamic input and involved in correct integration of thalamic afferents into layer 4 of S1BF (Marques-Smith et al., 2016).

The involvement of deep layer SST INs in correct thalamic integration was at the same time confirmed by Tuncdemir et al. (2016). They showed that SST interneu-

rons, which receive transient thalamic innervation, are necessary for the establishment of mature thalamocortical inputs to both pyramidal and PV interneurons in infragranular layers (Tuncdemir et al., 2016).

1.1.7 A transient, translaminar L5b-L4 loop modified by sensory activity

The transient circuit described by Marques-Smith et al. (2016) is a reciprocal loop between layer 5b (L5b) SST positive interneurons and layer 4 (L4) excitatory neurons (spiny stellates). At approximately postnatal day 8 (P8), this connection disappears and it is not present in the mature cortex (Marques-Smith et al., 2016). The L5b SST INs involved in this reciprocal loop are a subtype of SST-positive Martinotti cells labelled by the Lpar1-EGFP transgenic line (Hoerder-Suabedissen & Molnár, 2012a; Pedraza, Hoerder-Suabedissen, Albert-Maestro, Molnár, & De Carlos, 2014). Figure 1.1 illustrates this connectivity change, showing the L5b-L4 reciprocal loop before P8 followed by the subsequent weakening of L5b-L4 connections and strengthening of thalamic input onto layer 4. Thalamic input was observed to first engage with L5b SST+ve Lpar1-INs in early development before strengthening connections to L4 cells.

This transient, reciprocal connection is dynamically controlled by sensory activity. If the infraorbital nerve (ION) is severed at P1, the L5b to L4 GABAergic input is still observed at P10-P15. This suggests that normal whisker-dependent sensory experience is required for the maturation of L4 S1BF GABAergic circuitry from an early L5b to a late L4 GABAergic circuit. Additionally, if early circuitry is biased toward enhanced PV+ input onto SSN INs through overexpression of Ig-Neuregulin-1type 1 (Nrg1type1-tg) in the cerebral cortex, GABAergic input from L5b onto L4 SSNs is not observed. The decrease in input from L5b INs in Nrg1type1-tg L4 SSNs

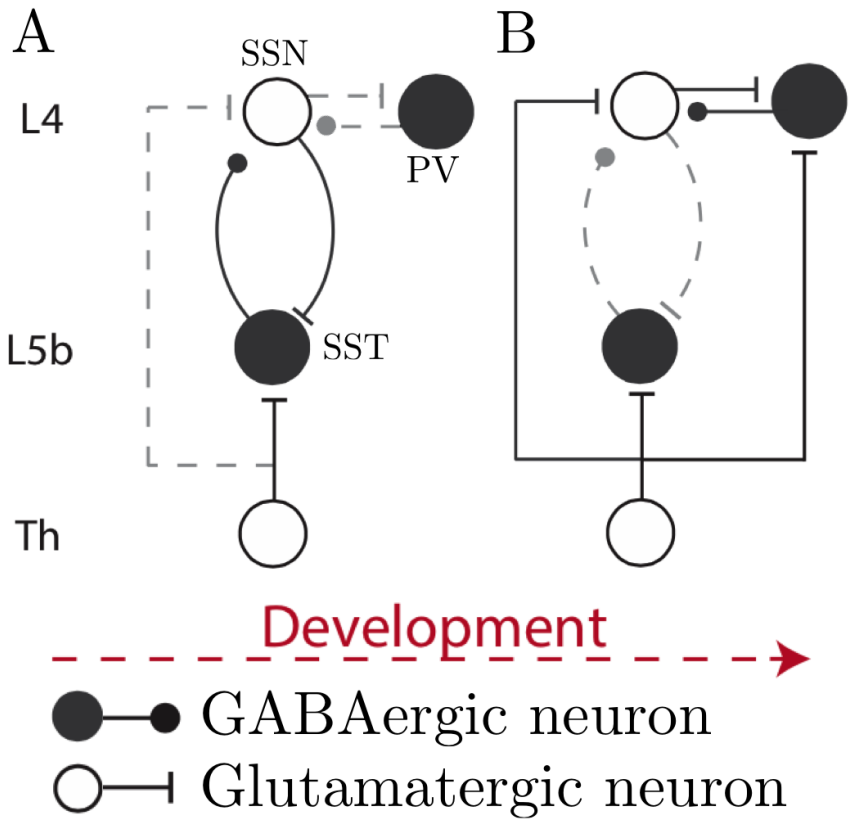


Figure 1.1: Dynamics of the L5b-L4 transient translaminar connection in the neonatal somatosensory cortex, showing collapse of the reciprocal loop and strengthening of thalamic input onto layer 4. **A)** The L5b-L4 transient translaminar connection from P4-P7. **B)** The L5b-L4 transient translaminar connection from P9+. Dashed lines represent weak/immature connections.

was revealed to be compensated for by an increase in local synaptic input within L4. Together, these results point to a dynamic balance of cell type-specific GABAergic input onto L4 during neonatal development that is modulated by sensory input.

Not only can the time course of this transient connection be modified by sensory information, but early GABAergic input onto L4 SSNs appears critical for proper integration of thalamic information into L4. In Nrg1type1-tg mice lacking L5b to L4 GABAergic input, EPSCs could not be evoked in L4 SSNs upon thalamic electrical stimulation. In older mice (post critical period) some recovery of the thalamic to L4 connection was seen, however, these connections were still smaller in amplitude than in WT animals. This recovery is likely mediated by the subplate (unpublished data). This indicates that the transient L5b-L4 circuit plays an important role in timely integration of thalamocortical synapses onto L4 SSNs in S1BF.

If early transient networks (such as the L5b-L4 loop found in S1BF) precede thalamic engagement, are required for correct integration of thalamocortical projections, and can be modified by incoming sensory information, it might be expected that these would be found in multiple primary sensory regions before the critical period. It is possible that there is a common mechanism for sensory integration across modalities and that the quality of this information directs modality-specific re-modelling of cortical circuits.

1.2 Thesis objectives

This thesis seeks to investigate the extent to which sensory information remodels cortical circuits during neonatal development. Although all regions of the adult neocortex appear to have common canonical circuitry, layer lamination and cell types, it is evident that unique sensory processing characteristics such as barrel fields or orientation selectivity exist in primary sensory cortices. The question is how

and when do the unique processing characteristics manifest themselves in primary sensory areas, and to what extent does sensory information remodel area-specific circuitry.

The involvement of sensory information in the development of specific cortical circuitry is a concept that has been around for several decades. However, the exact cellular components have only recently begun to be examined through new techniques such as optical circuit mapping, for example, laser scanning photostimulation (LSPS) (Anastasiades, Marques-Smith, & Butt, 2018; Shepherd et al., 2003; Zhao et al., 2009; Viswanathan et al., 2012; Brill, Mattis, Deisseroth, & Huguenard, 2016). The interaction with thalamic input combined with transient nature of the L5b-L4 reciprocal circuit makes it the ideal candidate to begin to address sensory-evoked circuit remodelling in primary sensory cortices.

The three main aims of this thesis, corresponding to the three results chapters, were as follows:

- **Aim 1: To investigate the default neonatal GABAergic circuits in a mouse model in which the neocortex is devoid of thalamic input**

- **Aim 2: To establish if common neonatal transient translaminar circuits exist across sensory modalities by comparing somatosensory and visual cortices**

- **Aim 3: To explore possible variance in thalamic input and SST cell populations between neonatal somatosensory and visual cortices**

The remainder of this chapter examines these aims in detail.

1.2.1 Transient cortical circuits in a sensory naïve mouse - Chapter 3

The first aim was to map the transient L5b-L4 connection in a mouse devoid of all sensory input. Although previous data (Marques-Smith et al., 2016) suggested that sensory perturbation as a result of ION sectioning resulted in a delay in the transition from L5b input to local GABAergic input in L4, ION damage can lead to alterations beyond simply abolishing transmission of sensory activity. For example, Takeuchi et al. (2012 and 2017) show rewiring of afferent fibres in the thalamus after peripheral nerve transection (Takeuchi et al., 2012; Takeuchi, Osaki, Yagasaki, Katayama, & Miyata, 2017). Therefore, in order to determine what developing cortical circuit dynamics were in the absence of sensory activity, a different model was needed.

The Celsr3|Dlx5/6 mouse line was the ideal candidate in which to interrogate the role of external sensory information in the maturation of neocortical circuits. In these mice, Celsr3, a cadherin receptor important for axon guidance (Nakayama et al., 1998), is conditionally deleted in the basal telencephalon where Dlx5/6 Cre is expressed (Zhou et al., 2008).

The precise area of Celsr3 deletion can be seen in Figure 1.2B (green regions). This conditional deletion of Celsr3 (Celsr3 $^{fl/fl}$) causes all three components of the internal capsule to be completely defective. As such, the thalamocortical, corticothalamic and subcerebral axonal projections all fail to reach their respective targets. This complete disconnect between the thalamus and the cortex was confirmed using histological approaches including DiI injections and tracing (Zhou et al., 2008). These conditional mutant mice live for approximately 21 days and have normal neurogenesis, as well as normal areal and laminar patterning, allowing for their use as a model for neonatal cortical circuit development in the absence of sensory input

(Zhou et al., 2010).

It was hypothesised that, as with ION sectioning, a lack of sensory input would delay any circuit remodelling and, therefore, timely development of a mature cortical circuit. To test this, GABAergic input onto L4 excitatory cells was mapped using LSPS in Celsr3|Dlx5/6 mice during the first two weeks of development.

1.2.2 Transient cortical circuits in the developing mouse primary visual cortex - Chapter 4

Due to the sensory-independent nature of the L5b-L4 reciprocal loop and its previously published role in the integration of thalamic connectivity into L4, it was further hypothesised that it might be present in other primary sensory cortices. The second aim of this DPhil was, therefore, to map cortical circuitry in the neonatal mouse visual cortex.

To investigate if the L5b-L4 connection was ubiquitous across sensory cortices, LSPS was used to map both GABAergic input onto L4 excitatory cells and glutamatergic input onto SST+ L5b INs in V1 of the mouse neocortex from P5 to P24. The extended time window was included to take into account the later critical period in V1.

In order to rule out the possibility that a similar translaminar circuit involving L5b SST+ve INs and a layer other than L4 existed, GABAergic input across cortical layers was mapped using LSPS.

To test if the L5b-L4 reciprocal connection is the default network found across modalities in the Celsr3|Dlx5/6 mouse, cortical circuitry was also mapped in V1 of Celsr3|Dlx5/6 mice.

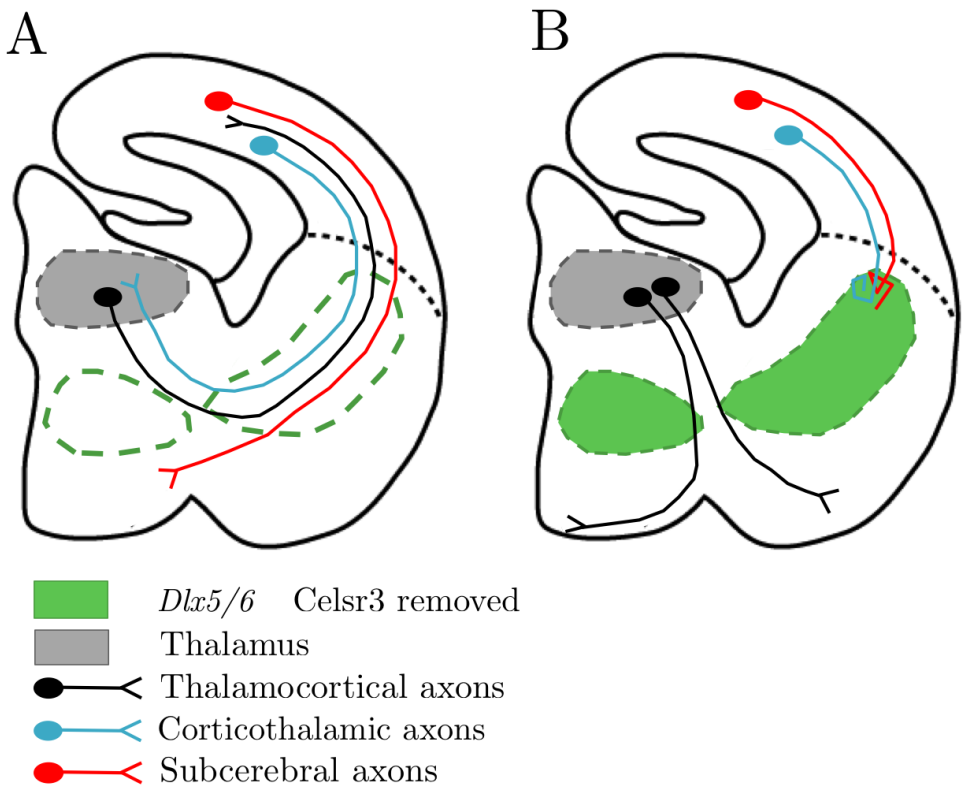


Figure 1.2: **Thalamocortical connections in Celsr3 conditional mutants. A)** Schematic summary of WT thalamocortical, corticothalamic and subcerebral projections. **B)** Schematic summary of Celsr3 conditional mutant thalamocortical, corticothalamic and subcerebral projections. Green indicates the areas of Dlx5/6 expression and consequently the areas of Celsr3 inactivation. Adapted from Figure S2 in (Zhou et al., 2008).

1.2.3 Thalamocortical input into neonatal V1 and S1BF - Chapter 5

The differences in circuit connectivity between V1 and S1BF in the absence of thalamic input suggest that early area-specific cortical circuitry is governed by intrinsic genetic mechanisms. As the SST+ Lpar1-EGFP INs were involved in the S1BF L5b-L4 reciprocal loop, it was hypothesised that this cell type might populate S1BF and V1 differently, driving differences in early circuitry. To investigate this, immunohistochemistry of both SST+ and Lpar1-EGFP cells on S1BF and V1 neonatal slices was performed.

As the L5b-L4 reciprocal circuit has been shown to be involved in the timing and strength of thalamic engagement with layer 4 in S1BF, and Lpar1-EGFP SST+ve INs receive thalamic input during early development, it was further hypothesised that developing thalamic afferents might engage differently with neonatal S1BF and V1.

A thalamus-specific Cre driver line was chosen to conditionally express channelrhodopsin. This allowed stimulation of cut thalamo-cortical axons (Petreanu, Huber, Sobczyk, & Svoboda, 2007) in order to accurately compare thalamic innervation in S1 and V1. Using the *Olig3*$^{\mathrm{cre/+}}$ mouse line, thalamic input onto L4 and L5b during neonatal development in S1BF and V1 was investigated.

The following chapter details the experimental methods used to investigate these three key areas.

Chapter 2

Methods

2.1 Mouselines

All animal work was approved by the local ethical review committee and conducted in accordance with Home Office personal and project (30/3052) and (30/2919) licenses under the UK Animals (Scientific Procedures) 1986 Act.

Mouse lines were maintained primarily on a C57/BL6 background. Some colonies were maintained on a mixed CD1, C57/BL6 background, as the original colony breeders were on a CD1 background. All experimental animals used were black or agouti in coat colour unless otherwise specified. No albino animals were used. This is because albino mice have altered chiasmatic decussation and show impaired visual function (Peirson, Brown, Pothecary, Benson, & Fisk, 2018).

The mice used in the project with red fluorescent protein expressed in layer 5a were generated by breeding *Rpb4*$^{cre/+}$ (retinol binding protein 4) with floxed *Ai14*$^{fl/fl}$ mice (The Jackson Laboratory - 007908, 2014). The *Ai14* contain the red fluorescent protein tdTomato. *Ai14* Mice were sourced from Jackson Laboratories and the *Rpb4*$^{cre/+}$ were sourced from an existing colony owned by Professor Zoltán Molnár (MMRRC - 031125-UCD, 2014) (Hoerder-Suabedissen, Korrell, et al., 2018;

Hoerder-Suabedissen, Hayashi, et al., 2018; Grant, Hoerder-Suabedissen, & Molnár, 2016).

All other mouse lines containing red fluorescent protein were bred using *Ai9*$^{fl/fl}$ animals (The Jackson Laboratory - 007909, 2014) containing the red fluorescent protein tdTomato.

The $P2X_2$ mice were bred by crossing *SST*$^{cre/+}$ (The Jackson Laboratory - 013044, 2014) mice with floxed-stop $P2X_2$ reporter mice (Anastasiades et al., 2016) to generate pups with $P2X_2$ expressed only in SST positive neurons.

For mice lacking thalamocortical input, the Celsr3|Dlx5/6 mouse line was used. The Celsr3|Dlx5/6 mouse line was generously provided by Professor Goffinet (The University of Louvain) (Zhou et al., 2010). The colony was maintained as two separate lines, the first being conditional floxed Celsr3 (*Celsr3*$^{fl/fl}$) mutant mice. These were maintained as a homozygous population. The second mouse line was a double heterozygous line (*Celsr3*$^{+/-}$;*Dlx5/6*$^{Cre/+}$). By crossing these two lines, *Celsr3*$^{f/-}$;*Dlx5/6*$^{Cre/+}$ could be generated.

In order to quantify Lpar1-eGFP cells in V1 and S1BF, the Lpar1-eGFP mouse was used (GENSAT Project at Rockefeller University, 2005; Hoerder-Suabedissen, Hayashi, et al., 2018; Pedraza et al., 2014)

In order to characterise the thalamocortical input into mouse neonatal S1 and V1, an *Olig3*$^{cre/+}$ crossed with Ai32 conditional channelrhodopsin-2 mouse line was used. The Cre dependent channelrhodopsin-2 mouse line was bought from Jackson Laboratories (The Jackson Laboratory - 012569, 2016). This line, commonly referred to as Ai32 (Ai32(RCL-ChR2(H134R)/EYFP)) consists of channelrhodopsin-2/EYFP fusion protein which is expressed following exposure to Cre recombinase. The *Olig3*$^{cre/+}$ mice were created and kindly provided by Professor Yasushi Nakagawa at the University of Minnesota (Vue et al., 2009).

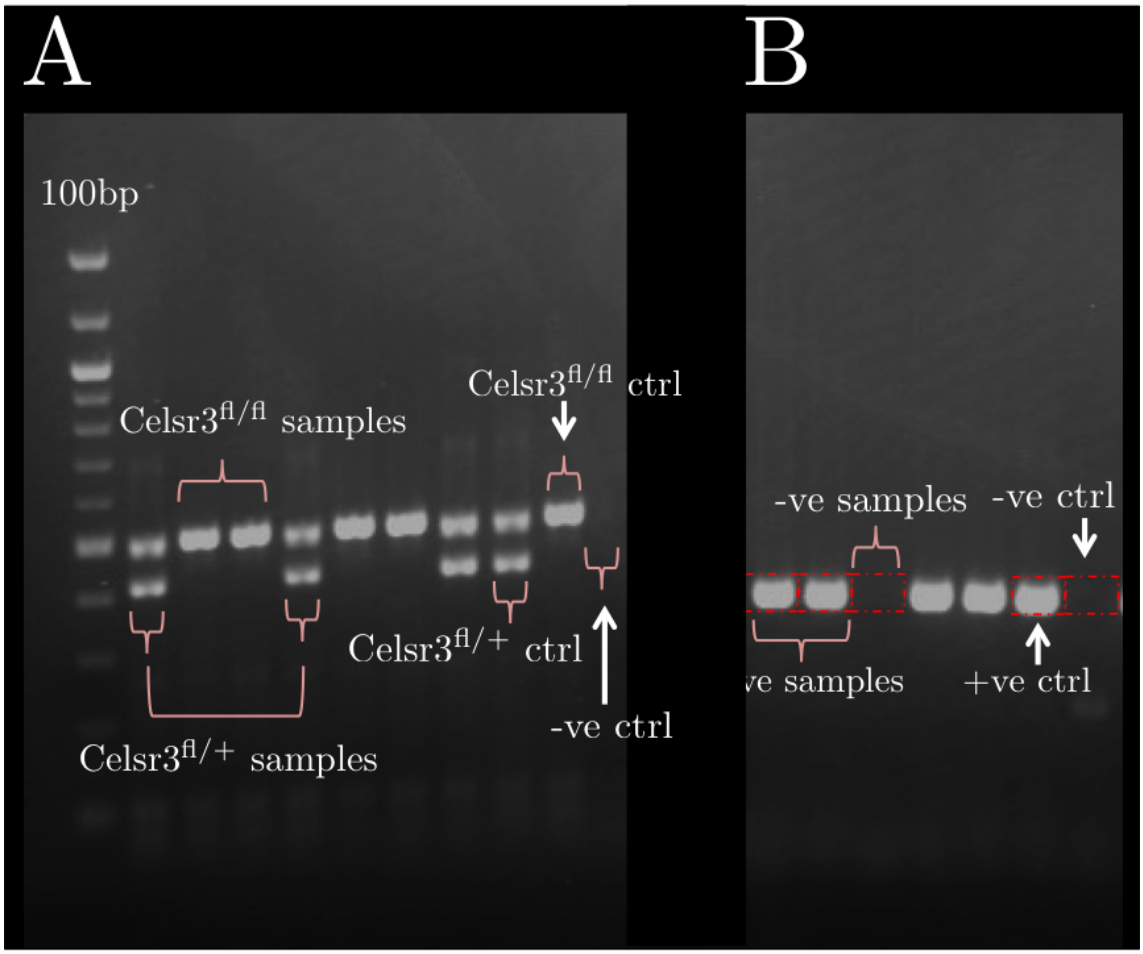


Figure 2.1: PCR gel showing the results of genotyping for both *Celsr3*$^{fl/fl}$ and *Dlx5/6*$^{Cre/+}$. **A)** Genotyping for *Celsr3*$^{fl/fl}$ and *Celsr3*$^{fl/+}$ shows two bands at 400 bp (WT) and 500 bp (flox). **B)** Genotyping for *Dlx5/6*$^{Cre/+}$ shows a single band at 350 bp indicating EGFP presence. Ladder is 100 bp.

2.1.1 Genotyping

In order to maintain the (*Celsr3*$^{+/-}$;*Dlx5/6*$^{Cre/+}$) mouse line, males from the experimental cross which were positive for Cre and heterozygous for Celsr3 were kept as breeders. *Celsr3*$^{fl/fl}$ gave a PCR band at 500 bp while a *Celsr3*$^{fl/+}$ gave a band at both 500 and 400 bp (Figure 2.1A). Genotyping for Dlx5/6 cre only gave a band at 350 bp when the attached EGFP sequence was present (Figure 2.1B).

Professor Nakagawa provided a PCR protocol for the presence of *Olig3*$^{cre/+}$ (Vue et al., 2009). This protocol results in a single positive band at 300 bp when mice

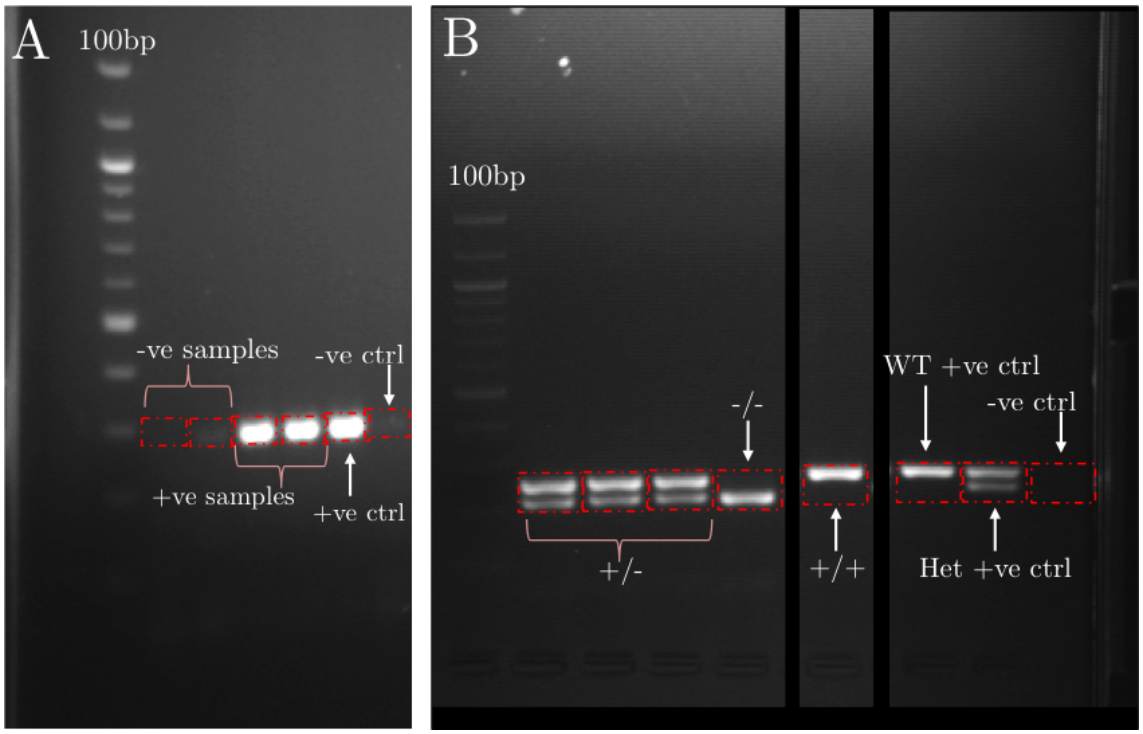


Figure 2.2: **PCR gel showing the results of genotyping for both *Olig3*$^{cre/+}$ and Ai32(EYFP). A)** Genotyping for *Olig3*$^{cre/+}$ shows a single band at 300bp if the mouse is positive for *Olig3*$^{cre/+}$. **B)** Genotyping for Ai32(EYFP) shows two bands. A wildtype band at 297 bp and a band indicating EYFP presence at 212 bp. Ladder is 100 bp.

carry *Olig3*$^{cre/+}$. As the mice could not be genotyped for homozygosity, they were maintained as a heterozygous colony, following the recommendation of Professor Nakagawa (Vue et al., 2009). Figure 2.2 shows positive and negative samples alongside a positive and negative control.

The PCR protocol for Ai32/EYFP recommended by Jackson Laboratories was followed to genotype breeding and experimental animals. This procotol resulted in two bands; a wildtype band at 297 bp and a mutant band at 212 bp (Figure 2.2). This allowed identification of both heterozygous and homozygous animals. Results for the PCR of Ai32 mice can be seen in Figure 2.2B. Figure 2.2B contains samples from wildtype, heterozygous and homozygous mice, as well as positive and negative controls. To breed mice for experimental protocols, Ai32$^{-/-}$ mice were bred with

Olig3$^{cre/+}$ mice.

2.2 Slice Preparation

Mice were deeply anaesthetized with 4% isoflurane (in 100% O_2) before decapitation with surgical scissors. For mice less than P21 in age, the brains were dissected in ice-cold, normal artificial CSF (ACSF); composition (in mM): 125 NaCl, 2.5 KCl, 25 $NaHCO_3$, 1.25 NaH_2PO_4, 1 $MgCl_2$, 2 $CaCl_2$, 20mM glucose); pH equilibrated with 95%O_2 / 5% CO_2 to pH7.2-7.4. For mice older than P21, brains were dissected in ice-cold high-sucrose ACSF composition (in mM): 125 NaCl, 3 KCl, 25 $NaHCO_3$, 1.25 NaH_2PO_4, 5 $MgSO_4$, 1 $CaCl_2$, 15 glucose, 130 sucrose. All chemicals were sourced from Sigma unless otherwise specified.

Different slice protocols were used depending on the area under investigation. For somatosensory cortex, both thalamocortical (Agmon & Connors, 1991) and coronal slice angles were used. For visual cortex, sagittal, thalamocortical (MacLean, Fenstermaker, Watson, & Yuste, 2006) and coronal slice angles were cut. Coronal sectioning was chosen as the most appropriate for further investigation in V1. Brains were sectioned at 400 μm preserving the regions of interest. The sectioning was performed in ice-cold ACSF for mice <P21 and in ice-cold high sucrose ACSF for mice >P21. Both solutions had been previously infused with a 95%O_2 / 5% CO_2 gas mixture for a minimum of 10 minutes. Brains were sectioned using a vibratome (Vibratome 3000 Plus; The Vibratome Company) before being transferred and stored in an incubation chamber (Harvard Apparatus, UK) containing room temperature, oxygenated ACSF. The ACSF had been oxygenated by infusing a 95%O_2 / 5% CO_2 gas mixture for a minimum of 10 minutes. The slices were left to rest for a minimum of 1 hour before recording.

2.3 Whole-cell patch-clamp electrophysiology

Individual slices were transferred to the recording chamber and continuously perfused with ACSF that was kept at room temperature and infused with 95%O_2 / 5% CO_2. The appropriate area and layer of interest were identified under a low power objective (10x) prior to switching to a 40x objective for patch-clamp electrophysiology.

Whole-cell patch clamping was performed using borosilicate glass microelectrodes (5 - 8 MΩ; Harvard Apparatus) pulled using a Narishige PC-10 electrode puller (Narishige, Japan).

To record GABAergic input, electrodes were filled with a Cesium-based intracellular solution containing: (in mM): 100 Gluconic acid, CSOH by titration to pH 7.2-7.4, 0.2 EGTA, 5 $MgCl_2$, 40 HEPES, 2 Mg-ATP and, 0.3 Li-GTP. For recordings P21+, the intracellular solution for GABAergic recordings also contained lidocaine (QX-314) (5mM), as caesium alone seemed insufficient to allow a positive holding potential.

This solution allows a stable voltage clamp at depolarized potentials. Therefore, the cell could be held at the reversal potential for glutamate (E_{Glut}), determined empirically using glutamate uncaging. When the cell was held at (E_{Glut}), outward currents represented GABA-mediated inhibitory postsynaptic currents (IPSCs) (X. Xu & Callaway, 2009).

To record glutamatergic inputs, electrodes were filled with standard whole-cell patchclamp solution containing (mM): 128 K-gluconate, 4 NaCl, 0.3 Li-GTP, 5Mg-ATP, 0.0001 CaCl2, 10 HEPES, 1 glucose and KOH by titration to pH 7.2-7.4. To enable reconstruction of recorded cell morphologies, biocytin (3 mg/ml) was included.

The microelectrode was lowered onto the target neuron using a motorised mi-

cromanipulator (Luigs and Neumann Mini 25-ZR), whilst constant positive pressure was applied via a mouthpiece connected to the pipette by silicon tubing. As the microelectrode was lowered towards the cell, a 25 mV pulse at 20 Hz frequency was applied in voltage clamp mode (Multiclamp 700B, Molecular Devices, SUA, CA). Once a dip in the test pulse and/or a dimple in the cell body membrane was observed, indicating proximity to the target cell body, the positive pressure was changed to negative pressure. This was applied until a tight seal between the microelectrode and cell membrane was formed. A tight, gigaohm seal was indicated by a flat test pulse. Once the seal had been established, a short sharp pulse of negative pressure was used to break through the cell membrane and enter whole-cell patch clamp configuration.

2.4 Intrinsic properties of recorded neurons

Intrinsic properties were ascertained for all cells recorded using standard electrode solution. The cell was held in current clamp, while positive current was injected in a ramp fashion until reaching the threshold of action potential firing (Figure 2.1A).

This allowed an approximation of cell excitability, so that subsequent pulse magnitudes could be adjusted to the intrinsic excitability of the cell. To measure a range of intrinsic properties, 500 ms square depolarizing or hyperpolarizing current pulses at 0.5 Hz were delivered via Clampex software (Molecular Devices, CA, USA) (Figure 2.3B). Current protocols varied depending on the intrinsic parameter of interest. For each cell the pulses were adjusted to produce; a threshold spike, hyperpolarization to -100 mV to determine the presence of rebound spike, hyperpolarization responses <20mV to allow measurement of input resistance, (Figure 2.1C) and large depolarization to measure maximum firing frequency (Figure 2.1D). From these recordings, additional intrinsic properties of resting membrane poten-

tial (RMP), spike height, spike half-width, afterhyperpolarization (AHP) amplitude, AHP delay, and decay constant could also be determined. During the calculation of a cell's intrinsic electrophysiological parameters, the action potential threshold was calculated using the maximum of the second derivative of the voltage trace (Wilent & Contreras, 2005; Platkiewicz & Brette, 2010; Henze & Buzsaki, 2001).

Intrinsic properties were monitored occasionally throughout recordings, in order to check cell health and access. A healthy cell was determined on the basis of no deterioration in RMP, spike height (above +10mV) and spike threshold (<30mV). Cells showing deterioration in access were discarded from further analysis. All cells were analysed offline using Clampfit (v10.1, Molecular Devices, CA, USA).

2.5 Laser scanning photostimulation - glutamate uncaging

LSPS was used to map synaptic inputs onto a given cell type within the neocortex through simultaneous whole-cell patch recording and stimulation of the surrounding cortical tissue (Anastasiades et al., 2018; Shepherd et al., 2003; Zhao et al., 2009; Viswanathan et al., 2012; Brill et al., 2016). LSPS of caged-glutamate was performed using an ultraviolet (UV) laser (DPSL-355/30) and a UGA-40/42 targeting module (Rapp OptoElectronic GmbH), focused through a Zeiss Axioskop FS2-plus microscope and 10 x UPLFLN objective (Olympus). The laser intensity was adjusted to achieve a stimulation spot of approximately 50 μm.

Caged-glutamate (100μM methyl 1-[5-(4-amino-4-carboxybutanoyl)] -7nitroindoline-5-acetate hydrate-caged glutamate (Tocris, UK)), was made up in high divalent cation (HDC) solution. HDC ACSF differs from ACSF in that is has raised levels (4mM) of $MgCl_2$ and $CaCl_2$. This solution was infused with a 95%O_2 / 5% CO_2 gaseous mixture. The HDC/caged-glutamate solution was washed into the recording

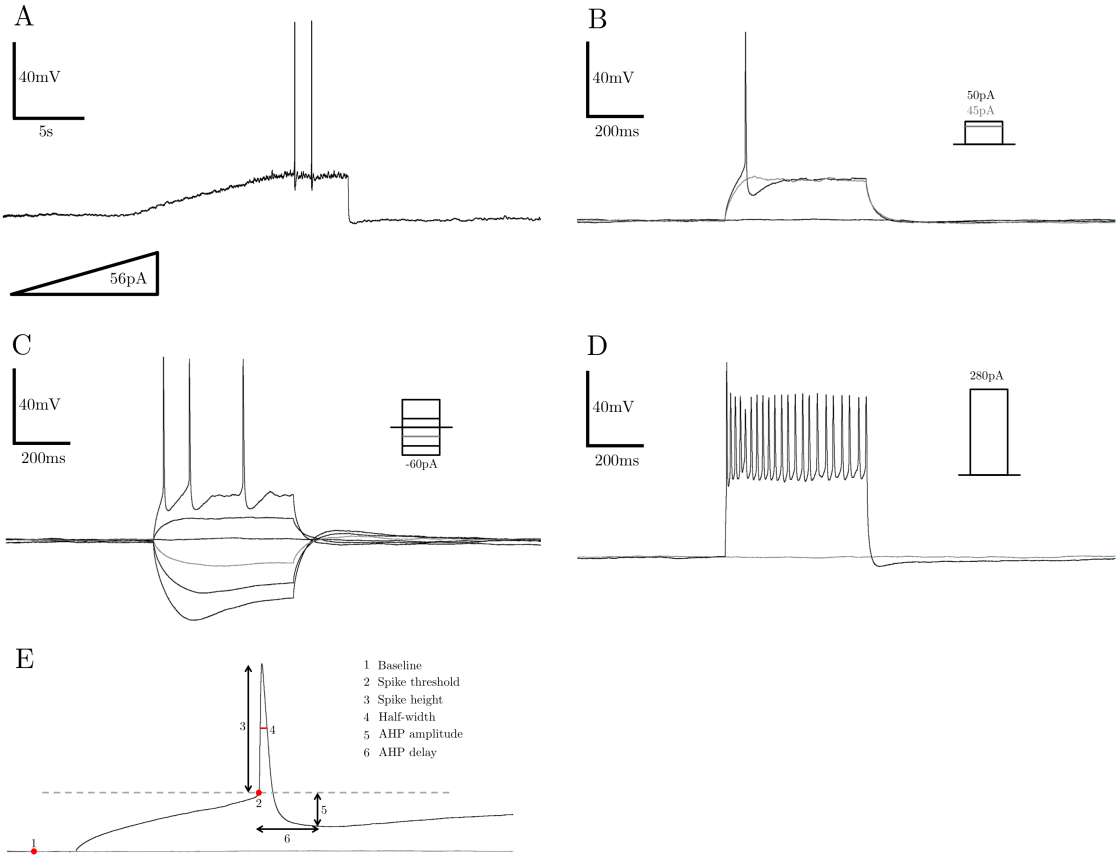


Figure 2.3: **Current input protocols used to calculate electrophysiological parameters.** A) Ramped current injection is used to determine a rough spike threshold and spike height, as well as the health of the cell and quality of the cell access. B) Stepped current injection to determine spike threshold. C) Voltage response to hyperpolarizing current steps. Input resistance and membrane time constant is calculated from the smallest hyperpolarizing step (grey line). D) Current steps are increased until maximum firing frequency is reached. E) The action potential caused by minimum current input to spike is also used to calculate a number of electrophysiological properties.

chamber for 4-6 minutes at room temperature before LSPS recording began.

The laser power was calibrated to evoke 3 action potentials when the laser was fired directly at the cell soma, but minimize suprathreshold responses elicited at distal sites to ensure good spatial resolution (Anastasiades, Marques-Smith, & Butt, 2017). The laser targeting grid was manually programmed in custom software provided by Rapp Optoelectronic (Hamburg, Germany). The mapping grid was a 17×9 spot grid. The width of the grid was 450 μm, while the height of the cortex determined the total length (650 − 850 μm). Spot stimulation order was pseudorandom to prevent neighbouring spots being stimulated sequentially. The laser was fired at 1 Hz, with each pulse lasting 100 ms. The map was aligned perpendicular to the surface of the slice and the position of the electrode was assigned a specific stimulation point. For areas longer than one standard grid, multiple overlapping grids were used to ensure that all areas were stimulated. Cells were mapped 2-3 times each under voltage clamp. The current traces were analysed offline using Minianalysis 6.0 (Synaptosoft Inc.). Recorded EPSCs/IPSCs that occurred within the putative monosynaptic window (160-400 ms laser fires at 100 ms) (Anastasiades & Butt, 2012) were extracted and the number and amplitude were analysed using a customized Matlab R2011 script (The MathWorks). Individual maps were generated from the sum IPSC amplitude, evoked in the recorded cell from each stimulating point. The average maps were calculated from the average of these individual sweeps. A photomicrograph of the targeting grid overlaid on the acute *in vitro* slice using the Axiovision v4.6 module of the UGA - 40/42 allowed the laser points to be assigned to the layers of the cortex.

Glutamatergic inputs were mapped at a holding potential of -70 mV. To map GABAergic input, cells were held at the glutamate reversal potential (E_{Glut}) in voltage clamp. The reversal potential for each cell was determined empirically by adjusting the holding potential, while uncaging glutamate proximal to the cell body

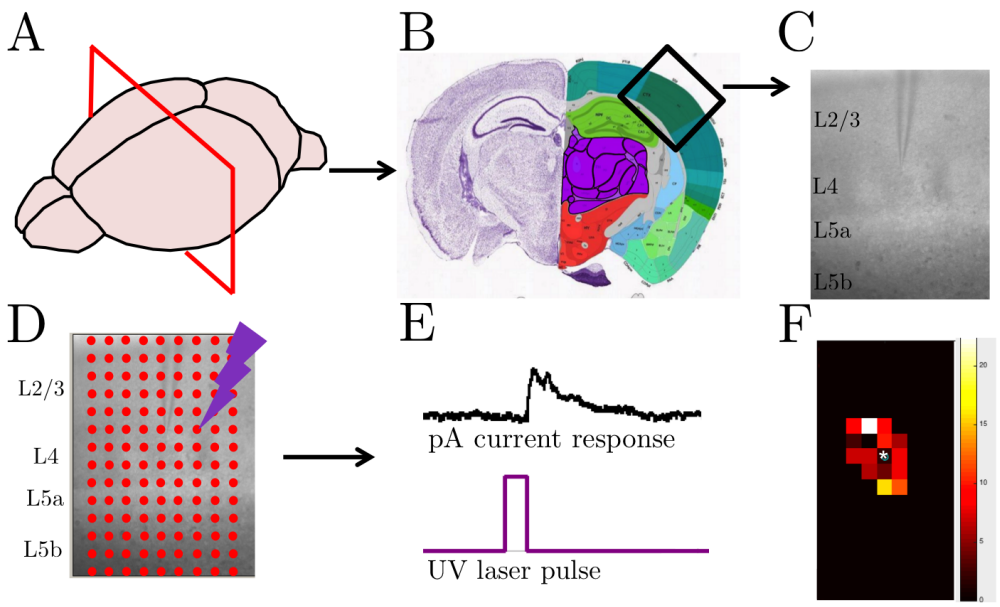


Figure 2.4: **Steps in LSPS methodology A)** The brain is sliced **B)** A slice containing the cortical region of interest is selected **C)** A cell in the region and layer of interest is patched. **D)** A 17×9 grid is overlaid on the slice and a UV laser uncages a compound (either glutamate of ATP) at each spot in a pseudorandom pattern. **E)** When the recorded cell receives input from a cell that has been activated through LSPS, a current response is observed. **F)** From multiple LSPS sweeps, averages of current responses are calculated to create a 'heat map' of connectivity onto the recorded cell.

until the direct current response was attenuated or absent (E_{Glut}).

2.6 Laser scanning photostimulation - ATP uncaging

For SST specific input, an optogenetic activator conditionally expressing in SST interneurons using SST-ires-Cre;$P2X_2$ was used. This enables selective activation of these interneurons in response to focal ATP uncaging (Zemelman, Nesnas, Lee, & Miesenböck, 2003; Miesenböck, 2011; Anastasiades et al., 2016). When using this technique, normal ACSF, as opposed to HDC, was used to dilute the caged-ATP (Invitrogen, Molecular Probes DMNPE-caged ATP, 0.22mM). Other than this

alteration, the procedure for LSPS using caged-ATP was the same as described above for caged-glutamate mapping.

2.7 Analysis of LSPS data

For all LSPS experiments, traces were analysed offline using Minianalysis 6.0 (Synaptosoft Inc.). All EPSC and IPSCs were logged. All synaptic events were then analysed using a customized Matlab script (The MathWorks). The number and amplitude of PSCs that occurred within the event detection window were extracted. The amplitude of responses across all sweeps was averaged for each stimulation point and plotted using a heat map.

When multiple cell recordings were collated into a single averaged heat map, each cell was first normalised before being grouped. This ensured that each cell contributed equally to the final heat map distribution.

For statistical comparisons, both total input and normalised input were used. For total input, the total input (pA) from each cortical layer was averaged and the SEM calculated. For normalised input, the percentage of total GABAergic input that originated from each layer was calculated for each cell. The mean and SEM of this was calculated for multiples cells of a given phenotype or age group. Figure 2.4 illustrates the steps undertaken during LSPS, from brain slicing through to data analysis.

2.8 Optogenetic stimulation of thalamocortical afferents

To stimulate the channelrhodopsin, a blue LED (Cool-LED pE-100, 450-490 nm) was used at increasing light intensity. The LED was triggered within a Clampex software

program (Molecular Devices, CA, USA). The blue light illuminated all surrounding tissue through a 40x objective (Olympus LUMPLFLN 40XW Objective). To avoid strong activation of the channelrhodopsin-2, a YFP filter was used to predominately excite the YFP protein fused to the channelrhodopsin-2.

In coronal slices containing S1BF a thalamic cell was recorded and stimulated using increased level of blue light intensity in order to further verify the function of the transgenic channelrhodopsin-2 expression in thalamic cells and to ascertain stimulation parameters. In both V1 and S1 cortices, cells in layer 4 and layer 5b were targeted for recording. The thalamocortical afferents were stimulated using either 10ms (<P10) or 1ms (≥P10) of blue light. Light intensity was varied to find minimal stimulation parameters. Minimal stimulation was then repeated every 20 seconds for 2-5 sweeps, in order to calculate average response amplitude.

To further investigate whether evoked responses were monosynaptic or polysynaptic in nature, Tetrodotoxin (TTX) (in concentrations 0.5μM - 2μM) and 4-Aminopyridine (4-AP) (in concentrations 300μM - 600μM) were added to the slice bath solution. On occasion, HDC ACSF was also used to attenuate polysynaptic activity.

2.9 Optogenetic stimulation analysis

The amplitude and latency of all responses from thalamic afferent optogenetic stimulation were analysed. The responses were subdivided based on cortical area (S1BF/V1), cortical layer (L4/L5b) and cell type (Pyr, SSN, NFS IN, FS IN). Other parameters such as LED power, response probability, length of stimulation, TTX concentration, 4-AP concentration and, bath solution (ACSF/HDC) were also noted, to allow separation of responses based on these parameters.

The standard error of the latencies of responses of 'jitter' was used as a mea-

surement of response consistency and, therefore, an indication of the likelihood that any given cell received mono-synaptic thalamic input. Any response recorded that was less than 5 ms or more than 22 ms was classed as spontaneous and excluded from the average amplitude and latency calculations. Additionally, any cell with an average response of less than 5 pA or any cell with a response probability of less than 10% was not classified as having a monosynaptic connection. Using these parameters, 42.3% of cells were excluded from mono-synaptic classification.

2.10 Statistics

Results were tested for normality using the one-sample Kolmogorov-Smirnov test. If data points were found to be normally distributed, a two sample t-test was used to test the null hypothesis that the data came from independent samples with equal means. If the data were found to not be normally distributed, a two-sided Wilcoxon rank sum test for independent samples was used.

2.11 Histochemistry

2.11.1 Slice preparation

Mice were anaesthetised with an intraperitoneal injection of a lethal volume of sodium pentobarbital. Once deeply anaesthetised mice were perfused with 4% paraformaldehyde in PBS. The brain was removed and stored in 4% paraformaldehyde in PBS at 4°C for 2 hours before being washed three times with PBS. Perfused brains were then dehydrated in 10% sucrose solution in PBS overnight followed by 30% sucrose solution in PBS for a second night. Brains were then mounted in O.C.T (Fisher Scientific) and frozen at -80°C. Brains were sliced on a cryostat at 20 μm thickness and mounted on superfrost microscope slides (Fisher Scientific). Slides

were stored at -20°C.

2.11.2 Antibody staining

Slices were dried for 30 minutes before being post-fixed to 10 minutes in 4% paraformaldehyde in PBS. Slices were then washed in PBS 3×5 mins, after which they were blocked with 5% donkey serum for 2 hours at RT. Primary antibody was then incubated in 0.2% PBST and 1% donkey serum overnight at 4°C. The following primary antibodies were used: Ctip2 rat [1:200], Brn2 goat [1:100], antiGFP chicken [1:200] Slides were then washed 3×5 minutes with PBS before secondary antibody in 0.2% PBST and 1% donkey serum was applied. Secondary antibodies were the following: donkeyαrat 488 nm, donkeyαgoat 468 nm, donkeyαrabbit 468 nm, donkeyαmouse 488 nm. This was left for 2 hours before washing the slides again in PBS 3 x 5 minutes. Secondary antibodies were all used at [1:500]. DAPI [1:1000] was applied for 10 minutes and washed off with PBS 3×5 minutes. Slides were then mounted and imaged using a standard fluorescence microscope (Leica HC FSA, Camera - Leica DFC 500) at 10×. Antibodies were sourced from the following: CTIP2 (Abcam ab18465), Brn2 (Santa Cruz Biotechnology), AntiGFP (Abcam ab13970).

2.11.3 Morphological reconstruction of biocytin filled neurons

After recordings, the 400 μm slices were fixed overnight at 4°C in 4% paraformaldehyde in PBS. The slices were then washed in PBS 2×10 minutes and PBST (0.05% Triton-X). Slices were incubated overnight in streptavidin-conjugated Alexa-Fluor 588 nm (ThermoFisher) in PBST at a concentration of [1:500]. Images were taken using a 10× objective with the Zeiss LSM710 confocal microscope using a z-stack to capture all projections. Neurons were traced using the Simple Neurite Tracer Fiji

(Image J) plugin. This plugin was also used for Scholl analysis of traced morphologies using standard axes and no normalization of intersections. Scholl analysis data was plotted as a linear Scholl plot (Ferreira et al., 2014). To assign cell type, the following publications were used to classify cells: (Sun, Huguenard, & Prince, 2006; Feldmeyer, Egger, Lübke, & Sakmann, 1999; Otsuka & Kawaguchi, 2009; Markram et al., 2004; Rudy, Fishell, Lee, & Hjerling-Leffler, 2011; Anastasiades et al., 2016; Steger et al., 2013; Jacob, Petreanu, Wright, Svoboda, & Fox, 2012; Sippy & Yuste, 2013). For final morphology images, confocal stacks were stacked to the highest pixel intensity.

2.11.4 DiI tracing

DiI tracing was performed on P5 Celsr3|Dlx5/6 and littermate control mouse brains. Perfused mouse brains were mounted in 5% agarose. Professor Zoltán Molnár performed the dissection and placement of the tracing dye (Molnár, Adams, & Blakemore, 1998). The posterior of each brain was carefully sliced to reveal the thalamus. A small number of individual DiI (1,1'-dioctadecyl 3,3,3'3'-tetramethylindocarbocyanine perchlorate) crystals were placed in the left thalamus and right somatosensory cortex using a fine stainless steel wire, under an operating microscope. Brains were then stored in PBS containing 0.1% Na azide and placed in an incubator at 37°C for 3 weeks after which time they were sliced at 100 μm thickness using a vibrating blade microtome (Leica). Slices were mounted on superfrost microscope slides (Fisher Scientific) and imaged using a standard fluorescence microscope (Leica HC FSA, Camera - Leica DFC 500) at 5× as well as a Zeiss LSM710 confocal microscope at 10×.

The following chapters make use of the methods presented here to address the key aims of this thesis.

Chapter 3

Thalamic input is not required for the development of the L5b-L4 GABAergic connection

Laser scanning photostimulation (LSPS) is a technique within neuroscience used to describe a method of cell activation, whereby a laser is scanned over a region of brain tissue, either *in vivo* or *in vitro*, to stimulate cells. This stimulation can be achieved in a variety of ways, including photolysis of a caged compound or activation of transgenically expressed light-sensitive ion channels (Boyden, Zhang, Bamberg, Nagel, & Deisseroth, 2005; Petreanu et al., 2007; Zhang, Aravanis, Adamantidis, de Lecea, & Deisseroth, 2007; Anastasiades et al., 2017; Anastasiades & Butt, 2012; Marques-Smith et al., 2016; Anastasiades et al., 2016; Brill et al., 2016; Zemelman et al., 2003; Shepherd, 2012). Both of these approaches, as well as a combination of the two techniques (in the case of transgenically-expressed ATP-activated $P2X_2$) were used in this dissertation.

Our current knowledge regarding the role of spontaneous and sensory-evoked activity, suggests that patterned spontaneous activity is instructive for initial circuit

formation and, that sensory evoked activity is required for maintenance (in the case of ODC), remodelling and even presence (in the case of barrels) of cortical features (Morishita & Hensch, 2008; Van der Loos & Woolsey, 1973; Hubel & Wiesel, 1962; H. Li et al., 2013; Erzurumlu & Gaspar, 2012). At early stages of development, sensory-specific thalamic input is also able to re-assign cortical identity. Many studies have also shown sensory activity-dependent changes at the cellular level, in terms of cell maturation, synapse formation, cell morphology and pre-synaptic characteristics (Hofer et al., 2009; García et al., 2015; Chattopadhyaya et al., 2004; Tuncdemir et al., 2016; Frangeul et al., 2017). These data strongly suggest that patterned and stimulus-driven activity is a key component of early cortical development.

However, our knowledge of the middle ground, circuits, and the effect that sensory activity has on their development is currently more limited. More recently, advances in optical mapping techniques have made the interrogation of developing circuits in the brain more accessible (Anastasiades et al., 2018; Shepherd et al., 2003; Zhao et al., 2009; Viswanathan et al., 2012; Brill et al., 2016). This has lead to a handful of studies over the last few years which have begun to shed light on the dynamics and functions of neonatal cortical circuits. The reciprocal L5b-L4 circuit, identified in S1BF, is of particular interest for the question of how sensory activity interacts with developing circuits. This is because the connection appears to be both modulated by sensory activity perturbations and essential for timely innervation of thalamic afferents into L4 (Marques-Smith et al., 2016).

Marques-Smith et al. (2016) showed that ION sectioning caused a developmental delay in the remodelling of the L5b-L4 circuit and, consequently, delayed thalamic innervation of L4 SSNs (Marques-Smith et al., 2016). It is, however, important to note that ION sectioning may lead to thalamic re-wiring and, therefore, unexpected changes to thalamic input onto S1BF (Takeuchi et al., 2012, 2017). For this reason, a mouse devoid of all thalamocortical and corticothalamic connections was used

to map the L5b-L4 transient circuit. Importantly, although this mouse line lacked thalamic innervation of the cortex, the lamination and areal patterning, neurogenesis and interneuron migration were all unaffected (Zhou et al., 2010).

Using this 'Neocortex Isolé' mouse line (Celsr3|Dlx5/6) (Zhou et al., 2008) allowed the developing circuitry to be mapped in the absence of both thalamic-driven spontaneous and sensory-evoked activity. The development of any circuits observed was, therefore, expected to be intrinsically controlled. Conversely, the absence of any connections normally seen in the WT animal would determine that these required thalamic-driven activity to form.

In this chapter, GABAergic connections onto S1BF L4 SSNs were mapped in P5-P13 Celsr3|Dlx5/6 mice using LSPS. Alongside LSPS circuit mapping, the intrinsic electrophysiological properties, morphologies and spontaneous IPSCs onto SSNs cells were compared between Celsr3|Dlx5/6 mice and littermate controls to further explore activity and developmental differences.

3.1 Characterisation of Celsr3|Dlx5/6 mouse line

3.1.1 Whole Brain DiI tracing of reciprocal thalamocortical connectivity in Celsr3|Dlx5/6 mice

It was important to verify that the connections between thalamus and neocortex were disrupted in the mice maintained in our colony. This was done by replicating the whole brain carbocyanine dye tracing in fixed tissue done in the initial publication (Zhou et al., 2008). Three Celsr3|Dlx5/6 mice and two WT littermate controls were perfused with 4% paraformaldehyde at P5 and single carbocyanine (DiI) crystals were placed unilaterally with DiI into either the thalamus or cortex. Figure 3.1E shows a picture of a P5 mouse brain with DiI placement site in the

thalamus. DiI crystal placed into the left thalamus (Figure 3.1A) of a WT control reached S1BF in the neocortex. DiI crystal placed into the right S1BF reaches the thalamus. In contrast, cortical crystal placement of DiI in a Celsr3|Dlx5/6 mouse failed to label the thalamus (Figure 3.1B), while a thalamic crystal placement of DiI in a Celsr3|Dlx5/6 mouse did not label the neocortex (Figure 3.1B). A higher magnification confocal stack of the cortex of both the WT and Celsr3|Dlx5/6 mice after thalamic crystal placement of DiI shows thalamocortical afferents projecting across the depth of the neocortex in the WT control, but a complete absence of such fibres in the neocortex of the Celsr3|Dlx5/6 mouse (Figure 3.1C, D). These results confirm that the Celsr3|Dlx5/6 mice used for the following experiments had a fully defective internal capsule as previously described (Zhou et al., 2008).

Other hallmark characteristics of the Celsr3|Dlx5/6 mouse were observed, although not quantified, during experiments. These include a reduced thickness of the neocortex, lower weight compared to WT littermates and compete lack of barrels in L4 of S1BF. Zhou et al. (2010) reported a 15.7% reduction in cortical area. The Celsr3|Dlx5/6 mice also died at approximately P21, which was also reported in (Zhou et al., 2010).

3.1.2 Anatomy and cell morphologies of Celsr3|Dlx5/6 layer 4 spiny stellate cells

The morphology and electrophysiological properties of layer 5 pyramidal cells in Celsr3|Dlx5/6 mice have previously been described by (Zhou et al., 2010) who reported that L5 pyramidal cells in mutant mice show dendritic atrophy and reduced electrical excitability. However, these pyramidal cells are not involved in the layer 5b SST to layer 4 spiny stellate cortical circuit (Marques-Smith et al., 2016). Therefore, the morphology and electrophysiological properties of L4 SSN/excitatory cells

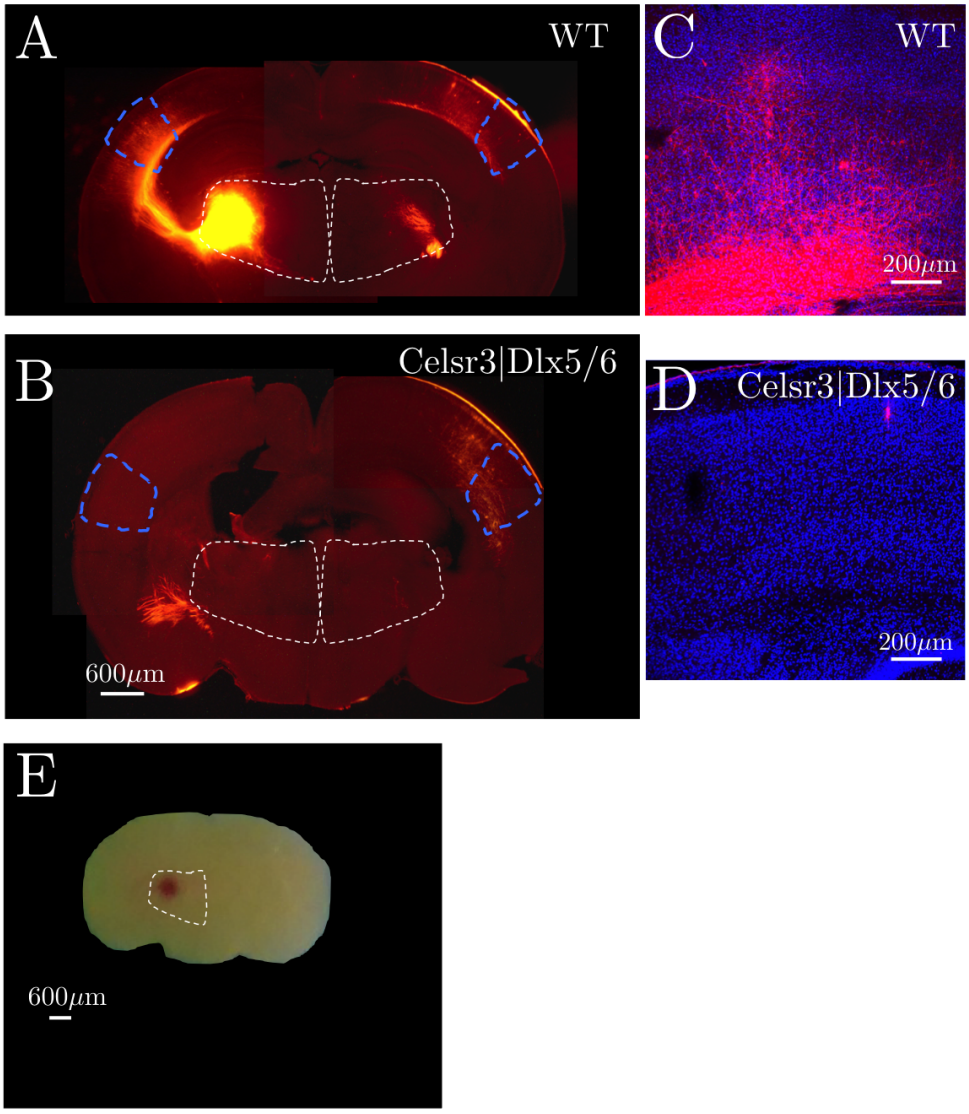


Figure 3.1: **Anatomical verification of a defective internal capsule in Celsr3|Dlx5/6 mice**. **A,B)** Sections from P5 WT and Celsr3|Dlx5/6 mice following DiI crystal placement in cortex and thalamus.**A)** In WT mice, DiI crystal placement in the cortex (right side, blue dotted line) reaches the thalamus (right side, white dotted line). DiI crystal placement in the thalamus (left side, white dotted line) reaches the cortex (left side, blue dotted line). **B)** In Celsr3|Dlx5/6 mice, DiI crystal placement in the cortex (right side, blue dotted line) fails to reach the thalamus (right side, white dotted line). DiI crystal placement in the thalamus (left side side, white dotted line) fails to reach the cortex (left side, blue dotted line). **C)** Confocal image of thalamic fibres (red) in the neocortex (S1BF) after thalamic DiI crystal placement in a P5 WT mouse. **D)** Higher magnification confocal image showing absence of thalamic fibres in the neocortex (S1BF) after thalamic DiI crystal placement in a P5 Celsr3|Dlx5/6 mouse. **E)** Picture of a P5 mouse brain after DiI crystal placement (red) in the thalamus (white dotted line). A total of 3 Celsr3|Dlx5/6 and 2 WT mice were used for these carbocyanine dye tracing experiments. All showed the same phenotype as shown in A and B.

was characterised during circuit mapping in the Celsr3|Dlx5/6 mouse. A total of five WT control and nine Celsr3|Dlx5/6 layer 4 spiny stellate/excitatory morphologies were recovered. An example of a WT and Celsr3|Dlx5/6 layer 4 spiny stellate morphology is shown in Figure 3.2A-D. In Figure 3.2A, three filled and stained WT L4 excitatory neurons are seen. One of these cells is reconstructed in Figure 3.2B. WT layer 4 spiny stellate cells lacked a prominent apical dendrite as previously described (Harris & Shepherd, 2015; Douglas & Martin, 2004). However, in Celsr3|Dlx5/6, layer 4 excitatory cells had prominent apical dendrites that extended to layer 1 (Figure 3.2C and D). A linear Scholl plot of reconstructed cell morphologies showed that the mean number of crossings for the apical dendrite remained higher for Celsr3|Dlx5/6 layer 4 cells than the WT control at distances of 100 μm or more away from the cell body (Figure 3.2E). The mean apical dendrite length is also statistically ($p<0.05$) longer in Celsr3|Dlx5/6 ($n = 9$) layer 4 excitatory neurons than their WT control ($n = 5$) (Figure 3.2F) .

3.1.3 Intrinsic firing properties of Celsr3|Dlx5/6 L4 spiny stellate cells

The intrinsic electrophysiological properties of Celsr3|Dlx5/6 L4 spiny stellate cells were recorded to assess whether the electrophysiological properties of these cells developed at the same rate as WT control cells. It was possible that absence of thalamocortical inputs might delay the maturation of cortical cells and confound any circuit mapping results. The following intrinsic properties were measured: resting membrane potential (RMP), spike threshold, absolute spike height, total spike height, firing frequency, input resistance, afterhyperpolarization (AHP) amplitude, afterhyperpolarization (AHP) delay, membrane time constant, spike half-width and, spike frequency adaption. The intrinsic electrophysiological properties of Celsr3|Dlx5/6

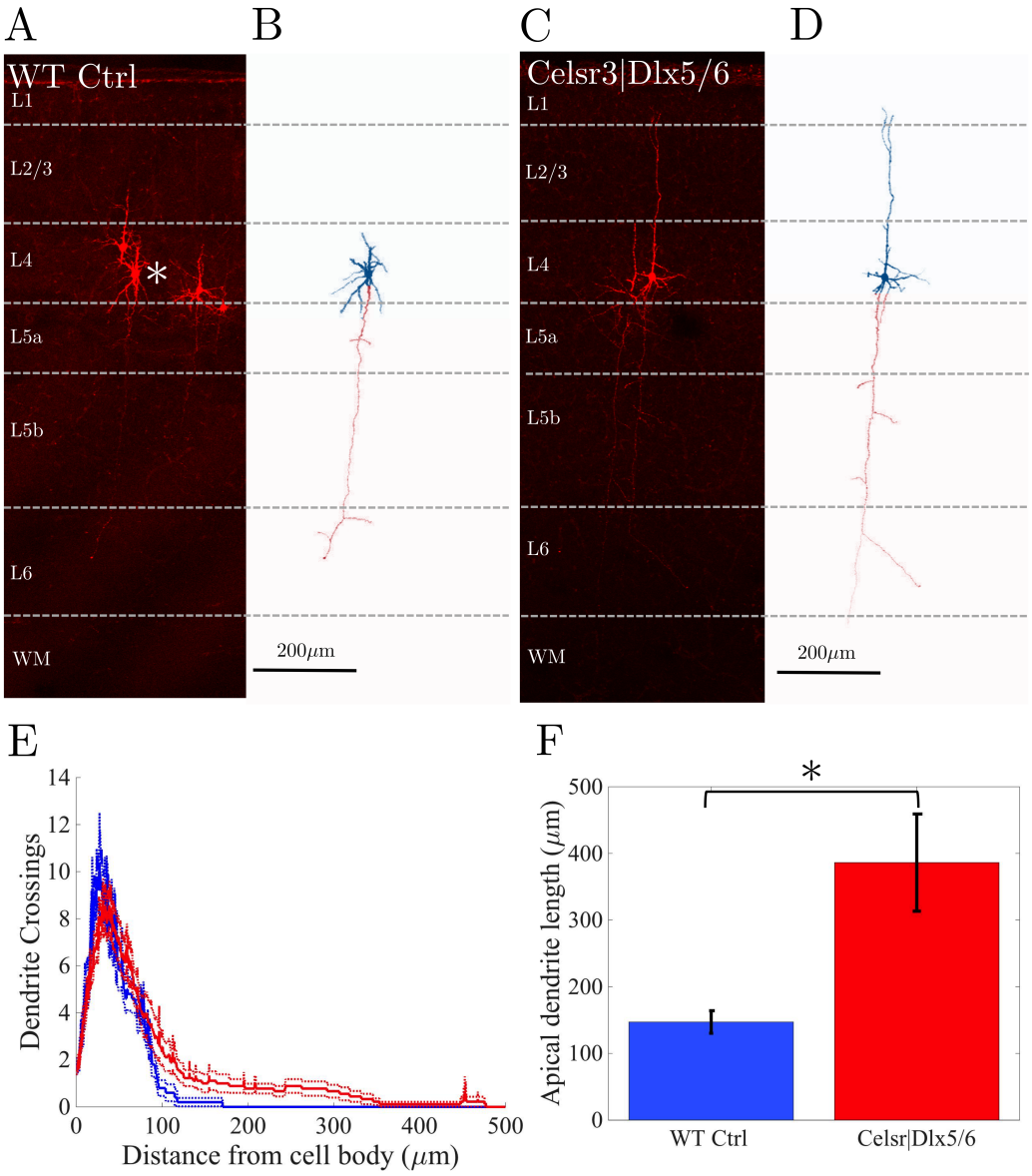


Figure 3.2: **Morphological analysis of apical dendrite length in WT and Celsr3|Dlx5/6 spiny stellate cells**. **A)** Layer 4 S1BF WT spiny stellate cells recorded, filled and then stained with streptavidin/RFP. **B)** Reconstruction of A) (white asterisk) with the dendrite shown in blue and the axon shown in red.**C)** Layer 4 S1BF Celsr3|Dlx5/6 spiny stellate cells stained with streptavidin/RFP. **D)** Reconstruction of C) with the dendrite shown in blue and the axon shown in red. **E)** Linear Scholl plot of WT spiny stellate cell dendrites (n = 5, blue) and Celsr3|Dlx5/6 spiny stellate cell cell dendrites (n = 9, red). The solid line is the mean number of crossings, while the dotted lines above and below are the standard error of the mean. **F)** Mean total dendrite length for WT spiny stellate cells (blue) and Celsr3|Dlx5/6 spiny stellate cells (red). Error bars are standard error of the mean. *=p<0.05 Statistical analysis used the two-sided Wilcoxon rank sum test for independent samples. WT control n = 5 cells (n = 4 P8 and n = 1 P11), Celsr3|Dlx5/6 n = 9 cells (n = 4 P8, n = 2 P9, n = 2 P10, n = 1 P13).

Intrinsic Property	WT Mean±SEM	Celsr3|Dlx5/6 Mean±SEM
RMP (mV)	-59.2±2.2	-54.8±3.4
Spike Threshold (mV)	-37.61±1.2	-36.2±0.9
Absolute Spike Height (mV)	40.1±2.8	33.5±3.2
Total Spike Height (mV)	77.7±3.3	69.7±3.8
Firing Frequency (Hz)	21.7±2.4	24.8±1.1
Input Resistance (MΩ)	994.7±51.3	1094.1±107.1
AHP Amp (mV)	13.2±1.8	11.2±1.8
AHP delay (ms)	90.7±12.4	45.4±9.4 **
Membrane Time Constant (ms)	59.1±2.1	63.7±6.6
Spike Half-width (ms)	2.7±0.1	2.7±0.1
Spike Frequency Adaption (%)	48.2±4.9	36.8±2.4

Table 3.1: Intrinsic electrophysiological properties of WT and Celsr3|Dlx5/6 L4 Excitatory Neurons (P7-P10). n=8 cells (5 animals) for Celsr3|Dlx5/6 and n=7 cells (4 animals) for WT. **=p<0.01, statistical analysis used the two-sided Wilcoxon rank sum test for independent samples. RMP is resting membrane potential, AHP is afterhyperpolarization.

L4 spiny stellate cells between ages P7 and P10 were not found to be significantly different to WT littermate control cells, with the exception of afterhyperpolarization delay (p<0.01) (Table 3.1).

3.2 *In vitro* electrophysiology

3.2.1 GABAergic input onto L4 excitatory cells in S1

GABAergic input onto layer 4 excitatory neurons was mapped in young Celsr3|Dlx5/6 mice from P5 through to P11 and compared to WT littermates in order to investigate if thalamic input was required for the L5b-L4 connection.

Figure3.3A, B and C show an example of an LSPS recording as well as two examples of how the evoked IPSCs inform the heat maps for WT P5-8 and WT P9+. The GABAergic input maps for individual cells for WT P5-8 and P9+ are shown in Figure 3.3, illustrating the variability between cells, information which is

lost in the average heat map data.

The early transient layer 5b GABAergic input onto layer 4 excitatory cells was observed in young WT littermates (Figure 3.4A), similar to previous reports in Marques-Smith et al. (2016). This connection disappears in animals aged P9 or older (Figure 3.4C). Again, this is in line with the dynamic of the L5b-L4 cortical circuit published in (Marques-Smith et al., 2016).

When GABAergic input onto L4 excitatory cells was mapped in young Celsr3|Dlx5/6 mice, a similar layer distribution of input was observed. Layer 5b GABAergic input was present in young animals (P5-P8) (Figure 3.4B), but this infragranular layer input was absent in older mice (P9+) (Figure 3.4D).

In order to obtain a clear picture of the distribution of input across the layers, each cell was normalised and the percentage of total GABAergic input onto L4 cells that originated from each cortical layer was quantified. When the younger (P5-P8) WT recordings (n = 7) were compared to the older (P9+) WT recordings (n = 4), significantly more GABAergic input came from layer 5b in the younger animals ($p<0.05$), while the older animals had significantly more of the GABAergic input from layer 4 ($p<0.05$) (Figure 3.5A). Although the GABAergic heat maps for Celsr3|Dlx5/6 mice appear to show the same cortical circuit dynamics as WT littermates, when the distribution was quantified, it could be seen that none of the layers had significantly different percentages of total input between young and older pups (Figure 3.5B). The percentage of total input for layer 5b is higher in younger animals than older animals, but the difference is not significant (Figure 3.5B).

The layer contributions of GABAergic input in younger mice are not significantly different between WT and Celsr3|Dlx5/6 recordings (Figure 3.5C). When comparing the distribution of GABAergic input onto layer 4 in older animals (P9+), WT recordings show significantly more input from layer 4 than Celsr3|Dlx5/6 cells (Figure 3.5D).

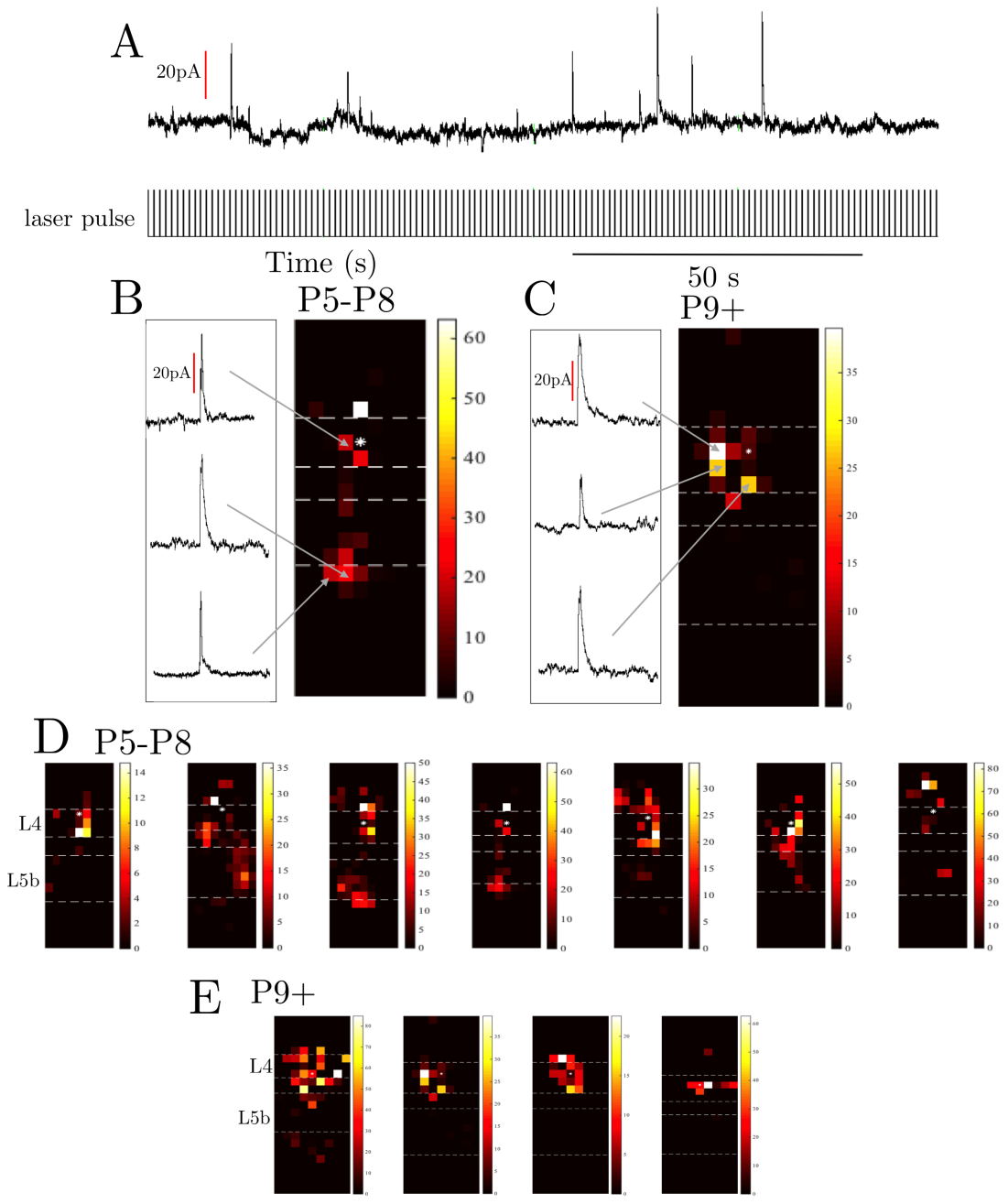


Figure 3.3: **Raw IPSC data and connectivity mapping variability for the L5b-L4 circuit**. **A)** Representative recording trace showing evoked IPSCs (upper trace) and laser stimulation (lower trace). **B)** Evoked IPSCs from a single upper-layer sweep aligned to the grid points of the heat map which they contribute to. Animal is P5-8. **C)** Evoked IPSCs from a single upper-layer sweep aligned to the grid points of the heat map which they contribute to. Animal is P9+. **D)** Individual heat maps of connectivity for P5-8 WT mice. **E)** Individual heat maps of connectivity for P9+ WT mice. White asterisks show recorded cell position and dotted white lines delineate layer boundaries.

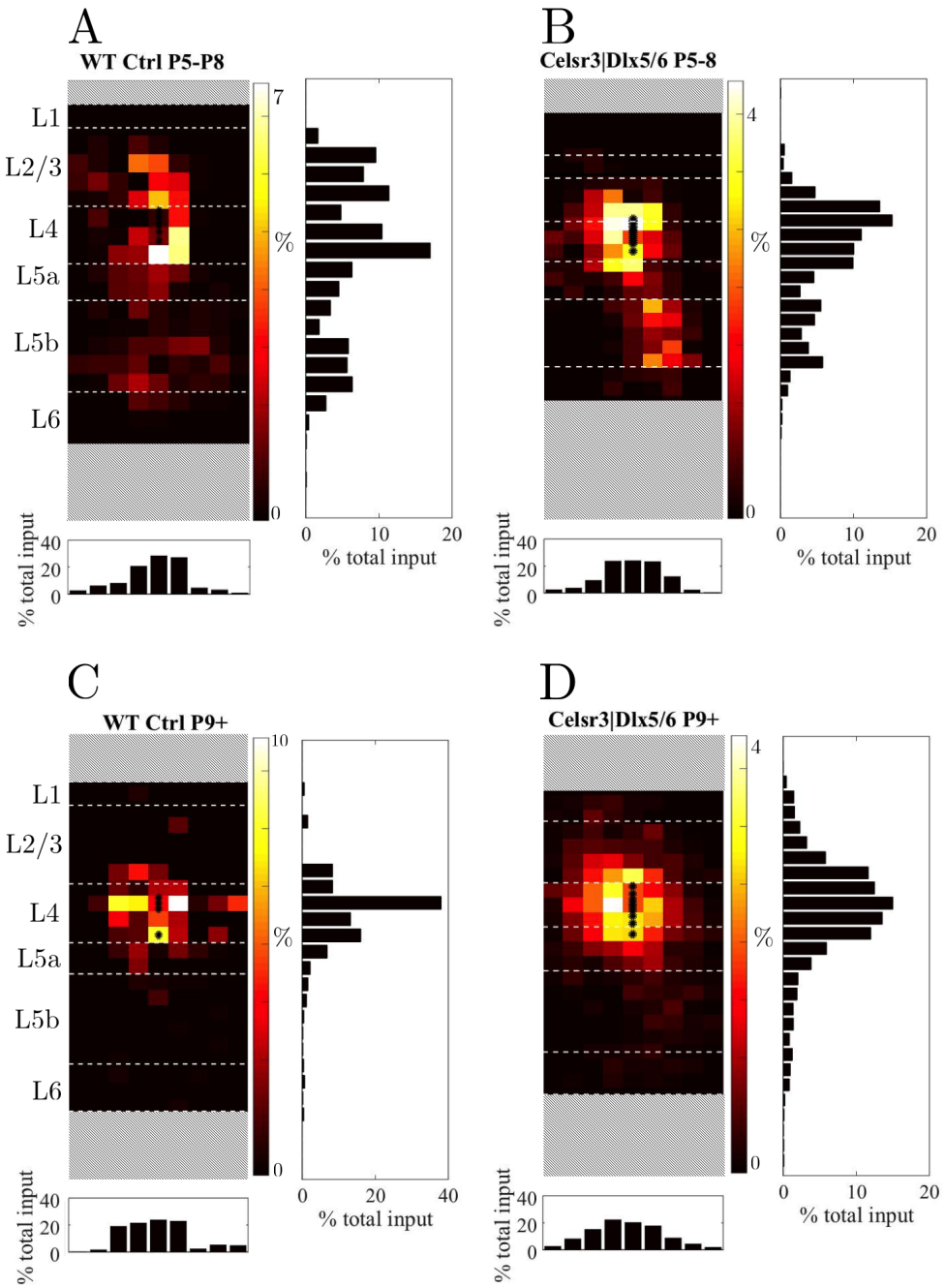


Figure 3.4: **Heat maps of GABAergic input onto WT and Celsr3|Dlx5/6 layer 4 S1BF excitatory cells**. **A)** Average heat map showing the distribution of GABAergic input onto WT P5-P8 layer 4 S1BF excitatory cells. **B)** Average heat map showing the distribution of GABAergic input onto Celsr3|Dlx5/6 P5-P8 layer 4 S1BF excitatory cells. **C)** Average heat map showing the distribution of GABAergic input onto WT P9+ layer 4 S1BF excitatory cells. **D)** Average heat map showing the distribution of GABAergic input onto Celsr3|Dlx5/6 P9+ layer 4 S1BF excitatory cells. All bar graphs show the percentage of the total input for each column and row of the averaged heat map. n = 7 cells (4 animals) WT P5-P8, n = 4 cells (3 animals) WT P9+, n = 12 cells (7 animals) mutant P5-P8, n = 9 cells (5 animals) mutant P9+.

Data from the heat-maps, combined with the quantification of input distribution, would indicate that while Celsr3|Dlx5/6 cells show reduced L5b-L4 connectivity from postnatal day 9+, they do not develop the same precision of layer 4 GABAergic input onto layer 4 excitatory cells as that seen in controls.

In addition to quantifying the distribution of input, the total (pA) GABAergic input from each layer onto layer 4 was also quantified. The total GABAergic input originating from layer 4 was significantly ($p<0.05$) higher in older WT animals as compared to younger WT recordings (Figure 3.6A). The total pA input originating from layer 5b was slightly higher in younger WT recordings as compared to older, but this was not a significant difference. When the total pA GABAergic input was compared between P5-8 and P9+ Celsr3|Dlx5/6 cells, the P9+ recordings showed significantly more GABAergic input originating from layer 2/3 ($p<0.05$), layer 4 ($p<0.01$) and layer 5a ($p<0.01$) (Figure 3.6B). Total GABAergic input was not significantly different between P5-8 WT and Celsr3|Dlx5/6 recordings (Figure 3.6C). Total GABAergic input originating from layer 2/3 was significantly ($p<0.05$) different between P9+ WT and P9+ Celsr3|Dlx5/6 recordings, suggesting that the post critical period Celsr3|Dlx5/6 GABAergic input is not specific to layer 4, as it is in WT animals (Figure 3.6D).

The differences between P5-8 and P9+ Celsr3|Dlx5/6 recordings indicate an increase in total GABAergic input across all layers. This increase in total pA input in older Celsr3|Dlx5/6 can be clearly seen in Figure 3.6E. Total pA input across all layers for P9+ Celsr3|Dlx5/6 is significantly higher, not only compared to the younger P5-P8 Celsr3|Dlx5/6, but also compared to the WT control of the same age group, indicating that while the distribution of input might roughly follow the WT pattern, the level of total input within the cortex is significantly higher in Celsr3|Dlx5/6 mice after the S1BF critical period. Given that there were four recordings for WT P9+, it is possible that this difference between WT and Celsr3|Dlx5/6 P9+ recordings

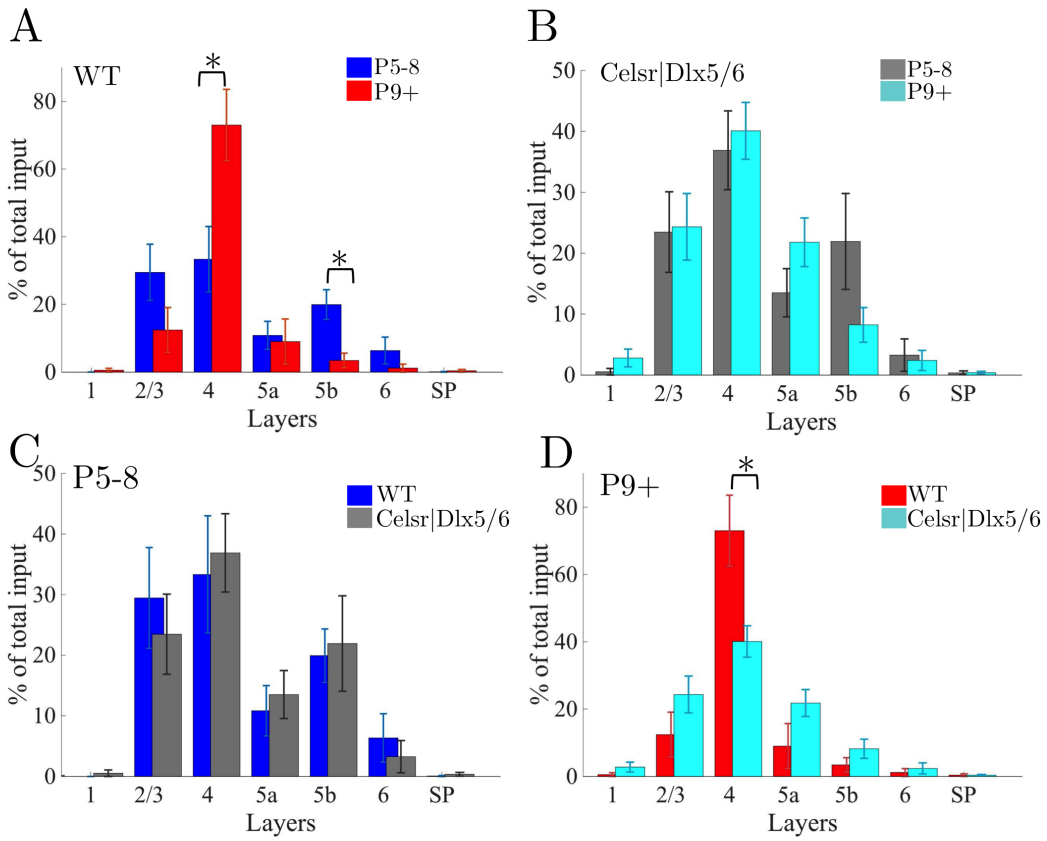


Figure 3.5: **Percentage of total GABAergic input that originates from each cortical layer for WT and Celsr3|Dlx5/6 layer 4 spiny stellate cells A)** Comparison of GABAergic input distribution between WT P5-8 and WT P9+ recorded cells. **B)** Comparison of GABAergic input distribution between Celsr3|Dlx5/6 P5-8 and Celsr3|Dlx5/6 P9+ recorded cells. **C)** Comparison of GABAergic input distribution between WT P5-8 and Celsr3|Dlx5/6 P5-8 recorded cells. **D)** Comparison of GABAergic input distribution between WT P9+ and Celsr3|Dlx5/6 P9+ recorded cells. *=$p<0.05$ Statistical analysis used the two-sided Wilcoxon rank sum test for independent samples. n = 7 cells (4 animals) WT P5-P8, n = 4 cells (3 animals) WT P9+, n = 12 cells (7 animals) mutant P5-P8, n = 9 cells (5 animals) mutant P9+.

arises from underpowered data.

3.2.2 Spontaneous GABAergic activity in layer 4

The total GABAergic input onto layer 4 from within the cortex is significantly higher in Celsr3|Dlx5/6 mice compared to WT control. It was, therefore, of interest to investigate the baseline level of excitability and activity within the cortices of Celsr3|Dlx5/6 and WT mice. To do this, spontaneous IPSCs outside the temporal monosynaptic laser-evoked response window were quantified, based on their frequency and amplitude. Although total evoked pA GABAergic input onto layer 4 excitatory neurons is higher in P9+ Celsr3|Dlx5/6 mice, no such corresponding difference was seen in the level of spontaneous activity. No significant difference in the frequency or amplitude of spontaneous GABAergic events was seen for P5-8 and P9+, WT and Celsr3|Dlx5/6 mice.

3.3 Discussion

In this chapter, the Celsr3|Dlx5/6 mouse line was used to dissect the role of thalamic connectivity in circuit remodelling of the previously published L5b-L4 GABAergic connection. From the findings of Marques-smith et al. (2016), that showed a delay in L5b-L4 loop remodelling when the ION nerve was sectioned, it was expected that a similar developmental delay would be observed in L5b GABAergic input of the Celsr3|Dlx5/6 mice. Surprisingly, it was clear from these results, that the L5b to L4 GABAergic connection was present in Celsr3|Dlx5/6 mice and its remodelling followed the same time course as WT littermate controls. When the results were normalised and the input from each layer measured as a percentage of the total input, GABAergic input originating from L5b was greater in young animals for both WT and Celsr3|Dlx5/6, but only significantly different for WT animals. The lack of

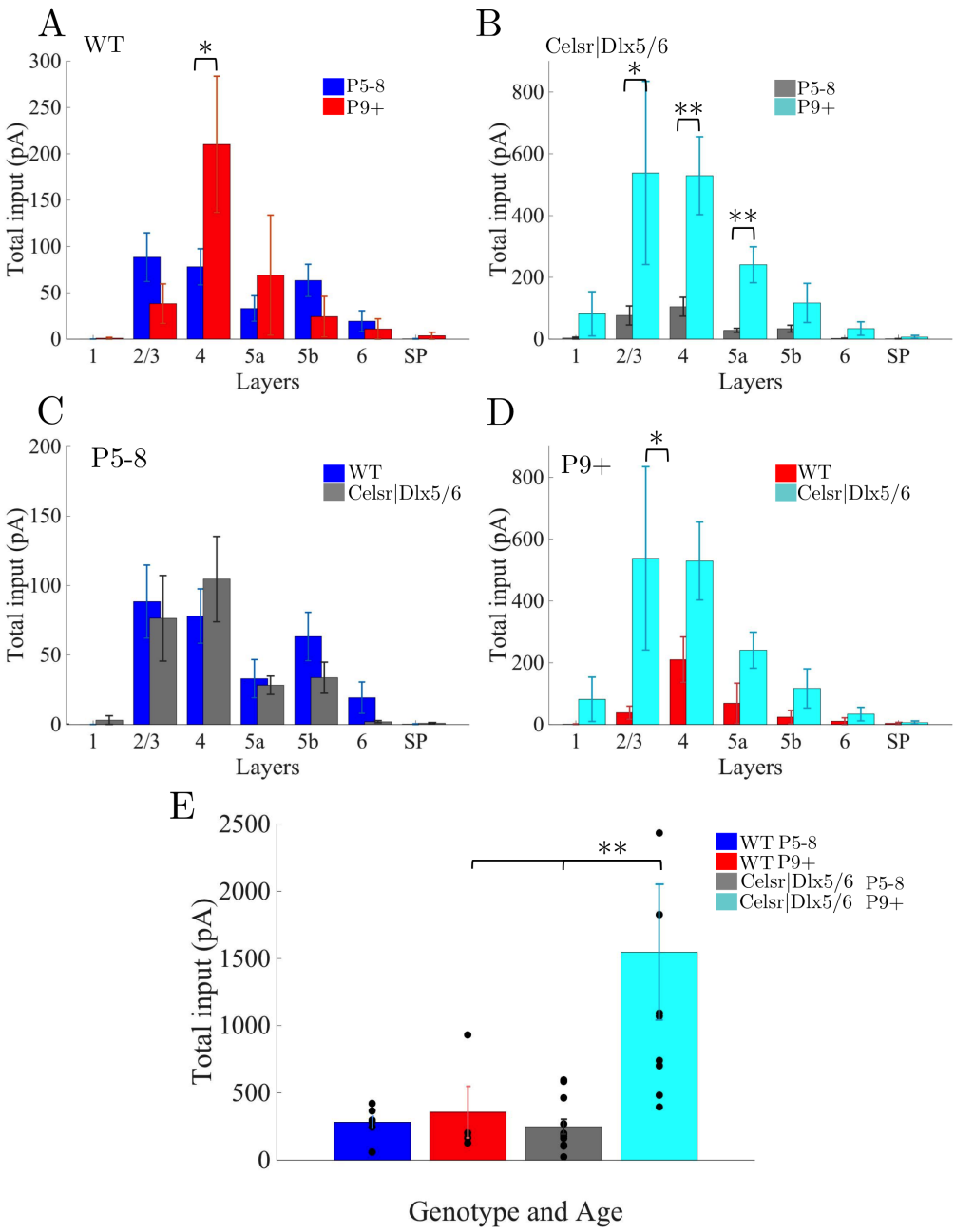


Figure 3.6: **Total GABAergic input that originates from each cortical layer for WT and Celsr3|Dlx5/6 layer 4 spiny stellate cells. A)** Comparison of total GABAergic input between WT P5-8 and WT P9+ cells. **B)** Comparison of total GABAergic input between Celsr3|Dlx5/6 P5-8 and Celsr3|Dlx5/6 P9+ cells. **C)** Comparison of total GABAergic input between WT P5-8 and Celsr3|Dlx5/6 P5-8 recorded cells. **D)** Comparison of total GABAergic input between WT P9+ and Celsr3|Dlx5/6 P9+ cells. **E)** Comparison of total GABAergic input summed across all layer for Celsr3|Dlx5/6 P5-8 and P9+ and WT P5-8 and P9+ cells. *=$p<0.05$ and **=$p<0.01$ Statistical analysis used the two-sided Wilcoxon rank sum test for independent samples. n = 7 cells (4 animals) WT P5-P8, n = 4 cells (3 animals) WT P9+, n = 12 cells (7 animals) mut P5-P8, n = 9 cells (5 animals) mut P9+.

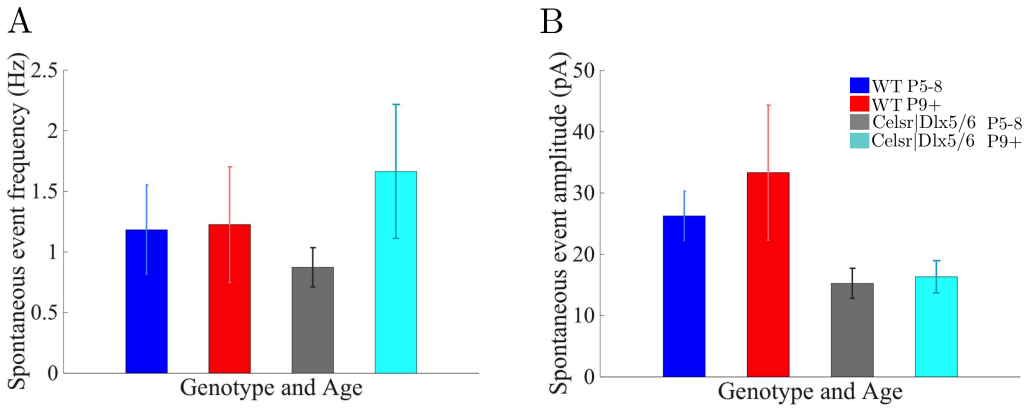


Figure 3.7: **Frequency and amplitude of spontaneous GABAergic events (sIPSCs) in WT and Celsr3|Dlx5/6 mice. A)** Average frequency of spontaneous GABAergic events in WT and Celsr3|Dlx5/6 mice. **B)** Average amplitude of spontaneous GABAergic events in WT and Celsr3|Dlx5/6 mice. Cell numbers: n = 7 cells (4 animals) WT P5-P8, n = 4 cells (3 animals) WT P9+, n = 12 cells (7 animals) mutant P5-P8, n = 9 cells (5 animals) mutant P9+.

statistical difference between L5b input in young and old Celsr3|Dlx5/6 is likely due to the larger variability in the young Celsr3|Dlx5/6 and the broader GABAergic input observed in older Celsr3|Dlx5/6 mice, with small residual L5b input.

These results show that the L5b-L4 transient loop is present in a mouse which lacks any input, either spontaneous or stimulus evoked, from the thalamus. The presence of this transient connection shows that thalamic input is not required for the dynamic development of certain cortical circuits. Instead, these results point to intrinsic cortical factors as the instructive cue for early circuit remodelling. This contradicts the central role thalamic input was hypothesised to play, given the wealth of information on the role of activity in cortical development and the previous observation that ION sectioning altered the time course of the L5b-L4 loop.

Marques-Smith et al. (2016) suggest that in the absence of sensory input, L5b SST IN input onto L4 SSN can compensate for the delayed maturation of local PV+ FS IN driven inhibition, causing the prolonged L5b-L4 connection in ION animals (Marques-Smith et al., 2016). As the L5b-L4 loop in Celsr3|Dlx5/6 remodels at a

similar time point to that in WT controls, it would be of interest to characterise the maturation of PV+ FS INs in Celsr3|Dlx5/6 mice to assess if this SST/PV see-saw relationship appears present, and if Celsr3|Dlx5/6 PV INs are able to mature in the absence of thalamocortical input.

When the total pA input for both age groups and genotypes was compared, it was clear that older Celsr3|Dlx5/6 mice had significantly more total GABAergic input for all layers as compared to young mice, and also significantly more total GABAergic input when all layers are combined than any other age or genotype. When viewing this data, it is important to consider the nature of mapping GABAergic input using LSPS. A concern in interpreting raw amplitude data in LSPS in that small adjustments in laser power can result in large differences in the amplitude of the response. In order to verify that the large differences in total pA input are not an artefact of methodology, it would be important to ensure stimulation parameters were identical for all cells and between genotypes. Additionally, total GABAergic input median values for P9+ WT mice have been reported to be higher in Marques-Smith et al. (2016) and closer in value to the Celsr3|Dlx5/6 mice, suggesting that more data is needed to verify any difference between WT and Celsr3|Dlx5/6 mice. If the significant increase in GABAergic input in Celsr3|Dlx5/6 mice post P8 is a genuine activity change in the cortices of these animals, it may be as a result of increased input into P9+ SSN cells in Celsr3|Dlx5/6 mice which have not remodelled the apical dendrite. The increase in evoked GABAergic activity is not reflected in spontaneous events.

No significant difference in the number or amplitude of spontaneous IPSCs was seen for any age group or genotype. This observation indicates that spontaneous GABAergic cortical activity in unaffected by the loss of a thalamic connection. Given that thalamic afferents provide strong input onto FS PV+ INs from P6-7 (Daw et al., 2007) and that thalamic activity drives spontaneous events such as

spindle bursts and EGOs, the lack of difference in spontaneous activity in the cortex of Celsr3|Dlx5/6 mice appears surprising. It further suggests that there are intrinsic factors which are able to guide early circuit development, independent of subcortical or peripheral input, and balance GABAergic activity in a homoeostatic manner.

The Celsr3|Dlx5/6 mouse line appeared, as previously described by Zhou et al. (2010) (Zhou et al., 2010), with absence of barrels in S1BF, reduced animal weight and reduced cortical depth. DiI crystal placement in fixed tissue into both the thalamus and cortex of P5 Celsr3|Dlx5/6 pups confirmed the lack of connection between the thalamus and cortex.

The electrophysiological maturation of L4 excitatory cells was unaffected by the absence of thalamocortical input. Previously, characterisation of the electrophysiological properties of large pyramidal cells *in vitro* reported that Celsr3|Dlx5/6 Pyramidal cells show a decreased electrical excitability (Zhou et al., 2010). The discrepancy between these two results may be due to the difference in cell types (SSNs in L4 and large pyramidal cells). It is possible that different cell types might require different levels of thalamocortical input in order to mature. In particular, the large pyramidal projection neurons which make up the Zhou et al. (2010) intrinsic properties data set are more adversely affected than any other cell type by the lack of thalamocortical and corticothalamic connections. Indeed, most layer 5 projection interneurons in the Celsr3|Dlx5/6 mouse died in the absence of subcortical projections (Zhou et al., 2010).

While electrophysiological properties of SSN appeared unaffected, the remodelling of the apical dendrite in L4 SSNs was not observed in the Celsr3|Dlx5/6 cortex. This suggests that the remodelling of dendrites into the final mature SSN requires thalamocortical input. Although SSNs are not found in mouse V1, ferrets have SSNs in V1 L4 (Harris & Shepherd, 2015; Douglas & Martin, 2004; Peters & Kara, 1985; Nassi & Callaway, 2009). In ferrets deprived of retinal input, a signif-

icant fraction of layer 4 excitatory neurons failed to remodel their apical dendrites into SSN morphology, further supporting the finding that sensory input plays a fundamental role in SSN morphology (Callaway & Borrell, 2011). Together, these results strongly suggest that sensory activity plays a key role in remodelling early neurites, in particular SSN morphology. It is, therefore, likely that mature S1BF SSN morphology requires thalamic input.

Together, somewhat surprisingly, these results suggest that the only major cortical changes observed between WT littermate controls and Celsr3|Dlx5/6 mice are the absence of barrels and the lack of apical dendrite remodelling in L4 SSNs.

Chapter 4

The L5b-L4 transient circuit is not observed in the primary visual cortex

Chapter 3 presented evidence that the L5b-L4 transient connection forms and disappears in the absence of thalamic input in S1BF on a similar time frame as normal thalamocortical connectivity. Therefore, the instructions which drive its development are intrinsically generated. As was previously published, this transient connection is involved in timely acquisition of thalamic input onto L4 in S1BF (Marques-Smith et al., 2016; Tuncdemir et al., 2016). Given that the L5b-L4 connection observed in S1BF is formed and dismantled independently of thalamic input and previous results show it is involved in establishing thalamic input onto L4, it was hypothesised that the same transient reciprocal connection might exist and fulfil the same role in other primary cortical areas.

Although S1BF provides an excellent model system for studying cortical development in the rodent brain, it is important to remember that it is a highly specialised sensory processing centre and S1BF developmental principles might not generalise

to other regions of the brain or to other mammals (Catania & Henry, 2006; Meng, Kao, & Kanold, 2014). Therefore, cortical circuit development in the visual cortex was mapped, with particular focus on GABAergic connections onto L4 in the mouse primary visual cortex (V1) in both the WT and Celsr3|Dlx5/6 mice.

In this chapter, LSPS was used to map both GABAergic input onto L4 excitatory cells and glutamatergic input onto SST+ L5b INs in V1 of the mouse neocortex through early postnatal life (P5 to P24) taking into account the later critical period plasticity in V1 (Gordon & Stryker, 1996). GABAergic input onto L2/3, L5a and L5b was also mapped, to rule out any additional GABAergic input onto excitatory cell transient translaminar connections between layers, other than L5b and L4. GABAergic input onto L4 in V1 was also mapped in Celsr3|Dlx5/6 mice to further explore the default GABAergic circuitry present in the absence of sensory input.

4.1 Characterisation of V1

While layer 4 in S1BF can be clearly identified due to the presence of barrels, layer boundaries are harder to delineate in visual cortex due to the lack of distinctive cytoarchitecture (Cajal, 1911; Van der Loos & Woolsey, 1973; W. Ji et al., 2015). While cortical layers can still be seen using DAPI staining (Figure 4.1A and B), additional layer makers were used to further confirm the position of a selected population of layer 5 and layer 4-2 cells. To define the relative depth of layers within the visual cortex and to examine any deviations from the layers within S1BF, immunohistochemistry was performed on sagittal sections of a P8 brain, with antibodies against the transcription factors Ctip2, a lower layer marker, and Brn2, an upper layer marker (Molyneaux, Arlotta, Menezes, & Macklis, 2007). Staining for the L2/3 marker, Brn2, appeared weaker and more diffuse in V1 (Figure 4.1C), compared to S1BF. Ctip2 did not show much difference between V1 and S1BF (Figure 4.1D).

The band of cells which stained for Ctip2 in V1 was, however, narrower (93 μm) than the band in S1BF (266 μm). This could be partially attributed to the differing thickness of the two cortical areas with S1BF (1225 μm) twice the depth of V1 (613 μm).

4.1.1 Targeting layer 4 in V1

Layer 4 of S1BF in a wildtype mouse is easily identifiable from P5 onwards by the presence of barrels. The location and boundaries of layer 4 in V1 under DIC are less clear. In order to correctly identify layer 4 in acute *in vitro* slices, the *Rpb4*$^{\text{cre/+}}$ mouse line was used. When crossed with Ai14 reporter line, Rpb4|Ai14 mice express red fluorescent protein (RFP; tdTomato) in layer 5a (Figure 4.2A) (Hoerder-Suabedissen, Korrell, et al., 2018; Grant et al., 2016). This allowed confirmation of layer 5a cells and targeting of layer 4 by recording cells directly above layer 5a. Figure 4.2B shows a DIC image during recording of a filled cell from Figure 4.2A. In Figure 4.2B, the DIC image with stimulation grid overlay and recording electrode is aligned with the cortical boundaries and filled cell shown in Figure 4.2A. By aligning the fluorescence and DIC image from a recording, it is possible to accurately assign layer boundaries in V1. Figure 4.2C shows this layer identification in an alternate mouse V1 section.

4.2 *In vitro* electrophysiology in V1

4.2.1 GABAergic input onto L4 excitatory cells.

The total GABAergic input onto layer 4 excitatory cells was mapped in wildtype mice from P5 to P24. These recordings were split into three age groups, P5-P8, P9-P12, and P13-P24. The two earlier age groups allowed direct comparison with

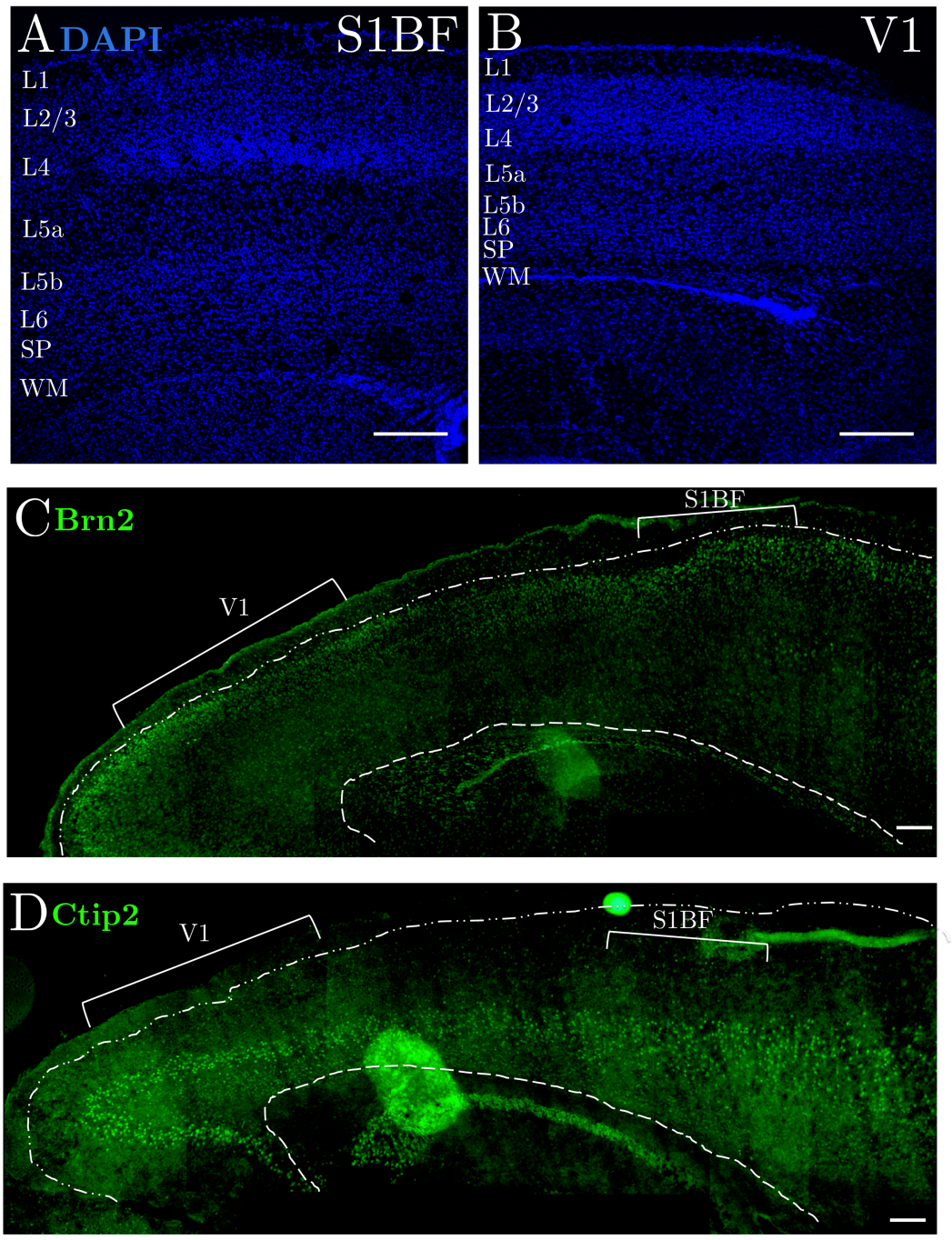


Figure 4.1: **V1 and S1BF DAPI staining on P10 coronal sections and Brn2 and Ctip2 staining on P8 sagittal sections**. **A and B)** DAPI staining on P10 coronal sections for S1BF (A) and V1 (B) **C)** Brn2 immunohistochemistry staining on a P8 sagittal section. Brackets show V1 and S1BF position. Dotted lines delineate both the boundary between L1 and L2 and the white matter. **D)** Ctip2 immunohistochemistry staining on a P8 sagittal section. Brackets show V1 and S1BF position. Dotted lines delineate both the boundary between L1 and L2 and the white matter. Scale bar = 200 μm. Area boundaries were defined using the Allen Brain Atlas.

Figure 4.2: **Layer identification in V1 using the Rpb4 Cre; Ai14 mice. A)** P8 Rpb4 Cre; Ai14 V1 section showing the expression of RFP in layer 5a (red) and three Streptavadin-488 labelled recorded neurons (green). **B)** A DIC image with stimulation grid overlay and recording electrode during the recording of the cell marked with a white arrow in (A). The DIC image is aligned with (A) to allow layer 5a identification. **C)** A DIC image of a V1 slice with layer boundaries marked. Scale bars are 200μm. SP is subplate and WM is white matter

S1BF GABAergic input maps, while the third, P13-P24, was recorded to include the later time points for a later V1 critical period and the period after which eye opening occurred (P12).

In V1, no age group showed GABAergic input from L5b onto excitatory cells in layer 4 (Figure 4.3, Figure 4.4A). GABAergic input in all ages originated mainly from layer 4 (43.82±3.3%, P5-P24, n=28), with a smaller amount from neighbouring layer 3 (20.5±4%) and 5a (31.5±4%) (Figure 4.3A). The progression of the L4 GABAergic input profile in V1 from P5 to P24 can be seen clearly in Figure 4.4A. While GABAergic afferent input extended into layers immediately adjacent to L4, very little was evident from L5b (2.7±0.7%) or L6 (0.1±0.07%).

GABAergic input onto L4 in V1 and S1BF for P5-P8 animals was quantified, both in terms of total pA input and percentage of total input. For L4 cells in S1BF (n=7), a significantly larger percentage of total GABAergic input originated in layers 5b ($p < 0.01$) and 6 ($p < 0.05$) when compared to V1 (n=9) (Figure 4.4B). This difference was also reflected in the total GABAergic input, with significantly ($p < 0.01$) more GABAergic input originating from layer 5b in S1BF compared to V1 (Figure 4.4C).

4.2.2 SST-specific GABAergic input onto excitatory cells in V1.

The L5b to L4 GABAergic input in S1BF is mediated by SST-positive L5b interneurons in S1BF (Marques-Smith et al., 2016). As glutamate uncaging includes GABAergic input from all interneuron types, it was unknown whether SST INs specifically provided any input onto L4 in V1 or whether the local GABAergic input observed originated from other IN populations, such as PV. Given the reported late emergence of PV interneuron inputs in V1 and their central role in determin-

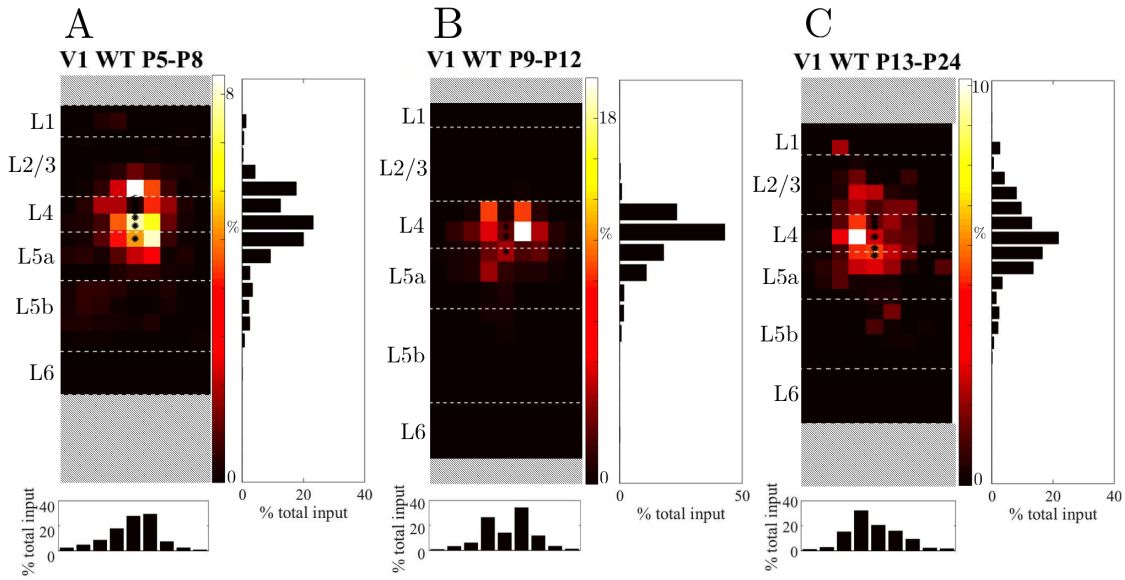


Figure 4.3: **Averaged heat maps of global GABAergic input onto layer 4 excitatory neurons in V1. A)** Averaged heat maps (normalised) of global GABAergic input onto layer 4 excitatory neurons in P5-P8 coronal sections (n=9 cells from 7 animals). **B)** Averaged heat maps (normalised) of global GABAergic input onto layer 4 excitatory neurons in P9-P12 coronal sections (n=4 cells from 2 animals). **C)** Averaged heat maps (normalised) of global GABAergic input onto layer 4 excitatory neurons in P13-P24 coronal sections (n=6 cells from 6 animals).

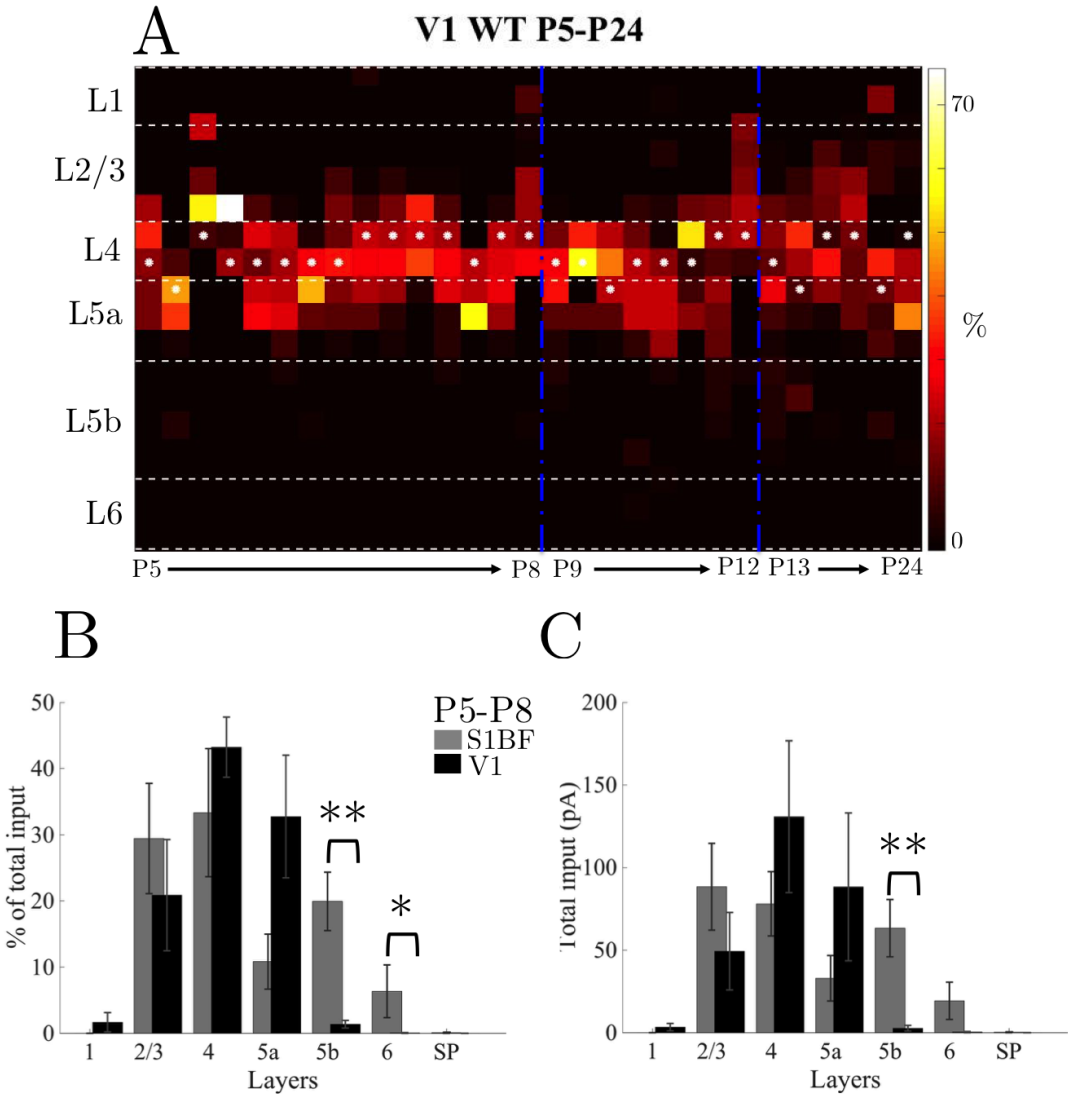


Figure 4.4: **V1 and S1BF have significantly different early GABAergic input profiles onto L4**. **A)** Temporal progression of the L4 GABAergic input profile in V1 from P5 to P24. Each column represents normalised GABAergic input onto a single layer 4 excitatory cell. The recorded cell's position is marked with a white asterisk. Data points are from coronal, sagittal, and thalamocortical slice angles. **B)** Percentage of GABAergic input onto L4 excitatory cells, originating from each cortical layer for S1BF and V1. **C)** Total GABAergic input (pA) onto L4 excitatory cells, originating from each layer for S1BF and V1. For B) and C) n=7 for S1BF and n=9 for V1. Dotted lines represent the average layer boundaries for A. *=$p<0.05$ **=$p<0.01$ Statistical analysis used the two-sided Wilcoxon rank sum test for independent samples. Errorbars are SEM.

ing the time frame of the critical period of plasticity (Pangratz-Fuehrer & Hestrin, 2011; Hensch, 2005), it was hypothesised that SST interneurons would contribute to the local GABAergic input onto L4 in V1, particularity at time points pre-critical period. For SST-specific input, an optogenetic activator (P2X2 receptor) was conditionally expressed under the control of SST Cre. This enabled selective activation of SST interneurons in response to focal ATP uncaging (Zemelman et al., 2003; Miesenböck, 2011; Anastasiades et al., 2016).

Figure 4.5 shows SST-specific input onto cells in layer 4 (n=3 cells from 3 animals). No translaminar SST-specific input can be seen from any cortical layer onto layer 4 (Figure 4.5A). Additionally, the distributions of input from SST-only cells and global GABAergic input (with caged-glutamate) were not significantly different for any layer (Figure 4.5B).

4.2.3 Alternative slice angles

Given the curvature of the visual area at the caudal aspect of the neocortex, the orientation of pyramidal cells might not always be perpendicular to the cutting angle in coronal sections, causing translaminar connections to be severed. To ensure that the L5b-L4 connection was indeed absent and not a product of severed connections, GABAergic input onto layer 4 of V1 was tested in sagittal and visual thalamocortical slice preparations (MacLean et al., 2006).

Figure 4.6 shows connectivity maps normalised and averaged for multiple cells for both sagittal and visual thalamocortical slice preparations. No translaminar GABAergic input onto layer 4 was seen in either preparation for P5-P8 mice (Figure 4.6B,E) (n=2, n=4) or P10-P12 mice (Figure 4.6C,F) (n=3, n=2), indicating that the absence of the L5b GABAergic connection in V1 is unlikely to be due to slice orientation.

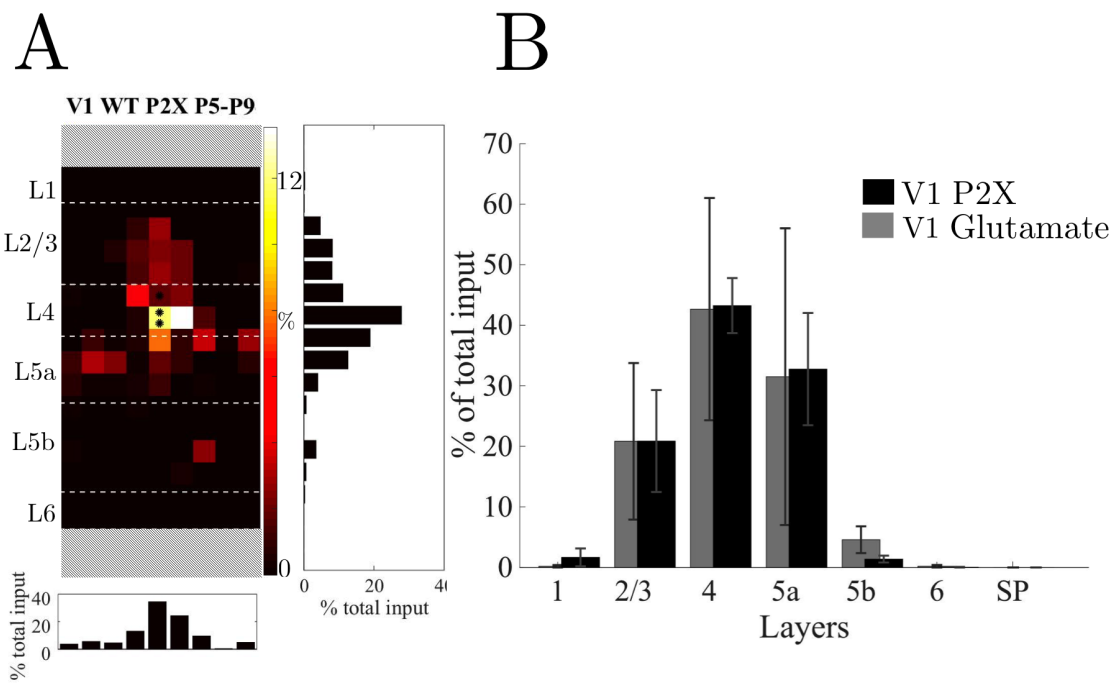


Figure 4.5: **SST-specific GABAergic input onto layer 4 in V1**. **A)** Averaged heat maps of SST-specifc input onto layer 4 of V1 in P5-P9 mice. **B)** Percentage of total GABAergic input (SST-specific and global) onto layer 4 V1, originating from each cortical layer. n=3 cells from 3 animals for P2X ATP-uncaging and n=9 cells from 7 animals for glutamate-uncaging. Error bars are SEM.

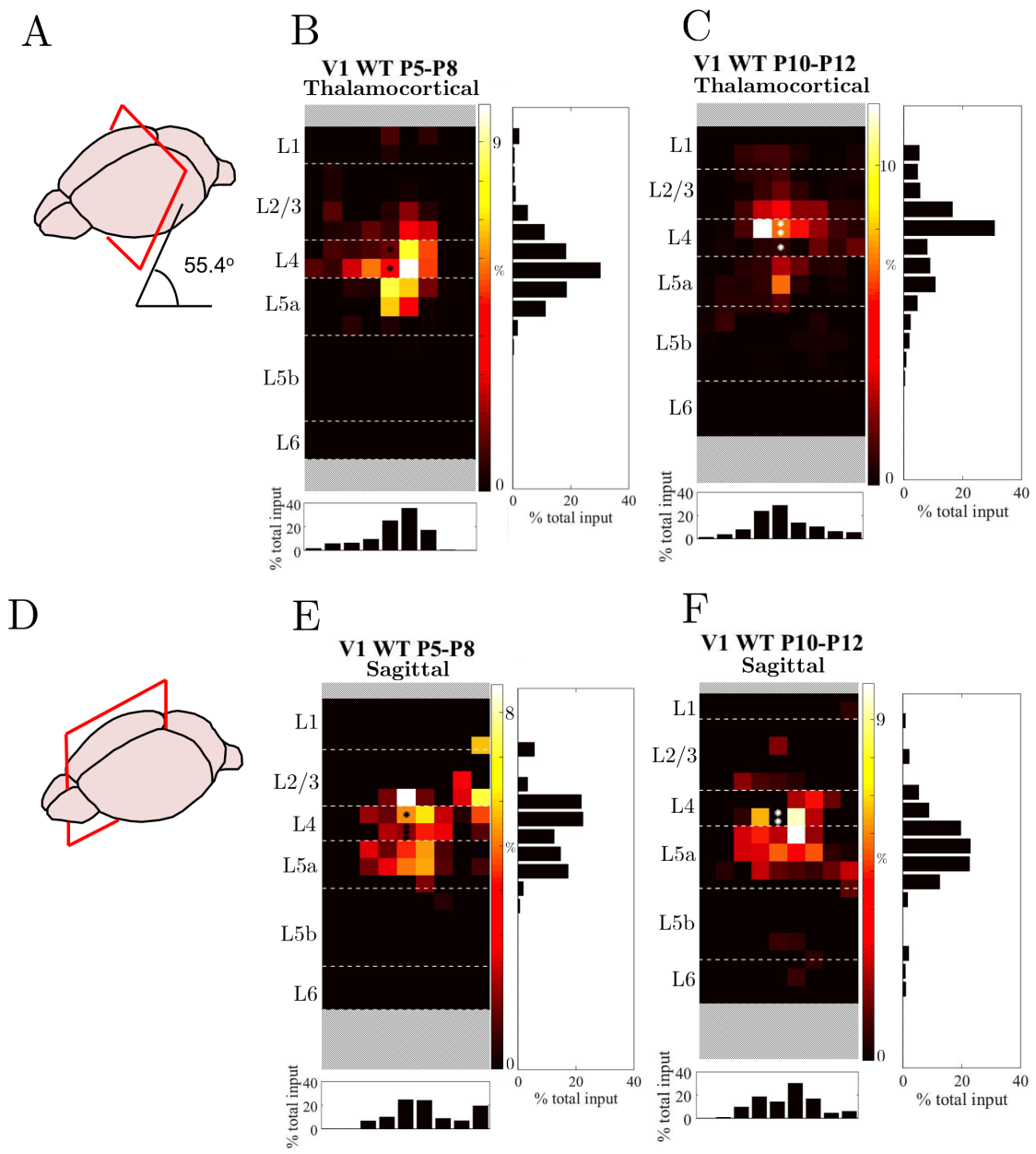


Figure 4.6: **GABAergic input onto layer 4 V1 in for sagittal and visual-thalamocortical slice preparations**. **A)** Diagram showing the slice angle for visual thalamocortical slices. **B)** Averaged heat maps (normalised) for GABAergic input onto layer 4 of V1 in P5-P8 mice. Thalamocortical sections (n=2 cells from 1 animal). **C)** Averaged heat maps (normalised) for GABAergic input onto layer 4 of V1 in P10-P12 mice. Thalamocortical sections (n=3 cells from 1 animal). **D)** Diagram showing the slice angle for sagittal slices. **E)** Averaged heat maps (normalised) for GABAergic input onto layer 4 of V1 in P5-P8 mice. Sagittal sections (n=4 cells from 2 animals). **F)** Averaged heat maps (normalised) for GABAergic input onto layer 4 of V1 in P10-P12 mice (n=2 cells from 1 animal). Sagittal sections. Black and white asterisks represent the position of the recorded layer 4 cell.

4.2.4 GABAergic input onto excitatory cells in all layers

While the L5b-L4 translaminar connection was not present in V1, it was possible that other GABAergic translaminar connections existed in V1 and served a similar function. To investigate whether GABAergic translaminar connections existed onto other cortical layers in V1, GABAergic input was mapped across cortical layers at early postnatal ages. No transient translaminar GABAergic connection was observed in layers 2/3, 5a or 5b (Figure 4.7), revealing that GABAergic input in V1 was primarily local in origin. In older animals, translaminar GABAergic inhibition from infragranular layers onto layer 2 appeared (Figure 4.8)

4.2.5 Glutamatergic input onto L5b SST+ cells in V1

In S1BF, L5b SST INs are the target of reciprocal translaminar input from L4 (Marques-Smith et al., 2016). While L5b to L4 GABAergic input was not observed in V1, it was possible that L5b SST INs still received glutamatergic input from layer 4.

In order to investigate this possibility, SST Cre was crossed with Ai9 (RFP) reporter line. This allowed visualisation and targeted recording of SST+ve interneurons in layer 5b. Figure 4.9D shows a P6 V1 coronal section with SST cells expressing RFP and three SST+ve cells filled with biocytin (during recording) and subsequently stained with streptavidin-GFP.

No translaminar glutamatergic input onto SST+ve interneurons in infragranualr layer was present in any of the three age groups (P5-P8, P9-P12 or P13-P24) (Figure 4.9). This indicates that the transient layer 4 excitation onto layer 5b SST interneurons is not present in V1.

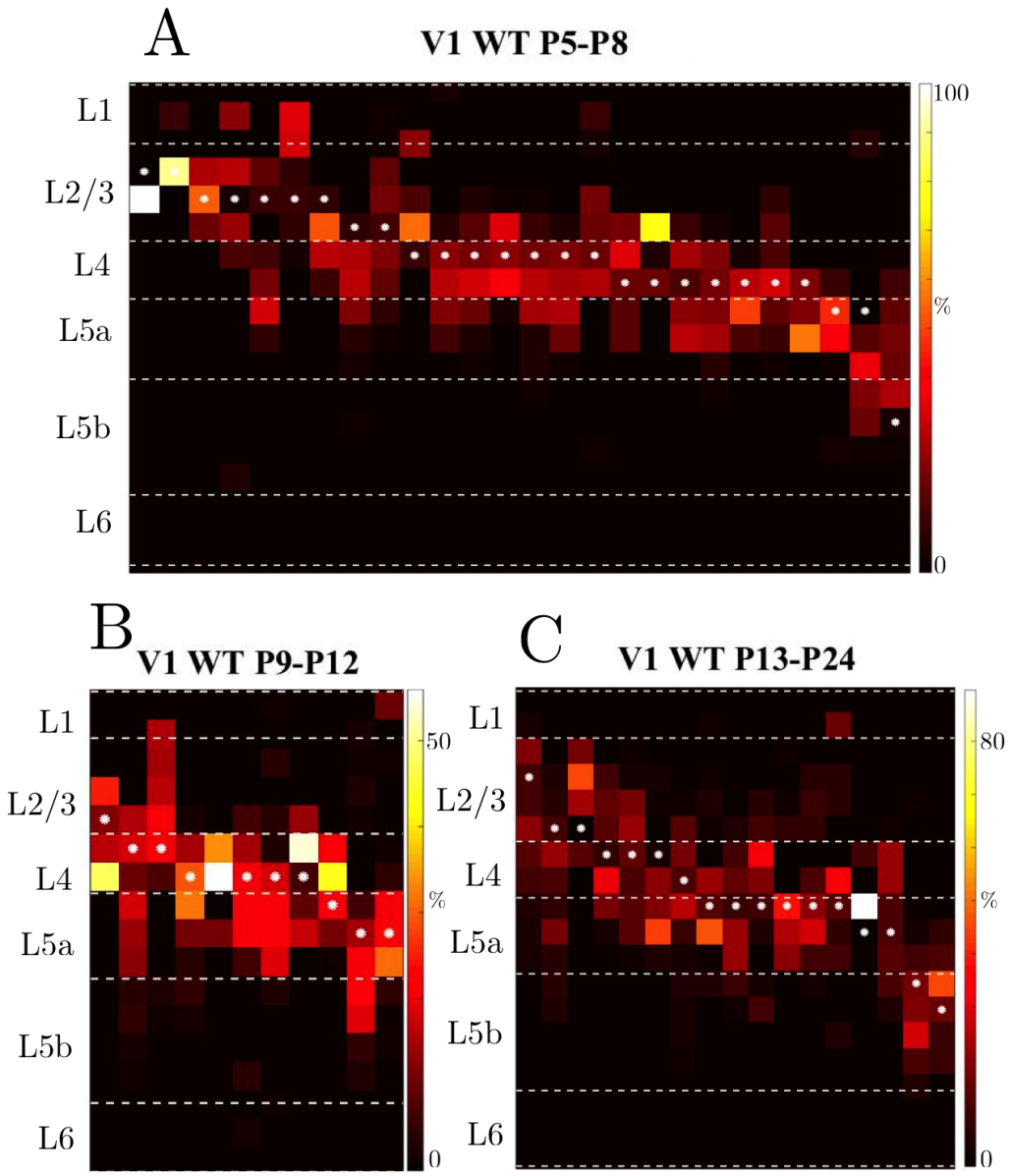


Figure 4.7: **GABAergic input onto each cortical layer from P5-P24 A)** GABAergic input onto layers 2/3, 4, 5a and 5b from P5-P8. **B)** GABAergic input onto layers 2/3, 4, 5a and 5b from P9-P12. **C)** GABAergic input onto layers 2/3, 4, 5a and 5b from P13-P24. Each column represents normalised GABAergic input onto a single excitatory cell. White asterisk indicates the recorded cell's position within the heat map. Data include coronal, thalamocortical and sagittal slice angles.

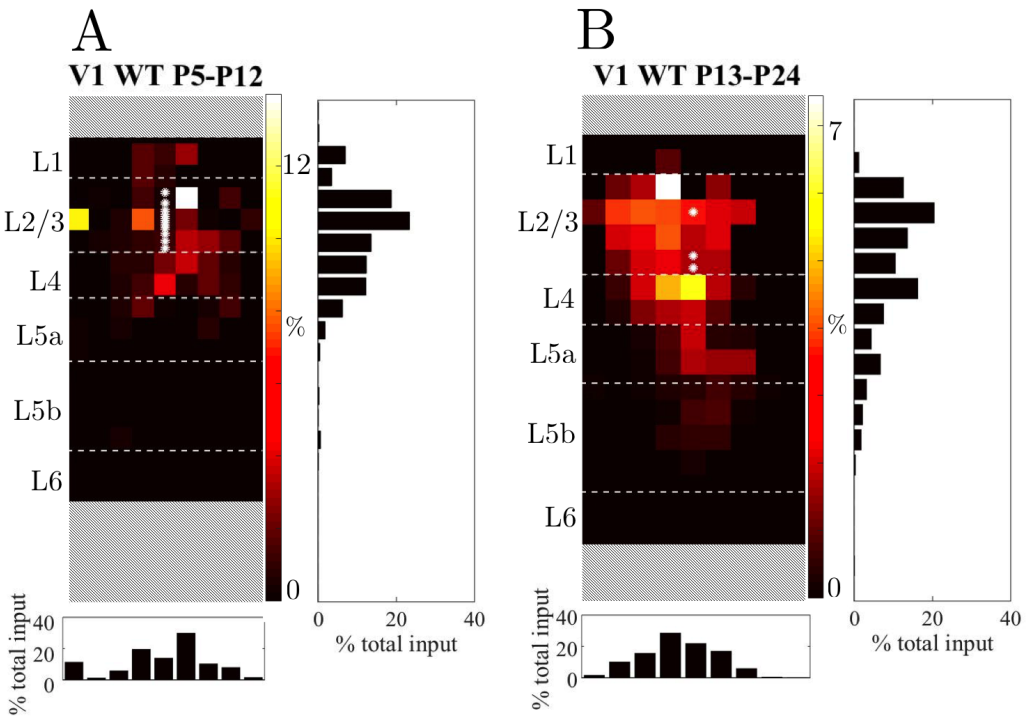


Figure 4.8: **Averaged heat maps of GABAergic input onto layer 2/3 in V1. A)** Averaged heat maps (normalised) of GABAergic input onto layer 2/3 excitatory cells of P5-P12 mice. **B)** Averaged heat maps (normalised) of GABAergic input onto layer 2/3 excitatory cells of P13-P24 mice. A) n=10 cells from 8 animals B) n=3 cells from 3 animals.

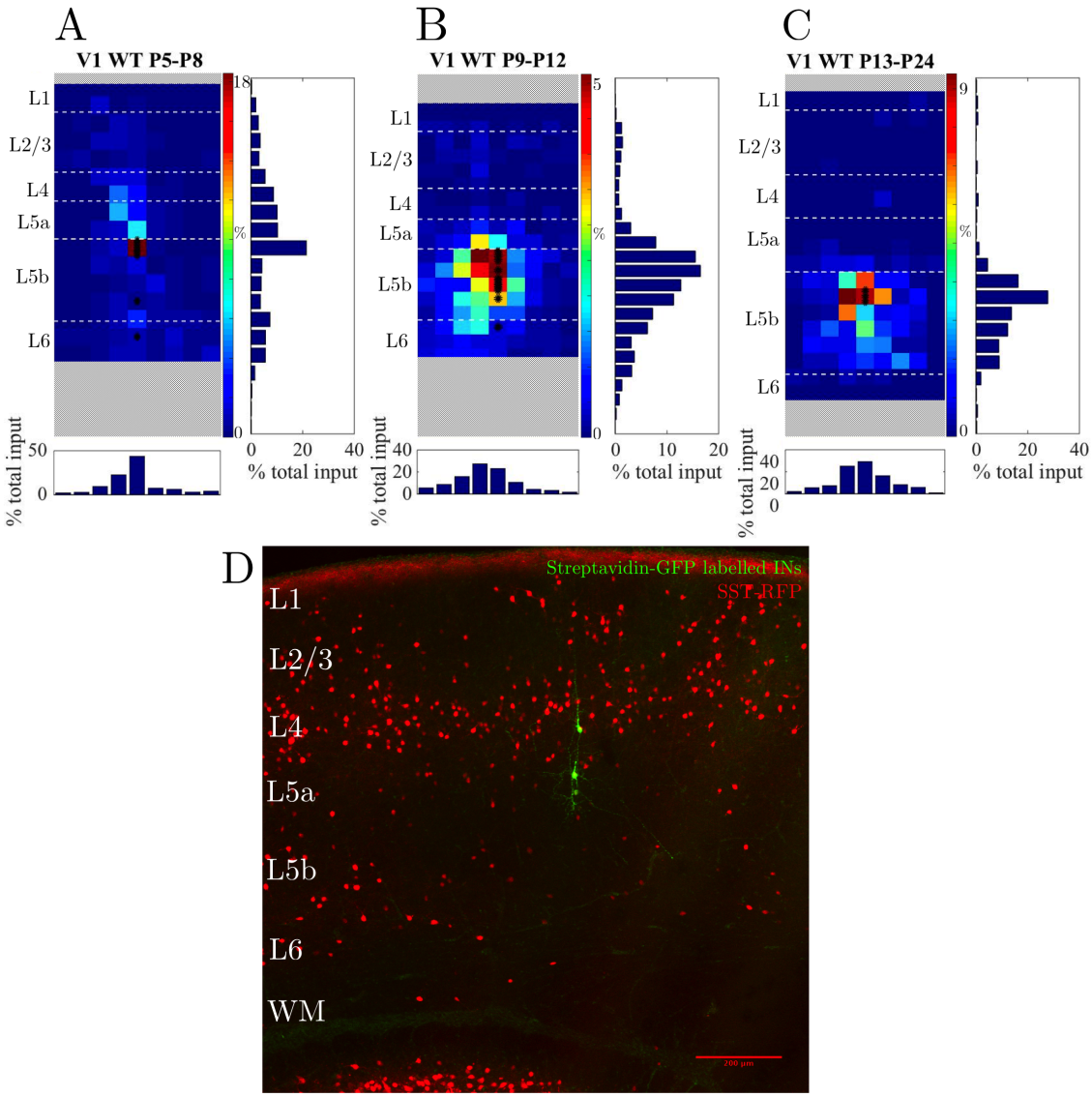


Figure 4.9: **Glutamatergic input onto L5b SST+ cells in V1. A)** Averaged heat maps (normalised) for glutamatergic input onto V1 layer 5b SST+ve interneurons for P5-P8 (n=8 cells from 7 animals). **B)** Averaged heat maps (normalised) for glutamatergic input onto V1 layer 5b SST+ve interneurons for P9-P12 (n=12 cells from 6 animals) **C)** Averaged heat maps (normalised) for glutamatergic input onto V1 layer 5b SST+ve interneurons for P13-P24 (n=3 cells from 4 animals). **D)** Confocal stack image showing SST-RFP expression (red) in a P6 SST|Ai9 mouse and three recorded SST+ve interneurons (green). Scale bar is 200μm.

4.2.6 GABAergic input onto V1 L4 excitatory cells in the Celsr3|Dlx5/6 mouse

It has been observed in previous sections that translaminar GABAergic input is present in S1BF of a mouse devoid of sensory input and absent in V1 of a wildtype mouse. It was unclear if this difference in GABAergic circuitry in V1 developed independently of any thalamic driven activity. For this reason, GABAergic input into layer 4 of V1 in the Celsr3|Dlx5/6 mouse was mapped. Such an experiment aimed to determine the role, if any, that early visual input had on L5b-L4 translaminar connections.

In the Celsr3|Dlx5/6 mouse, no L5b to L4 GABAergic connection was observed in neonatal (P6-P9) mice (Figure 4.10). This confirmed that the L5b to L4 GABAergic connection was not present in V1 in the absence of any visual input. The distribution of GABAergic input onto layer 4 in V1 was not significantly different between WT and Celsr3|Dlx5/6 mice (Figure 4.11A). There was no difference in total layer input between WT and Celsr3|Dlx5/6 mice, with the exception of significantly more total GABAergic input originating from layer 2/3 in Celsr3|Dlx5/6 mice ($p<0.01$, n=7 for Celsr3 and n=6 for WT) (Figure 4.11B). The total input for all layers was not significantly different between WT and Celsr3|Dlx5/6 V1 recordings (Figure 4.11C).

When comparing GABAergic input onto layer 4 of both Celsr3|Dlx5/6 V1 and Celsr3|Dlx5/6 S1BF, it is clear that Celsr3|Dlx5/6 mouse S1BF has translaminar L5b to L4 GABAergic input, while Celsr3|Dlx5/6 V1 does not. Figure 4.12A shows the distribution of GABAergic input from all cortical layers, comparing Celsr3|Dlx5/6 V1 and S1. Celsr3|Dlx5/6 S1 has a much higher, although not significant ($p=0.08$), percentage of the total GABAergic input originating from L5b, while Celsr3|Dlx5/6 V1 has a significantly higher percentage of the total GABAergic input originating from L2/3 ($p<0.05$, n=12 for Celsr3 S1BF and n=5 for Celsr3

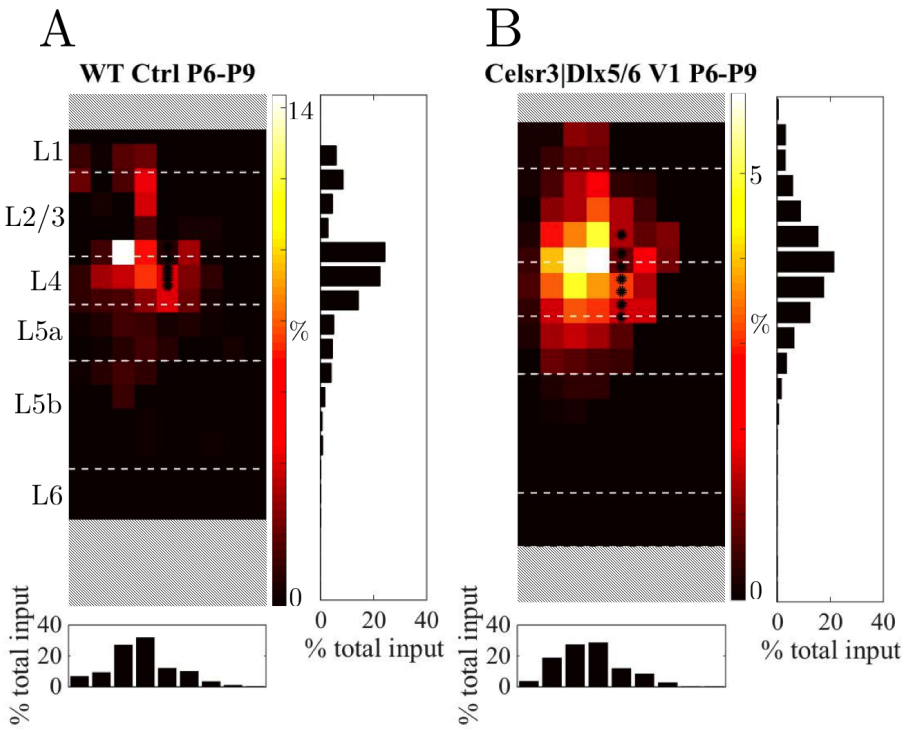


Figure 4.10: **GABAergic input onto V1 layer 4 in Celsr3|Dlx5/6 mice. A)** Averaged heat maps (normalised) for GABAergic input onto WT V1 layer 4 excitatory neurons for P6-P9 (n=6 cells from 3 animals). **B)** Averaged heat maps (normalised) for GABAergic input onto Celsr3|Dlx5/6 V1 layer 4 excitatory neurons for P6-P9 (n=7 cells from 6 animals).

V1). The total pA GABAergic input from each layer is not significantly different between the two mouse lines (Figure 4.12B).

4.3 Discussion

This chapter explored the early GABAergic circuits in V1 of the neonatal mouse. Contrary to expectations, there is no evidence of a transient translaminar L5b-L4 connection in mouse primary visual cortex (Marques-Smith et al., 2016). Instead, GABAergic input appears locally mediated during V1 neonatal development. From

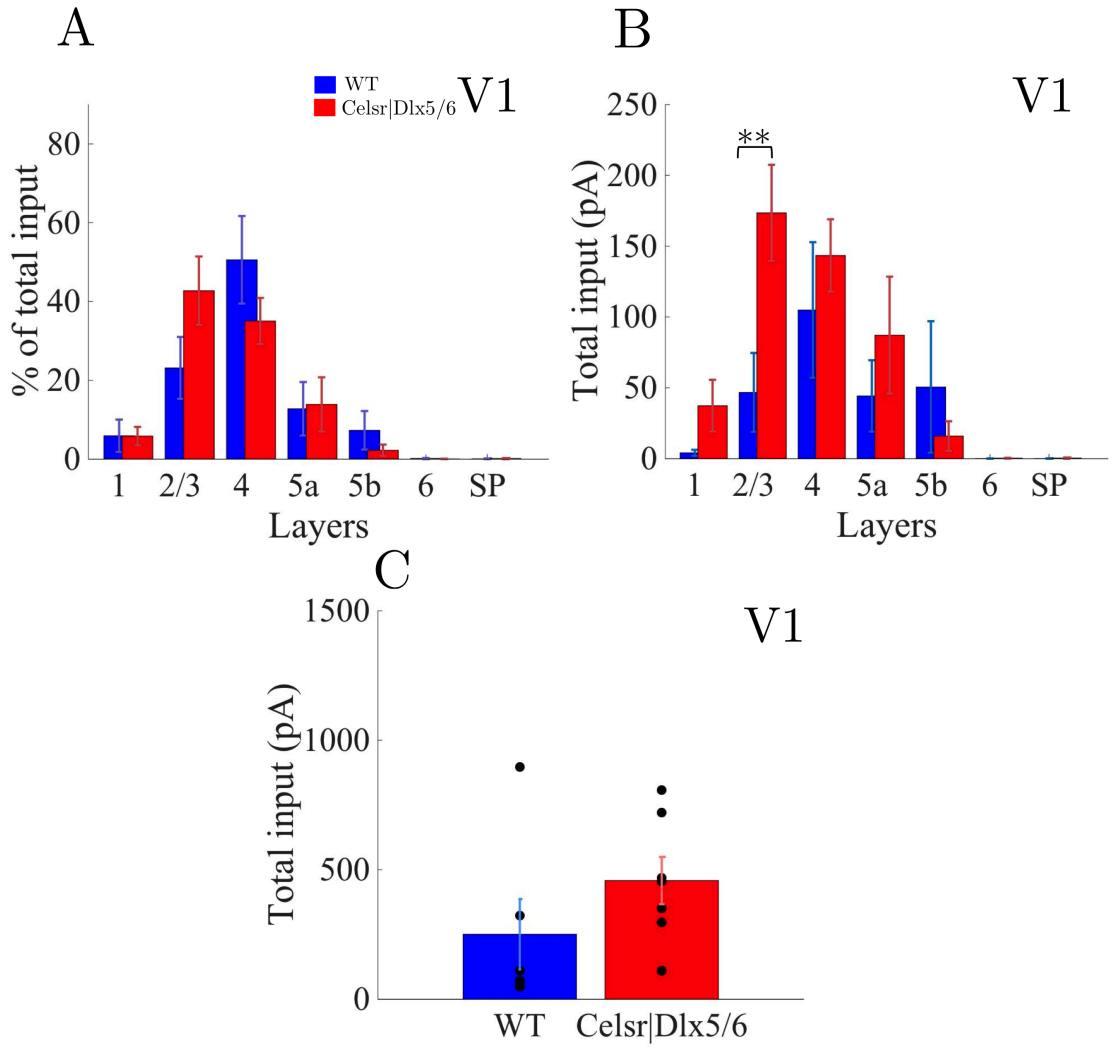


Figure 4.11: **Layer contributions to GABAergic input onto V1 L4 for Celsr3|Dlx5/6 and WT. A)** Normalised layer contributions for GABAergic input onto V1 layer 4 for Celsr3|Dlx5/6 and WT mice (P6-P9). **B)** Total pA layer contributions for GABAergic input onto V1 layer 4 for Celsr3|Dlx5/6 and WT mice (P6-P9). **C)** Total GABAergic input (pA) for P6-P9 WT and Celsr3|Dlx5/6 mice in V1. *=$p<0.05$ **=$p<0.01$ Statistical analysis used the two-sided Wilcoxon rank sum test for independent samples. Errorbars are SEM. n=7 cells from 6 animals for Celsr3|Dlx5/6 and n=6 cells from 3 animals for WT.

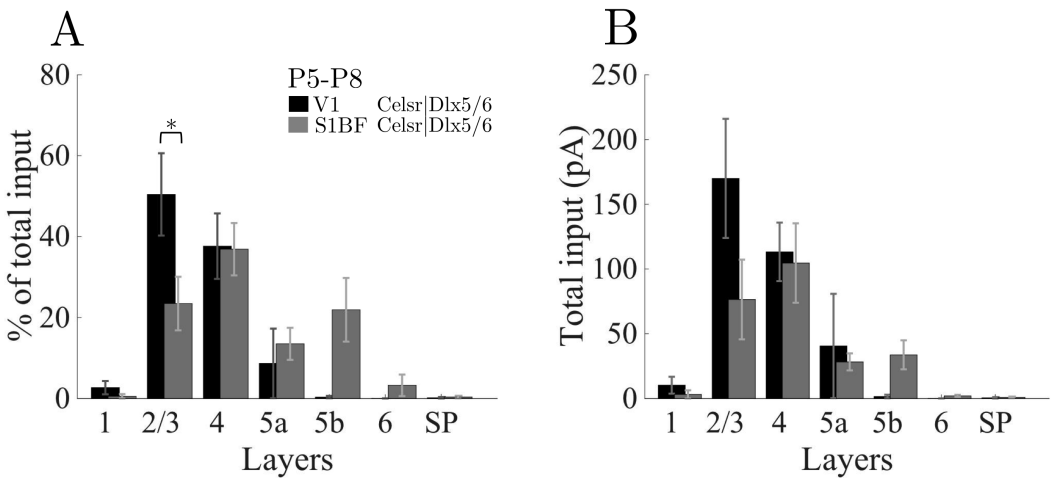


Figure 4.12: **Layer contributions for GABAergic input onto V1 and S1BF layer 4 for Celsr3|Dlx5/6 mice. A)** Normalised layer contributions for GABAergic input onto V1 and S1BF layer 4 for Celsr3|Dlx5/6 mice (P5-P8). **B)** Total layer contributions for GABAergic input onto V1 and S1BF layer 4 for Celsr3|Dlx5/6 mice (P5-P8). *=$p<0.05$ **=$p<0.01$ Statistical analysis used the two-sided Wilcoxon rank sum test for independent samples. Errorbars are SEM. n=12 cells for Celsr3|Dlx5/6 S1BF and n=5 cells for Celsr3|Dlx5/6 V1.

P5 onwards until the last recorded age (P24) no L5b GABAergic input onto layer 4 in V1 was observed in LSPS data. The local GABAergic input onto L4 in V1 was confirmed to be partly due to SST+ve INs via SST-specific excitation through SST Cre |$P2X_2$. The absence of L5b GABAergic input onto L4 was confirmed to not be an artefact of slice preparation. Additionally, no glutamatergic input from L4 onto L5b SST INs in V1 was observed, showing that neither component of the L5b-L4 loop is present in neonatal V1. Mapping of neonatal circuits in V1 Celsr3|Dlx5/6 mice from P6-P9 demonstrated that the absence of the L5b-L4 loop in V1 is the 'default state' and not influenced by thalamic-driven activity. Not only was the L5b-L4 loop absent in V1, but no infragranular translaminar GABAergic input was observed for any cortical layer in mice aged P5-P12. Together, these results point to fundamental differences in neonatal circuitry between S1BF and V1 that are independent of thalamic input.

What is the function of the early circuit difference between S1BF and V1? It

is possible that the highly specific organisation of the barrel field may require early developmental circuitry that is specialised for integration of whisker information and, therefore, not generally applicable to other sensory areas. The L5b-L4 reciprocal loop has been shown to play a role in the timely acquisition of thalamic input onto L4 in S1BF (Marques-Smith et al., 2016; Tuncdemir et al., 2016). In S1BF, whiskers map topographically onto somatosensory cortex of rodents and both the number and arrangement of whiskers and barrels are the same from animal to animal (Van der Loos & Woolsey, 1973; Knutsen & Ahissar, 2009; Woolsey & Van der Loos, 1970). Thalamocortical targeting in S1BF has been shown to be very precise to the target barrel from the earliest thalamic innervation (P0), while the same early precision of thalamic targeting is not seen in V1 (Agmon, Yang, Jones, & O'Dowd, 1995; Agmon, Yang, O'Dowd, & Jones, 1993; Krug, Smith, & Thompson, 1998). Perhaps the precise relationship between whisker, barreloid and then barrel requires cortical circuity to guide thalamic input into the correct barrel. Possibly, in the visual cortex, ODCs and retinotopy do not have as precise a pre-determined position and, therefore, retinal waves suffice to create the required cytoarchitecture without guidance in the form of early cortical circuits. Indeed, it appears that the development of topography in the visual cortex, including ocular dominance columns and orientation columns, is governed by a self-organising process in which initial conditions are random (Swindale, 1996).

The different timing of sensory input and subsequent critical period windows for S1BF and V1 could also be a factor in the requirement for an early specialised circuit in S1BF. S1BF and V1 receive behaviourally relevant sensory information at different times, with somatosensation beginning at birth, while eye opening does not occur until approximately P12 (Crowley & Katz, 2000; Yang et al., 2018). Additionally, the critical period of plasticity differs greatly between the two regions with S1BF between P3-P14 and V1 between P19-P32 (Gordon & Stryker, 1996; Stern et al.,

2001; Hensch, 2005; Rebsam et al., 2005). The different temporal requirements for incoming sensory information between S1BF and V1 could require the involvement of different IN subtypes (Butt et al., 2017). At P3-4, PV INs show no functional connectivity to either other PV INs or Pyramidal cells. By P5-6, 24% were connected through chemical synapses. It was not until P15-P18 that approximately half of PV cells were connected with GABAergic synapses (Pangratz-Fuehrer & Hestrin, 2011). In contrast, GABAergic input from SST INs is functional during the first postnatal week. In the hippocampus, SST INs are responsible for generating giant depolarizing potentials (Ben-Ari et al., 1989; Picardo et al., 2011). In the neocortex, SST INs have also been shown to have functional GABAergic connections from P5 and receive thalamic input (Anastasiades et al., 2016; Tuncdemir et al., 2016). The earlier connectivity of SST INs as compared to PV INs, combined with the earlier sensory processing requirements and critical period of S1BF, may explain why SST INs play a central role in early S1BF circuits. Tuncdemir et al. (2016) reports that in S1BF, early SST networks are required for the maturation of thalamocortical input onto PV cells. It has been demonstrated that PV cell maturation and function controls the timing of the critical period of plasticity (Fagiolini et al., 2004). It is possible that the L5b-L4 loop functions in S1BF to facilitate thalamocortical input onto PV cells and thereby the earlier S1BF critical period. Possibly, by the time of eye opening at P12, PV cell connectivity has matured sufficiently to not require the same SST IN mediated GABAergic circuits in V1.

The presence of translaminar GABAergic connection to layers other than L4 was investigated in V1. Some lower layer GABAergic input from L5 was seen for L2/3 in older animals (Figure 4.7). As this connection forms first in older mice and is present in the adult (Kätzel, Zemelman, Buetfering, Wölfel, & Miesenböck, 2011), it is not considered to be a transient connection. Therefore, in contrast to S1BF, there does not appear to be any GABAergic transient translaminar connection in V1 to any

layer. The building and dismantling of transient connections would be energetically expensive for a developing brain and, therefore, it is expected that such connections would only form if the required machinery for the final connections was not yet in place. The absence of transient GABAergic circuitry in V1 further supports the argument that the L5b-L4 reciprocal loop in S1BF functions as an intermediate step allowing thalamic innervation of sensory information before the onset of PV IN connectivity. Possibly, once the later critical period of plasticity occurs in the visual cortex, local PV GABAergic input is sufficient to regulate thalamic input and circuit maturation.

It is also possible that early subplate circuits differ between S1BF and V1 resulting in different requirements for transient cortical circuits. In macaque monkeys, the subplate zone appears earlier in S1 than V1 and also differs in width relative to the cortical plate between the two regions (Kostovic & Rakic, 1990). Subplate circuits themselves must differ between cortical regions as S1BF subplate neurites are orientated around the barrel and later septa of layer 4, something which is specific to S1BF (Piñon et al., 2009). It is also well known that the subplate consists of a molecularly and morphologically diverse cell population (Osheroff & Hatten, 2009; Hoerder-Suabedissen et al., 2008; Pedraza et al., 2014; Viswanathan et al., 2012; Hoerder-Suabedissen & Molnár, 2012b; Kostovic & Rakic, 1980; Luskin & Shatz, 1985; Marin-Padilla, 1970). Subplate cells act as an early relay between the thalamus and layer 4 and receive input from the thalamus, subplate and cortical layers before the L5b-L4 circuit is formed (Hanganu et al., 2002, 2008; Luhmann et al., 2009; Zhao et al., 2009; Hanganu, Kilb, & Luhmann, 2001). Because the highly connected subplate circuits appear at the earliest stages of cortical development, this cell population would be able to modulate the flow of sensory information into later cortical circuits (Dupont et al., 2006). Possibly area-specific subplate circuits, such as the dynamic integration of neurites into the barrel field (Piñon et al., 2009), lead

to different mechanisms of thalamic integration between the two regions, resulting in a requirement for a L5b-L4 circuit in S1BF but not V1.

Although neonatal V1 does not develop transient translaminar connections, the local GABAergic input seen in P5-P24 is still immature. The GABAergic input onto L4 originating from L4 (43.82%) is similar to the 44.2% reported for GABAergic input onto L4 from L4 cells in adult V1. However, in adult V1, 53% of GABAergic input also originates from layer 5 (5a and 5b combined) (Kätzel et al., 2011), something which was not observed in V1 up to P24. Therefore, the local GABAergic input seen in P5-P24 does not represent the complete mature cortical circuitry.

What is it that instructs the early circuit differences between S1BF and V1? Since the differences seen between V1 and S1BF are independent of thalamic input, it follows that factors within the neocortex itself must be responsible for these early circuit differences. Arealization of the neocortex begins with the secretion of morphogens at the perimeter of the dorsal telencephalon. These morphogens, such as FGF8, WNT, and BMP act as the first step in defining cortical area boundaries by controlling the differential expression of transcription factors within cortical progenitors. From the expression of transcription factors such as Emx2, COUP-TFI, Pax6 and Sp8 and their downstream targets, the positions of sensory areas within the neocortex are determined. (OLeary & Sahara, 2008; Suzuki-Hirano & Shimogori, 2009).

Given that the circuit differences observed between WT S1BF and V1 were unchanged in the Celsr3|Dlx5/6 mouse, they must be a product of signalling cascades and differential transcription factor expression set in motion during early cortical arealization. These genetic differences could influence circuit development in a number of ways. Firstly, it is possible that early spontaneous cortical activity differs between S1BF and V1 and, thereby, instructs circuit development. However, this is not a likely explanation given the similarity of early spontaneous activity between

the two areas. Both S1BF and V1 have spindle bursts and early gamma oscillations that are primarily driven by retinal waves and spontaneous movement (Khazipov & Milh, 2017). Local inactivation of the VPM profoundly reduces not only spindle bursts and gamma oscillations but the majority of spontaneous events (Yang et al., 2012). This suggests that the isolated cortex does not have circuitry mature enough to maintain intrinsic oscillations. Another possible candidate for intrinsically generated cortical activity could be large scale calcium waves which begin at E16. These waves are mediated by chemical synapses and propogate across an entire horizontal cortical slice. After birth, the frequency and amplitude of these waves changes differentially along the anterior/posterior axis. However, as these changes occur after thalamic input has reached the cortex, it is unclear whether these changes are directed by thalamic input (Moreno-Juan et al., 2017). Additionally, these calcium waves are thought to primarily enable the development of long range cortico-cortico connections and not columnar structures (Garaschuk, Linn, Eilers, & Konnerth, 2000). It is, therefore, unlikely that spontaneous activity differences between S1BF and V1 underlie the circuitry differences observed.

More plausible is that intrinsic genetic factors within different primary sensory areas instruct cell type and morphology, resulting in differing circuitry. Given the central role of Lpar1-EGFP SST INs in the L5b-L4 loop, it is also possible that genetic differences in V1 and S1BF influence either the morphology and survival of Lpar1-EGFP SST INs, or the tangential migration of interneuron subtypes. The differences in SST cell morphology and subtype between S1BF and V1 will be explored and discussed in Chapter 5. From these results, it is clear that intrinsic genetic factors have the ability to shape early circuit differences between primary sensory cortices completely independently of thalamic input. This evidence suggest that the developing neocortex is far from a 'blank slate' containing canonical circuitry before thalamic innervation.

Chapter 5

Thalamic innervation in V1 and S1BF during neonatal development

From the previous results chapters, it has been observed that the developing neocortex does not exist in a 'blank slate' state, ready for remodelling by thalamic afferents, but instead already contains area-specific circuitry that is independent of thalamocortical input.

Although the assembly, presence and disassembly of the L5b-L4 circuit is not affected by thalamic input, the circuit is required for correct thalamic integration in S1BF (Marques-Smith et al., 2016; Tuncdemir et al., 2016). This raises the possibility that thalamic integration into L4 of S1BF and V1 occurs through two different developmental mechanisms, and that perhaps the cells which receive thalamic input in the developing cortex may differ between S1BF and V1.

Of particular interest is the comparison between the V1 and S1BF L5b SST+ve INs. The particular subtype of SST+ve INs, Lpar1-EGFP cells, are known to be involved in the L5b-L4 reciprocal circuit and also receive thalamic input during early

development (Marques-Smith et al., 2016; Tuncdemir et al., 2016). It is possible that this cell population differs between V1 and S1BF and is one of the intrinsic differences driving the observed cortical circuitry differences.

Currently there is limited electrophysiological data documenting thalamic engagement in the neocortex during early development, particularly that of V1. The generalised model for thalamic engagement in sensory cortices is that thalamic afferents connect to the subplate before birth and then wait for their final targets, L4 neurons, to be born (López-Bendito & Molnár, 2003; Lund & Mustari, 1977; Rakic, 1976; Shatz & Luskin, 1986). Thalamic afferents then engage with the cortical plate, which will eventually transition into L4. By P4, thalamic afferents also give direct input onto L5, a connection which has also been confirmed more recently to involve SST+ INs (Molnár, Kurotani, Higashi, Yamamoto, & Toyama, 2003; Wess, Isaiah, Watkins, & Kanold, 2017; Price et al., 2006; Tuncdemir et al., 2016; Marques-Smith et al., 2016; Higashi, Molnár, Kurotani, & Toyama, 2002; Higashi, Hioki, Kurotani, Kasim, & Molnár, 2005).

For the visual cortex, the progression of functional thalamic connections during the first weeks of life is less clear. Similar to S1BF, thalamic afferents are thought to engage with the subplate before finding their final targets in L4 (López-Bendito & Molnár, 2003). Whether they also synapse directly onto infragraular layers during this time is not clear. Explant studies have shown that LGN axons will identify, innervate and terminate in L4, however, a small fraction of TC axons also terminated in lower layers (Yamamoto, Yamada, Kurotani, & Toyama, 1992; Yamamoto, Kurotani, & Toyama, 1989; Molnár & Blakemore, 1991; Yamamoto, Higashi, & Toyama, 1997). In adult mice (P50-P70), stimulation of virally injected ChR2 showed that some Pv+ INs and Pyramidal (Pyr) cells in all layers receive thalamocortical input, with the majority of thalamocortical input innervating L4. Fluorescent imaging of thalamocortical axons within the cortex showed high ChR2

expression in L4, along with a much fainter L5 band. Only SST+ve INs in L4 received direct thalamocortical input and this input was weaker than input onto either Pyr or PV+ INs (X.-y. Ji et al., 2015).

Traditionally, in order to investigate thamalocortical input in the somatosensory cortex, mouse brains are sliced at approximately 45 degrees (Agmon & Connors, 1991; Higashi et al., 2002, 2005), in order to preserve the thalamocortical connections. Using this preparation it is possible to stimulate thalamic cells or the thalamic axons electrically and evoke responses in connected cortical cells. For the visual cortex, however, this is very difficult to consistently achieve, given the route taken by the thalamic fibres from the lateral geniculate complex to the visual cortex (MacLean et al., 2006). In our experience, no slice angle is able to consistently preserve enough of the thalamo-cortical connection to make the electrical stimulation an option.

For this reason, a thalamus-specific Cre driver line was chosen to conditionally express channelrhodopsin in thalamic afferents. To limit the expression of the channelrhodopsin to the thalamus, the *Olig3*$^{\text{cre}/+}$ mouse line (Vue et al., 2009) was chosen. This line was particularly suitable, as it showed broad channelrhodopsin expression in the thalamus, including both the ventral posteromedial nucleus (VPM), projecting to S1 and the lateral geniculate complex, projecting to V1 (García et al., 2015). Other thalamic-specific Cre driver lines such as *VGlut2*$^{\text{cre}/+}$ did not have as broad an expression profile in the thalamus (García et al., 2015). For the Cre recombinase dependent channelrhodopsin, the Ai32 mouse line was chosen. This line expresses a channelrhodopsin-2/EYFP fusion protein and has previously been demonstrated to have sufficient expression at young ages (P8-12) to elicit reliable EPSCs when stimulated (García et al., 2015). Additionally, it has been shown that Ai32 expressing axons can be stimulated, even if they are severed from their parent somata (Petreanu et al., 2007). It was, therefore, a suitable candidate for

investigation of thalamic input into S1 and V1 in neonatal mice.

In this chapter, characteristics of SST INs and Lpar1-EGFP INs are compared between S1BF and V1, including morphology, cell number and layer distribution. Following this, the Olig3|Ai32 mouse was used to investigate thalamic input onto cells in S1BF and V1. Cells selected for recording were picked at random and later classified as one of four main cells types, fast-spiking (FS) IN, non-fast-spiking (NFS) IN, spiny stellate neuron (SSN) or pyramidal neuron (Pyr), based on both intrinsic electrophysiological properties and reconstructed morphologies.

5.1 Properties of layer 5 Lpar1-EGFP in S1BF and V1

5.1.1 Intrinsic electrophysiological properties of Lpar1-EGFP GABAergic cells in S1BF and V1 are not different

Layer 5 Lpar1-EGFP cells in S1BF and V1 were recorded to explore whether their intrinsic electrophysiological properties differed between S1BF and V1. None of the properties listed in Table 5.1 were significantly different between S1BF and V1 for layer 5b. This was tested using the two-sided Wilcoxon rank sum test for independent samples.

5.1.2 Lpar1-EGFP GABAergic layer 5 cells in S1BF have more extensive axonal arborisation than Lpar1-EGFP GABAergic layer 5 cells in V1

During the recording of electrophysiological properties, Lpar1-EGFP cells in S1BF and V1 were filled with biocytin, to allow staining and reconstruction of their axons

Intrinsic Property	**S1BF** Mean±SEM	**V1** Mean±SEM
RMP (mV)	-59.44±1.63	-56.54± 2.58
Spike Threshold (mV)	-38.05±1.67	-39.26± 0.79
Absolute Spike Height (mV)	16.17±3.13	20.62± 2.40
Total Spike Height (mV)	54.22±4.25	59.88± 2.95
Firing Frequency (Hz)	46.42±5.37	51.5± 5.23
Input Resistance (MΩ)	979±130.37	1071.7± 146.58
AHP Amp (mV)	15.53±1.22	15.97± 2.01
AHP delay (ms)	28.90±5.16	28.59± 4.79
Membrane Time Constant (ms)	59.51±8.50	64.49± 10.60
Spike Half-width (ms)	2.40±0.26	2.38± 0.24
Spike Frequency Adaption (%)	28.12±2.52	38.29± 1.58

Table 5.1: Intrinsic electrophysiological properties of Lpar1-EGFP GABAergic neurons in S1BF L5b and V1 L5b (P8-P9). n=7 cells for both S1BF and V1. RMP is resting membrane potential, AHP is afterhyperpolarization. Data from 4 animals

and dendrites. This allowed a comparison of the morphology of Lpar1-EGFP cells in layer 5b between S1BF and V1. Lpar1-EGFP cells in S1BF were found to have more extensive axon branching that reached further into superficial cortical layers (Figure 5.1). An example of the more extensive branching in S1BF Lpar1-EGFP neurons can be seen in Figure 5.1A and B, as compared to an Lpar1-EGFP cell in V1 (Figure 5.1C and D). This was quantified using Scholl analysis. Figure 5.1E shows the number of axon crossing of a circle surrounding the somata at increasing distances from the somata. S1BF Lpar1-EGFP cells have a higher number of axon crossings at distances of $\geq$ 250 μm away from the somata. The total length of all axon segments is significantly ($p<0.05$) higher for S1BF Lpar1-EGFP cells than for V1 Lpar-EGFP cells (Figure 5.1F).

5.1.3 The density and distribution of SST+ve and Lpar1-EGFP cells differs between S1BF and V1

During *in vitro* recordings it was often observed that the density and distribution of SST+ve and Lpar1-EGFP cells appeared different between S1BF and V1. Therefore,

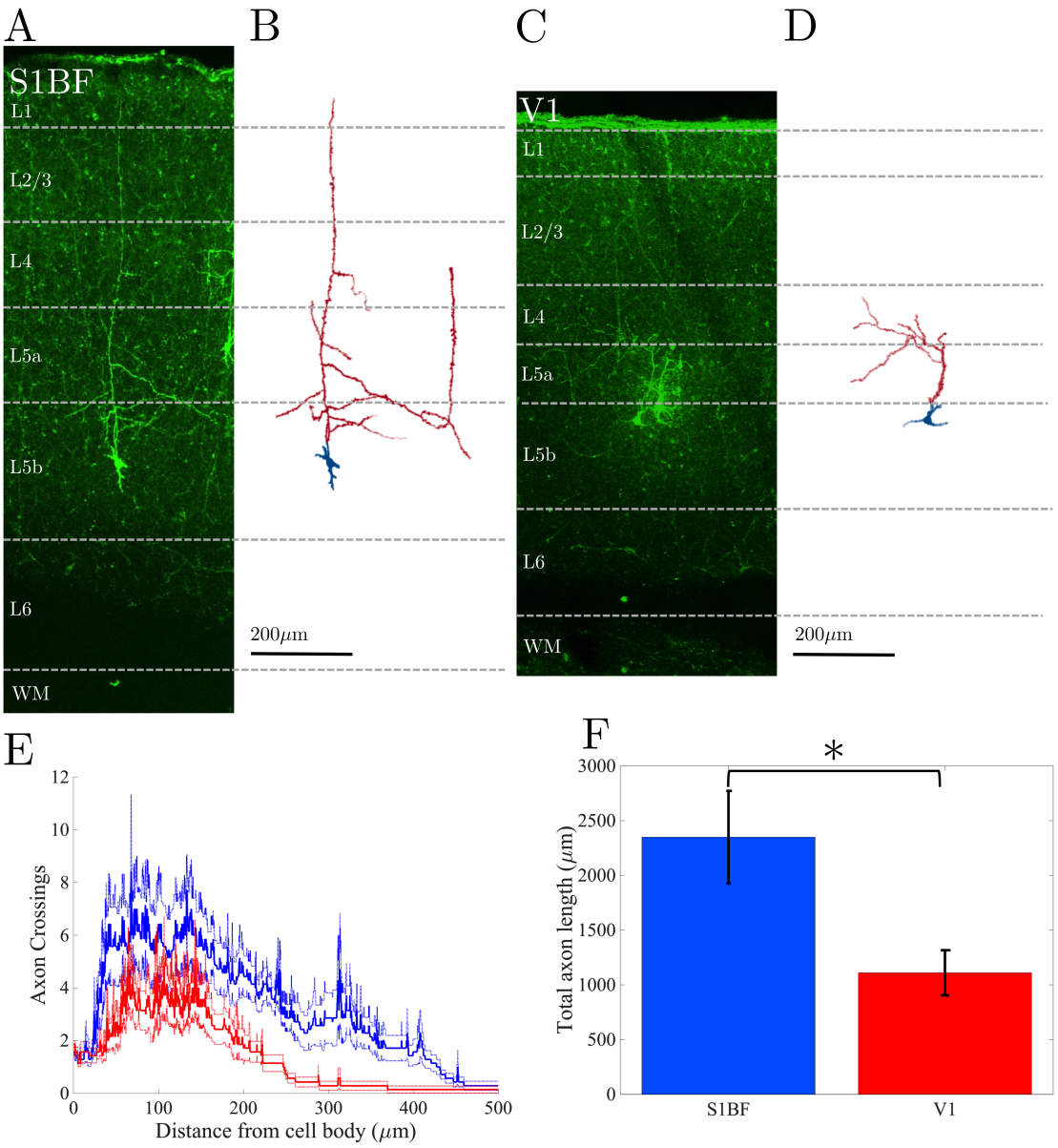


Figure 5.1: **Morphologies of Lpar1-EGFP cells in S1BF and V1 A).** Layer 5b S1BF Lpar1-EGFP cell stained with streptavidin/GFP. **B)** Reconstruction of A) with the dendrite shown in blue and the axon shown in red. **C)** Layer 5b V1 Lpar1-EGFP cell stained with streptavidin/GFP. **D)** Reconstruction of C) with the dendrite shown in blue and the axon shown in red. **E)** Linear Scholl plot of Lpar1-EGFP S1BF cell axons (n = 7, blue) and Lpar1-EGFP V1 cell axons (n = 7, red). The solid line is the mean number of crossings, while the dotted lines above and below are the standard error of the mean. **F)** Mean total axon length for Lpar1-EGFP S1BF cells (blue) and Lpar1-EGFP V1 cells (red). Error bars are standard error of the mean. $p<0.05$ Statistical analysis used the two-sided Wilcoxon rank sum test for independent samples. Data from 4 animals each for V1 and S1BF

immunohistochemistry staining of Lpar1-EGFP and SST+ve cells was carried out to quantify any differences in the cell populations. Lpar1-EGFP cells were stained using an anti-GFP primary antibody to detect expressed EGFP. SST+ve cells were stained with an anti-RFP primary antibody in mice, which expressed RFP under the control of the SST-Cre driver line (Figure 5.2). Cells in each layer of the cortex across a width of 1270 μm were counted. For each individual animal, three separate sections of tissues were counted. The somatosensory cortex was consistently deeper than the visual cortex. This was corrected for in the final cell counts.

The primary somatosensory cortex contained significantly ($p<0.05$) more Lpar1-EGFP cells in layer 5a and 5b (Figure 5.3A). This was consistent with observed cell density during *in vitro* recordings. This increase in S1BF Lpar1-EGFP cells, relative to V1 in lower layers, is also reflected in the normalised distribution across layers. There is a significantly ($p<0.05$) larger percentage of the total cell count of Lpar1-EGFP cells in layer 5a (Figure 5.3B).

The total number of SST+ve cells does not follow the same trend as Lpar1-EGFP. There are more SST+ve cells in V1, with significantly ($p<0.05$) more SST+ve cells in V1 layer 4, compared to S1BF (Figure 5.3C). However, the normalised distribution of SST+ve cells shows that SST cells in V1 are distributed more evenly across the cortex with significantly ($p<0.05$) more cells, as a percentage of the total cell count, in layer 4. SST+ve cells in S1BF are found more in lower cortical layers, with a significantly ($p<0.05$) larger percentage of the total cell count found in layer 5b (Figure 5.3D).

The distribution of SST+ve and Lpar1-EGFP cells in the subplate was different between S1BF and V1. Significantly ($p<0.05$) more of both SST and Lpar1-EGFP cells as a percentage of the total cell count were found in V1 subplate compared to S1BF. The total number of SST+ve cells was also significantly greater in V1 subplate compared to S1BF subplate.

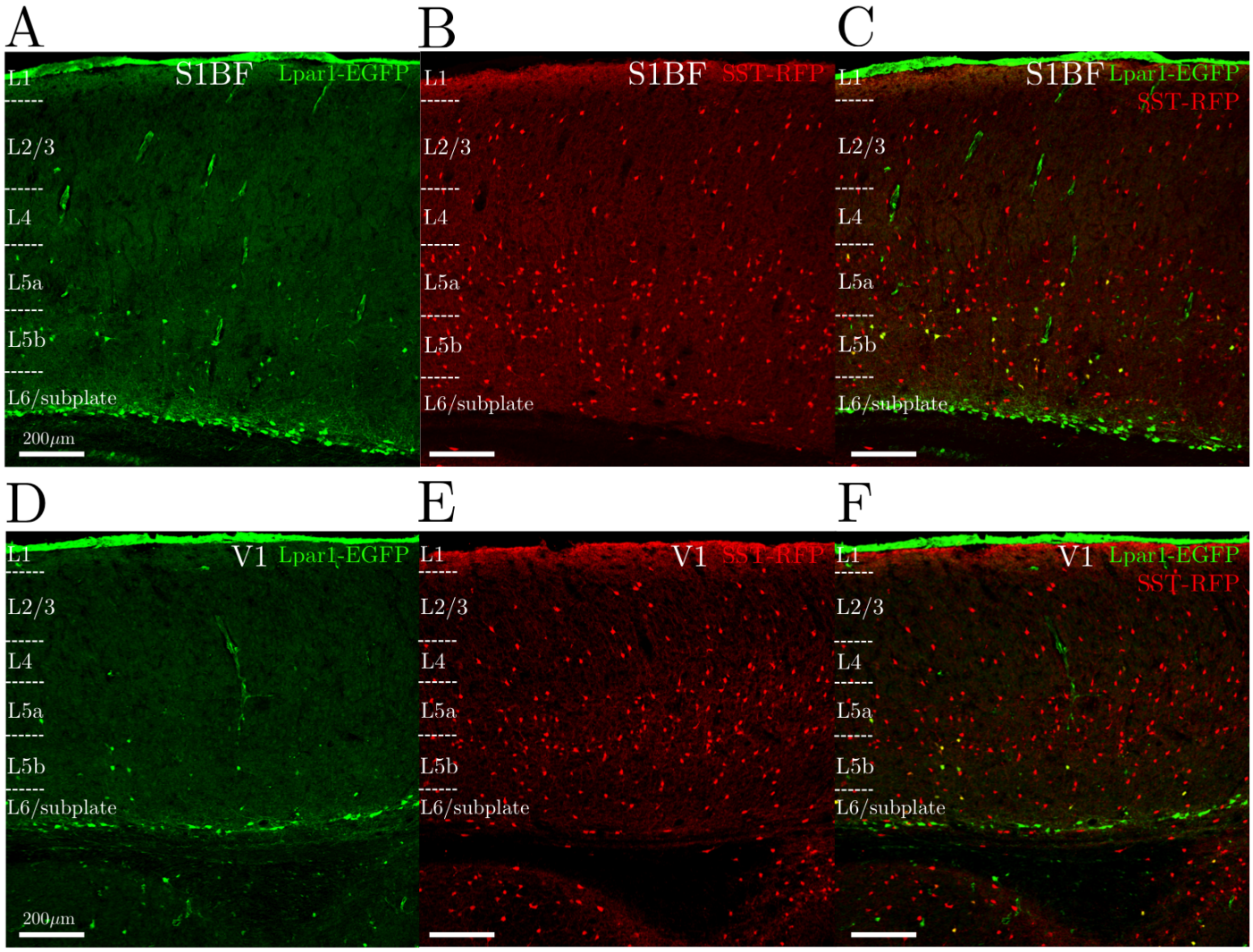


Figure 5.2: **Anti-GFP and anti-RFP immunohistochemistry showing the distribution and density of Lpar1-EGFP (green) and SST+ve (red) cells in V1 and S1BF of a P21 mouse**. **A)** Anti-GFP staining, showing Lpar1-EGFP cells in S1BF. **B)** Anti-RFP staining, showing SST cells in S1BF. **C)** Composite image of anti-GFP and anti-RFP staining, showing the overlap of Lpar1-EGFP and SST+ve cells in S1BF. **D)** Anti-GFP staining, showing Lpar1-EGFP cells in V1. **E)** Anti-RFP staining, showing SST cells in V1. **F)** Composite image of anti-GFP and anti-RFP staining, showing the overlap of Lpar1-EGFP and SST+ve cells in V1. Scale bar is 200 μm.

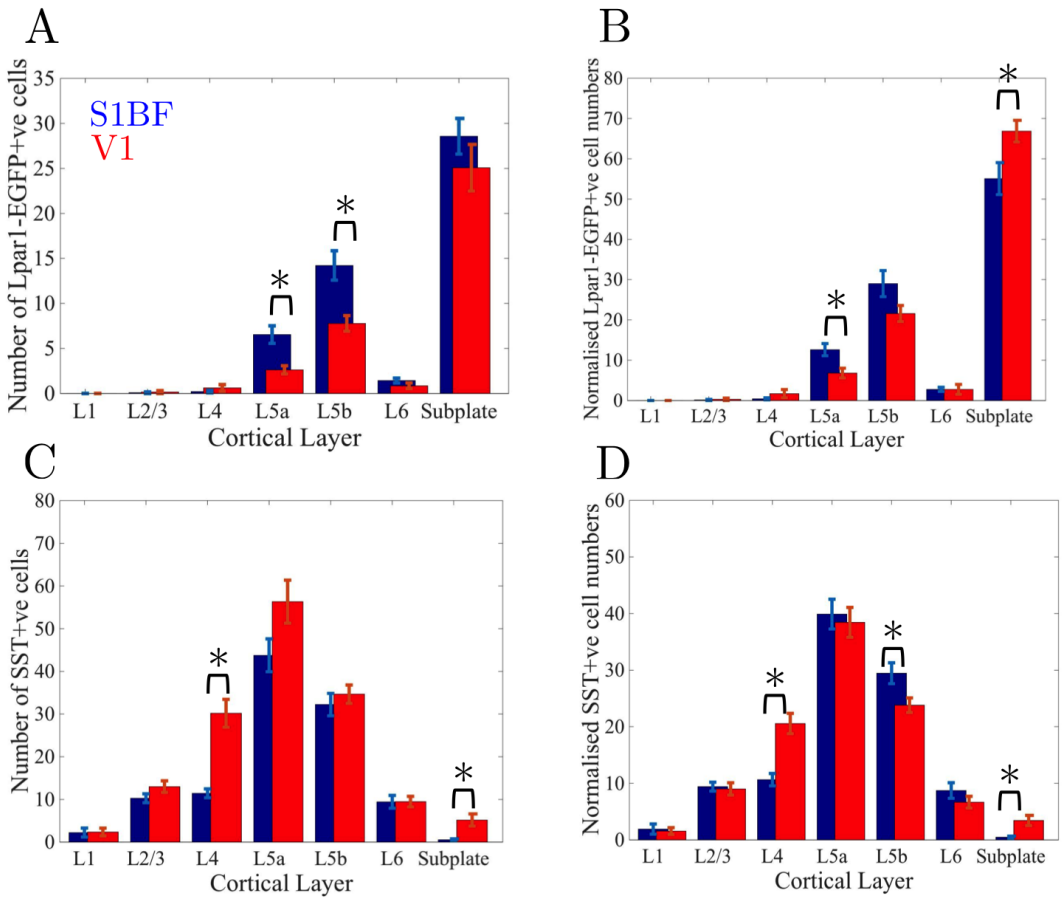


Figure 5.3: **Cell counts for Lpar1-EGFP and SST+ve cells in S1BF and V1. A)** Cell counts for Lpar1-EGFP cells in S1BF and V1, correcting for differences in cortex depth (P10 (n = 3) and P21 (n = 2) mice). **B)** Normalised cell counts for Lpar1-EGFP cells in S1BF and V1, showing layer distribution (P10 (n = 3) and P21 (n = 2) mice). **C)** Cell counts for SST+ve cells in S1BF and V1, correcting for differences in cortex depth (P21 (n = 2) mice). **D)** Normalised cell counts for SST+ve cells in S1BF and V1, showing layer distribution (P21 (n = 2) mice).

5.2 Characterisation of Olig3|Ai32

The mouse lines used for optogenetic stimulation of thalamo-cortical connections were characterised and validated in a number of ways, to ensure that subsequent experiments would have the desired conditional expression and function of channelrhodopsin-2 in neonatal pups.

To investigate differences in thalamocortical connections during development in both primary somatosensory and primary visual cortices of neonatal mice, an optogenetic activator expression under the control of a thalamus-specific promoter was used. A thalamus-specific Cre driver line was chosen to conditionally express channelrhodopsin, thereby allowing stimulation of cut thalamo-cortical axons (Petreanu et al., 2007). This is possible due to the presence of ChR2 in the cut axon terminals. This line was particularly suitable, as it showed broad expression in the thalamus, including both the ventral posteromedial nucleus (VPM), projecting to S1 and the lateral geniculate complex, projecting to V1 (García et al., 2015). Other thalamic-specific Cre driver lines, such as *VGlut2*$^{\text{cre}/+}$, did not have as broad an expression profile in the thalamus (García et al., 2015).

Importantly, *Olig3*$^{\text{cre}/+}$ did not show any expression in cortical cells (García et al., 2015). Any expression of a channelrhodopsin in cortical cells would have made it difficult to confirm that evoked responses were the result of thalamic connections and not intra-cortical connections. The absence of cortical cell expression was confirmed in both acute *in vitro* slices and through immunohistochemistry (Figure 5.4).

After brain tissue slicing, animals expressing Ai32/EYFP under the control of Olig3 were apparent by viewing live slices under a microscope with fluorescent light (Figure 5.4B and E). Figure 5.4A, B, D and E shows both S1 and V1 slices under DIC and fluorescence. Figure 5.4A shows a DIC image of a live P5 slice containing S1BF. The layer 4 barrel structures are visible. The red dotted region indicates a

single barrel. The same S1BF P5 slice is shown in 5.4B. In this panel, the EYFP fluorescence in layer 4 and layer 5b is clearly visible and comparable to previous characterisation (García et al., 2015). A similar distribution of fluorescence, with the brightest fluorescence in layer 4, is seen in the primary visual cortex at P5 (Figure 5.4D and E).

The presence of fluorescent thalamic afferents in V1 and S1BF confirmed that Olig3cre-driven Ai32|EYFP was expressed in both VPM and lateral geniculate nucleus (LGN) and that, by P5, there was sufficient expression in thalamic axons to be observed in live slices. This observation suggested that Ai32 would be sufficiently expressed to elicit evoked responses in early neonates. The efficacy of ChR2 to characterise thalamocortical connections at young ages, albeit via thalamic viral injection, is supported by Tuncdemir et al. (2016).

To further confirm that the *Olig3*$^{cre/+}$ mice had the same expression pattern as that which was previously reported (García et al., 2015) and that thalamic axons expressing the channelrhodopsin-2—EYFP fusion protein were reaching V1, sections of *Olig3*$^{cre/+}$/Ai32 brain were fixed and immunostained for EYFP.

Figure 5.4C and F show anti-EYFP immuno-histochemistry of an P10 Olig3|Ai32 mouse for both S1BF and V1. Using immunohistochemistry, the more prominent L4 and L5b EYFP fluorescent from thalamic axons is clearly seen in both S1BF and V1. When an intensity profile of S1BF and V1 EYFP immunohistochemistry is created, both L4 and L5b show increased brightness, compared to neighbouring layers (Figure 5.4C and F).

5.2.1 Characterisation of channelrhodopsin-2 response

Ai32 mice express a channelrhodopsin-2/EYFP fusion protein, following exposure to Cre recombinase. These mice can be used in optogenetic studies for rapid *in vivo* activation of excitable cells by illumination with blue light (450-490 nm). The Ai32

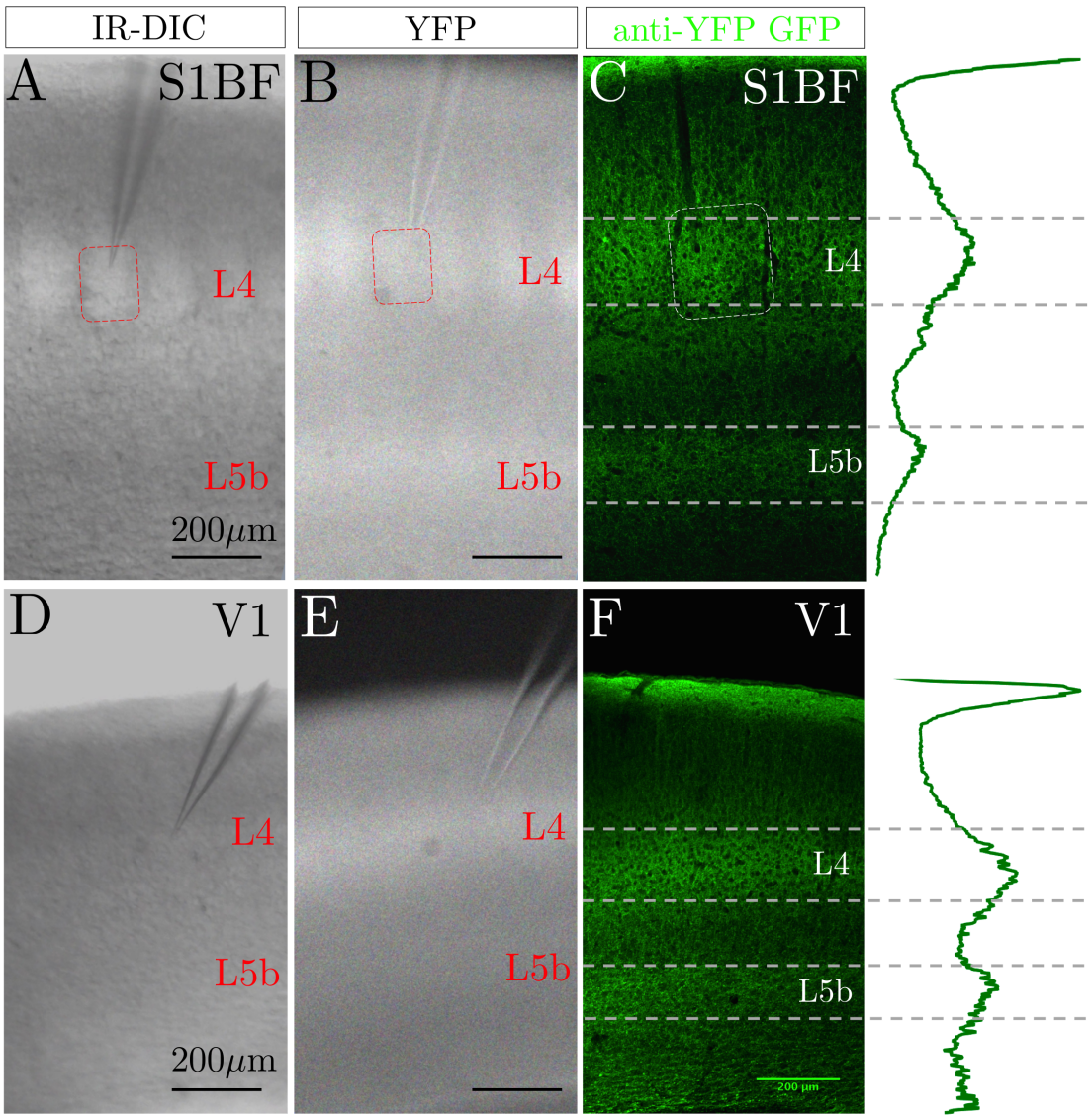


Figure 5.4: **Characterisation of EYFP cortical expression in the Olig3|Ai32 mouse**. **A, B, D, E)** DIC and fluorescent images of P5 live acute *in vitro* brain slices of Olig3|Ai32. **A)** DIC image of an S1BF slice, showing barrels. The red dotted line outlines a single barrel. **B)** The same S1BF slice as panel A, showing EYFP fluorescence in layer 4 and layer 5b. Again, the red dotted line outlines a single barrel in layer 4. **D)** DIC image of a V1 slice. **E)** The same V1 slice as panel D, showing EYFP fluorescence in layer 4 and layer 5b. **C), F)** Anti-EYFP immunohistochemistry of a P10 Olig3|Ai32 mouse, showing expression of EYFP in the thalamic fibres innervating S1BF and V1. **C)** EYFP expression in the thalamic fibres innervating S1BF with higher EYFP expression in layer 4 and layer 5b. **F)** EYFP expression in the thalamic fibres innervating V1 with higher EYFP expression in layer 4 and layer 5b. Intensity profile for both C and F shown to the right of the images. Scale bars are 200μm.

channelrhodopsin mouse line has previously been demonstrated to have sufficient expression at young ages (P8-12) to elicit reliable EPSCs when stimulated (García et al., 2015). Other studies have shown that viral injection of ChR2 into the thalamus results in cortical-evoked EPSCs from P5 (Tuncdemir et al., 2016).

Whether animals as young as P5 had adequate levels of ChR2 when driven by Olig3 to stimulate thalamic cells and axons was not known. Therefore, both thalamic cell responses and cortical EPSCs evoked from stimulation of cut thalamic afferents were characterised from P5 onwards.

5.2.1.1 Characterisation of thalamic cell response

To characterise light-evoked responses of channelrhodopsin-2 in neonatal mice, action potentials in thalamic cells were recorded over the time period of study (P5-P18). Figure 5.5A shows the position in the thalamus of a recorded thalamic cell (P12). This particular cell was located in the VPM thalamic nucleus. The position of both the VPM and posterior medial nucleus (POM) were determined using the Allen Brain Atlas (The Allen Institute, 2018). Images of filled thalamic cells were used to confirm that the recorded cell was located in the thalamus. A magnified confocal image of the same thalamic neuron is shown in Figure 5.5B. The morphology of recorded thalamic cells was compared to those previously described for the rodent VPM thalamic nucleus and found to be alike (Chiaia, Rhoades, Fish, & Killackey, 1991; Brecht & Sakmann, 2002). Intrinsic electrophysiological properties for all thalamic cells were recorded to verify cell identity. Examples of current injection for a P12 mouse is shown in Figure 5.5C and D. All thalamic cells which were recorded had a distinctive rebound spike after hyperpolarization, as previously published (Figure 5.5C) (Landisman & Connors, 2007; Chiaia et al., 1991; Brecht & Sakmann, 2002). Thalamic cells were then stimulated with 3 seconds of blue light at increasing light intensities. An example of such a stimulation at 10 W/cm^2 is

shown in Figure 5.5E. The firing frequency and corresponding light intensities for multiple thalamic cells is shown in Figure 5.5F. Each line represents a single cell. The age of the animal is shown at the end of each plotted line. The response to light stimulation varied considerably between cells. At P5, no stimulation intensity was able to elicit action potentials in thalamic cells. However, from P6 onwards, low intensity stimulation was able to cause multiple action potentials, with a frequency of approximately 4 Hz.

5.2.1.2 Characterisation of cortical cell response

The main challenge, when using the *Olig3*$^{cre/+}$;Ai32 mouse line to characterise thalamic input, was determining whether evoked responses were the result of a monosynaptic connection to the thalamus. To verify monosynaptic thalamic inputs on cortical neurons, TTX (in concentrations 0.5μM - 2μM) and 4-AP (in concentrations 300μM - 600μM) were added to the ACSF. This is a common approach for confirming monosynaptic activity (Cho, Deisseroth, & Bolshakov, 2013). Applying TTX, a voltage-gated sodium channel blocker, eliminates polysynaptic transmission within the cortex by preventing action potential propagation.

Blue light-evoked monosynaptic responses from thalamic afferents can be triggered directly by channelrhodopsin-2 excitation. However, this relies on enough channelrhodopsin-2 expression in the pre-synapse to cause sufficient depolarization. To enhance depolarization at presynaptic terminals, 4-AP was added, alongside the TTX, to the ACSF. 4-AP is a blocker of members of the Kv1 family of voltage-activated K^+ channels. The addition of 4-AP increases the depolarization in the synapse by blocking potassium shunting, making direct excitation of the synapse easier. Often, the addition of TTX alone eliminates all evoked responses and 4-AP is needed to rescue the light-evoked response (Root et al., 2014; Cho et al., 2013).

Figure 5.6 shows the effect of TTX on action potentials in a P18 S1BF cortical

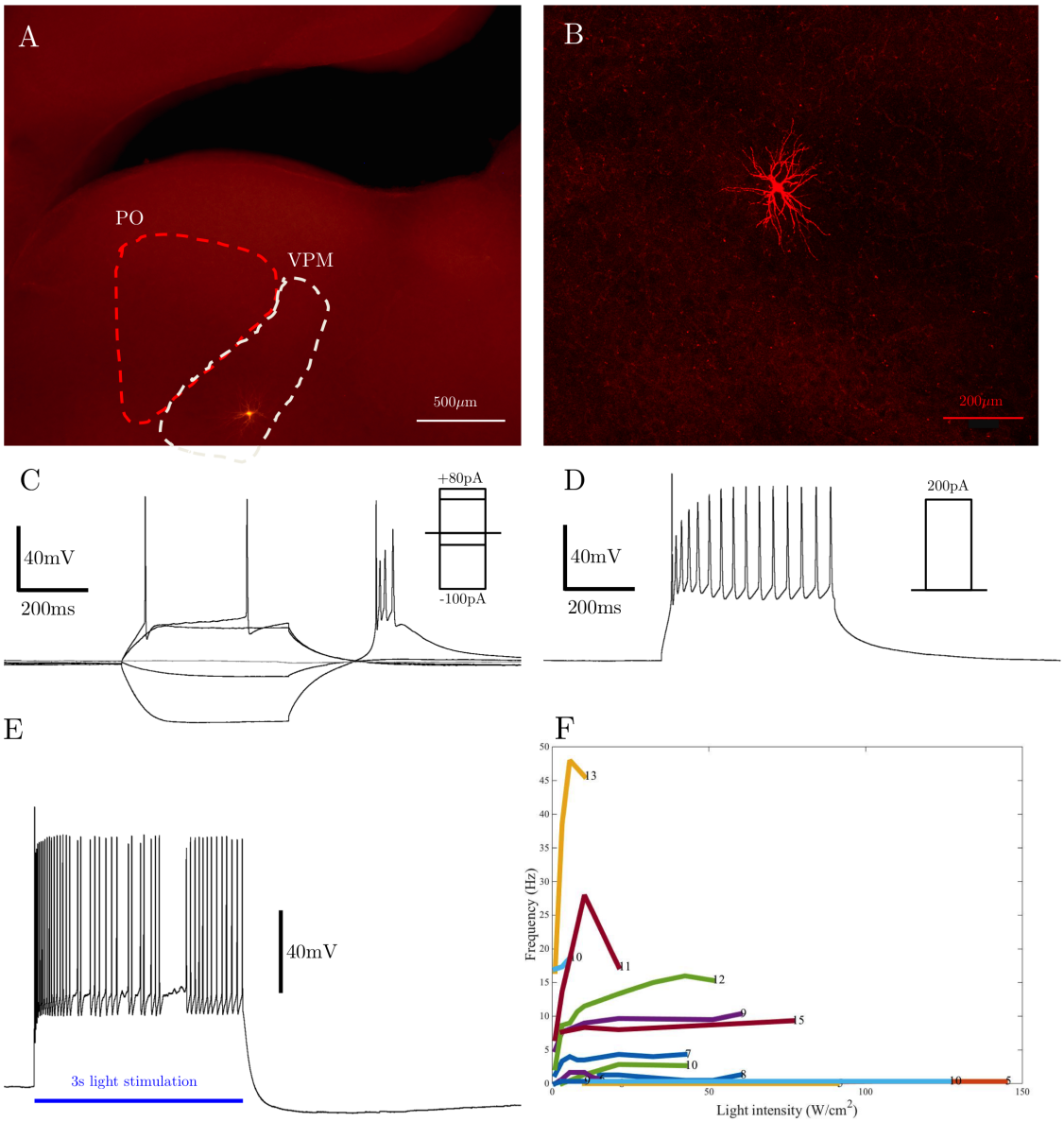


Figure 5.5: **Characterisation of ChR2 expressing thalamic cell response in neonatal Olig3|Ai32 mice to stimulation with blue light. A)** Image of streptavidin-RFP fluorescence of a biocytin filled thalamic cell. The thalamic cell is located in the VPM thalamic nucleus (outlined by the white dotted line). The neighbouring PO thalamic nucleus is outlined with the red dotted line. **B)** A magnified image of panel A, taken using a confocal microscope. **C)** Example trace of a P12 VPM thalamic cell after injection of depolarizing and hyperpolarizing current. **D)** Example trace of a P12 VPM thalamic cell after depolarizing current injection to measure the maximum firing frequency. **E)** Example trace of a P12 VPM thalamic cell after stimulation with three seconds of blue light at 10 W/cm^2 light intensity. **F)** Firing frequency of thalamic cells with respect to light intensity. Each line represents a single thalamic cell. The age for the animal in postnatal days is found at the end of each line.

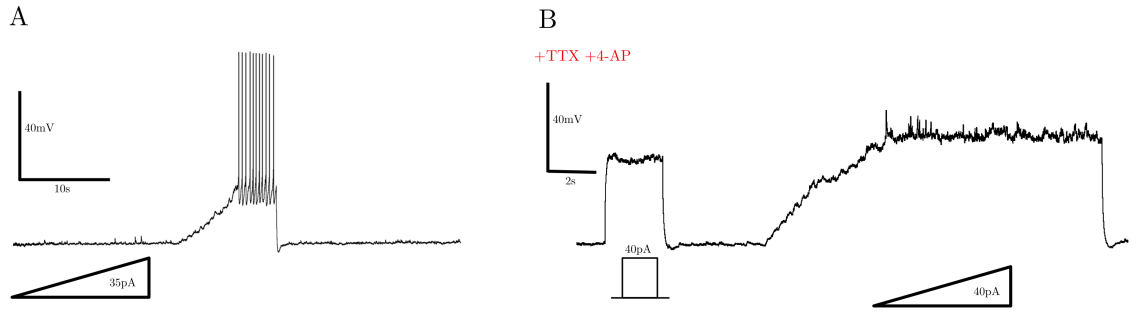


Figure 5.6: **Application of TTX inhibits action potential firing in cortical cells. A)** A P18 S1BF cortical cell firing during a ramped current injection before application of TTX and 4-AP. **B)** The P18 S1BF cortical cell's response to a larger ramped current injection after the addition of TTX (0.5 μM) and 4-AP (600 μM) into the bath solution.

cell. Application of 0.5 μM TTX resulted in the block of the Na_v transient action potential within 6 minutes. Before the addition of TTX, the cell spikes many times upon reaching the spike threshold voltage (Figure 5.6A). Figure 5.6B shows the same cell after the addition of TTX (0.5 μM). Injecting current to raise the cell's membrane voltage above the spike threshold elicits no action potentials from the cell. In this way, the addition of TTX inhibits action potential firing and, therefore, inhibits polysynaptic cortical-cortical connections.

In all recorded cells in animals younger than P17, the addition of TTX and 4-AP abolished all blue light-evoked responses from ChR2-EYFP loaded thalamic neurons. This could be due to either insufficient ChR2 in the pre-synapse or small initial evoked response amplitudes. This finding is consistent with previous reports. Marques-Smith et al. (2014) finds that evoked responses of less than 20 pA are abolished in the presence of TTX and cannot be rescued by the addition of 4-AP (Marques-Smith, 2014).

Only cells from P17 onwards were observed to have clear evoked responses after drug application. Figure 5.7A shows the effect of TTX and 4-AP on cells younger than P17. In all P17+ recordings, the amplitude of the response post-TTX is greatly

reduced. From P17 onwards, cells showed light-evoked monosynaptic responses in the order of 15 pA after TTX and 4-AP was added (Figure 5.7B). This reduction of response amplitude after TTX addition is shown for a single P18 layer 4 S1BF cell in Figure 5.7C-F. In Figure 5.7C, before drug addition, the evoked response is consistent and around 49 pA. Figure 5.7D shows the Figure 5.7C response enhanced, to more clearly see the latency and amplitude variability of the evoked response. Figure 5.7E and F show the same cell-evoked response after addition of TTX (0.5 μM) and 4-AP (600 μM). Although the response is consistently evoked, the amplitude has decreased to 8 pA.

For stimulation of thalamic afferents in S1BF and V1, stimulation protocols varied between age groups. Light stimulation lasting 10 ms was used in younger (<P10) mice, as 1ms stimulation did not evoke any responses. The response to 1 ms stimulation for P5-P18 cells is shown in Figure 5.8H. No evoked response was present in cells P5-P9, regardless of the intensity of LED stimulation. From P10 onwards, 10 ms stimulation was too long to observe minimal stimulation intensity and, therefore, the stimulation duration was shortened to 1 ms.

Both the length of the stimulation and strength of the blue light were observed to effect the latency of any evoked response. This was true both with and without addition of TTX and 4-AP. The variability in response latency can be seen in a P10 S1BF Pyramidal cell in layer 5b (Figure 5.8E-G). Figure 5.8E shows the evoked response to 10 ms of blue light stimulation, resulting in a 12 ms response latency (8 W/cm^2). When the cell is stimulated with a shorter (1 ms), stronger (60 W/cm^2) light stimulus the response latency shortens to 8.4 ms (Figure 5.8F). The response latency shortens further to 6 ms when the stimulation light intensity increases to 1 ms at (90 W/cm^2)(Figure 5.8G). This variability in response latency was also observed in monosynaptic responses, confirmed through the use of TTX and 4-AP. Figure 5.8 shows the change in the evoked response in a S1BF spiny stellate cell

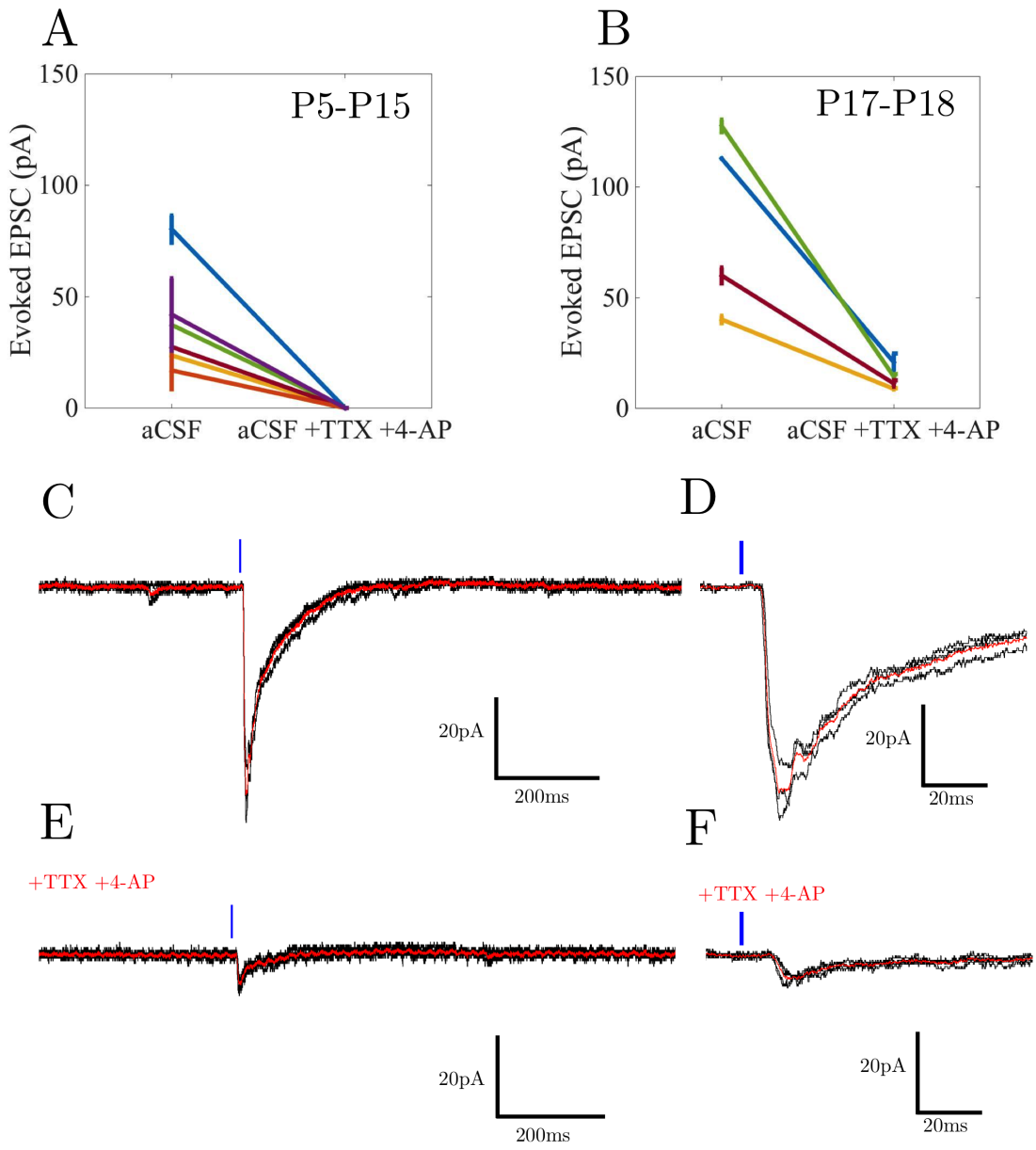


Figure 5.7: **The addition of TTX and 4-AP greatly reduces response amplitudes and eliminates evoked-responses in cells younger than P17. A)** Mean and SEM light-evoked response amplitudes for P5-P15 cells before and after TTX and 4-AP addition. **B)** Mean and SEM light-evoked response amplitudes for P7-P18 cells before and after TTX (0.5μM) and 4-AP (600μM) addition. **C-F)** Excitatory evoked responses in a P18 layer 4 S1BF cell after 1 ms blue light stimulation of thalamic axons before (49 pA response amplitude) and after TTX and 4-AP addition (8 pA response amplitude). **C)** Evoked responses to 1 ms blue light stimulation. **D)** An enhanced panel of the responses shown in C). **E)** Evoked responses to 1 ms blue light stimulation after addition of TTX and 4-AP. **F)** An enhanced panel of the responses shown in E). In all panels C-F, the black traces represent single stimulation sweeps and the red trace is the average of all sweeps. Blue lines represent the duration of the blue light stimulation.

after 1 ms and 10 ms light stimulation before and after TTX and 4-AP addition. Figure 5.8A and B show the evoked response to 1 ms light stimulation at 5.6 W/cm^2 before addition of TTX and 4-AP. Here, the response latency is 7 ms. Figure 5.8C and D show the same cell after the addition of TTX and 4-AP. The response latency for 10 ms light stimulation after addition of both drugs is 19 ms at 0.94 W/cm^2. Therefore, the latency of monosynaptic responses can be varied by the stimulation parameters.

5.2.1.3 Characterisation of evoked EPSC jitter

In Figure 5.8, response latency varies greatly within a single cell. Even after the addition of both TTX and 4-AP, a response latency of 19 ms was recorded, indicating that the kinetics of channelrhodopsin-2 stimulation could result in a monosynaptic connection with a long recorded latency. Because of this inconsistency, response latency appears to be an unreliable yardstick for determining whether an evoked response is monosynaptic in nature. The addition of TTX and 4-AP, although able to elucidate monosynaptic connections in recordings in older animals (P17-P18), abolished all evoked responses in younger animals. Therefore, a third parameter, 'jitter' was required to aid in the classification of responses, as either mono- or polysynaptic.

Response latency jitter is the variability of response latency over multiple sweeps. This is measured as the standard error of the latency (ms). For cells with monosynaptic connections from thalamic afferents, the evoked responses are expected to be more consistent than polysynaptic inputs and, therefore, have lower 'jitter' (0.59 ms $\pm$ 0.34 ms) (Petreanu et al., 2007).

Figure 5.9A shows the standard error of evoked response latencies plotted with respect to animal age. There does not appear to be an age-dependent change in latency jitter and, therefore, the same jitter threshold for monosynaptic classification

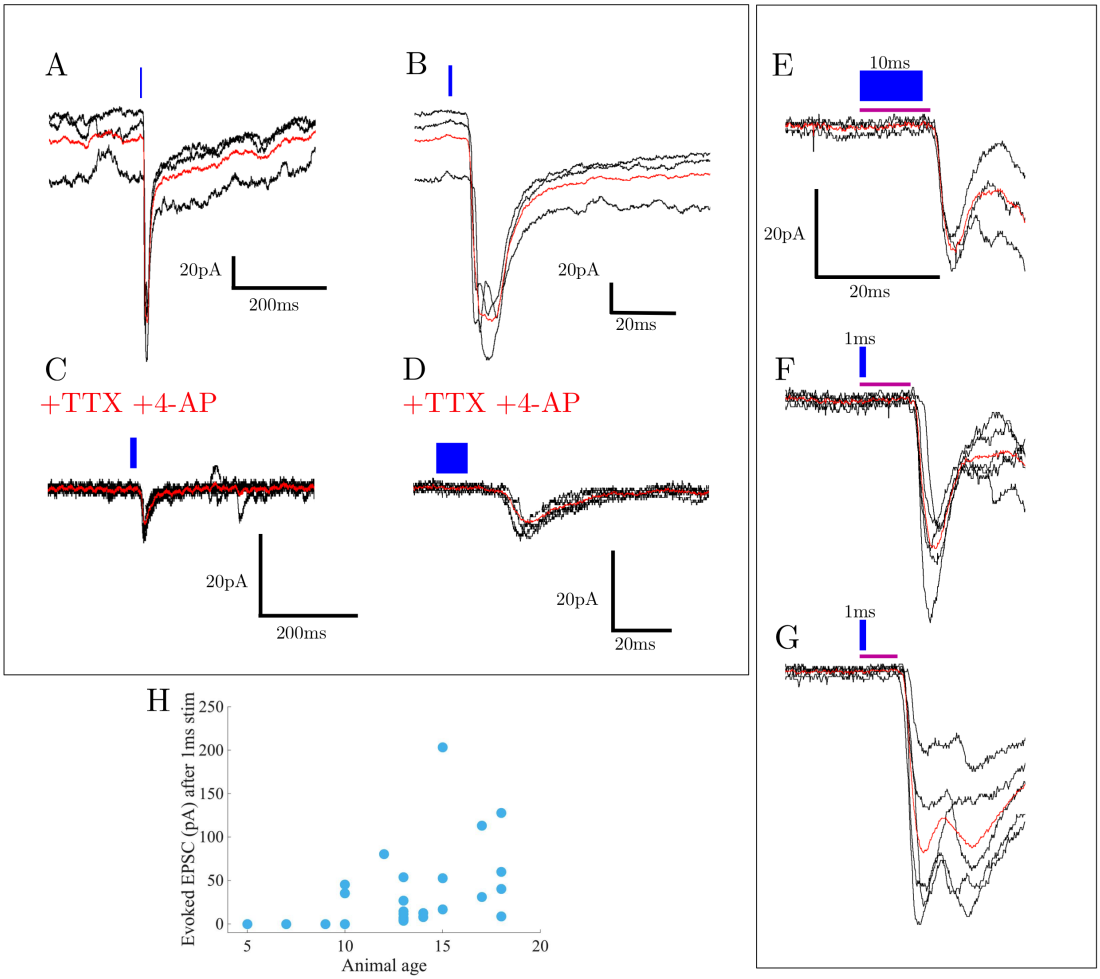


Figure 5.8: **Strength and duration of blue light stimulation alters evoked response latency with and without TTX**. **A-D)** Excitatory evoked responses in a P17 spiny stellate cell in S1BF L4 after both 1 ms and 10 ms of blue light stimulation of thalamic axons. **A)** and **B)** Evoked response in a spiny stellate cell after 1 ms stimulation of channelrhodopsin-2 expressed in thalamic afferents (5.6 W/cm^2). The brain slice is submerged in ACSF bath solution. **C)** and **D)** Evoked response in a spiny stellate cell after 10 ms stimulation of channelrhodopsin-2 expressed in thalamic afferents (0.94 W/cm^2). The brain slice is submerged in ACSF bath solution with TTX (0.5 μM) and 4-AP (600 μM). **E-G)** Excitatory evoked responses in a P10 Pyramidal cell in S1BF L5b after both 1 ms and 10 ms of blue light stimulation of thalamic axons. **E)** Excitatory evoked responses in a P10 Pyramidal cell in S1BF L5b after 10 ms stimulation (8 W/cm^2). **F)** Excitatory evoked responses in a P10 Pyramidal cell in S1BF L5b after 1 ms stimulation (60 W/cm^2). **G)** Excitatory evoked responses in a P10 Pyramidal cell in S1BF L5b after 1 ms stimulation (90 W/cm^2). Black traces show each stimulation sweep. The red trace is the average of all sweeps. Blue lines represent the duration of the blue light stimulation. Magenta lines show the length of the response latency. **H)** Amplitude of evoked EPSCs to 1 ms stimulation for ages P5-P18.

was deemed appropriate for all recordings. There is a slight age-dependent change in the mean latency of evoked responses (Figure 5.9B). The spread of all mean response latencies is shown in Figure 5.9E and indicates that there is no clear bimodal distribution that could represent mono- and poly-synaptic evoked responses.

Figure 5.9C shows the jitter of all evoked responses (both mono- and polysynaptic), plotted with respect to mean latency, indicating the spread of all responses. Figure 5.9D shows that all EPSCs, after the addition of TTX and 4-AP, have a latency jitter below 0.85 ms. This was in line with reported jitter for monosynaptic responses from ChR2 activation (Petreanu et al., 2007). Therefore, 0.85 ms was the threshold for jitter used to classify monosynaptic responses. Additional restrictions on the inclusion of responses for further analysis included a threshold of 10% or greater response probability, as jitter could not be calculated for cells with only one EPSC.

5.3 Functional thalamocortical synapses during neonatal development in S1 and V1

The development of monosynaptic thalamic input onto cells in L4 and L5b of both S1BF and V1 was interrogated using the *Olig3*$^{cre/+}$/Ai32 mouse line. After filtering all recorded responses for response probability and jitter, the amplitudes of these evoked EPSCs that were classified as monosynaptic were plotted with respect to animal age (Figure 5.10). Cells which fell outside the monosynaptic classification were plotted alongside with an amplitude of zero.

Figure 5.10A shows evoked excitatory responses in layer 4 cells within S1BF. P5 was the youngest age recorded from. At P5 monosynaptic thalamic input onto spiny stellates was seen in layer 4 of S1BF (Figure 5.10A). In the visual cortex, the first cell receiving thalamic input in L4 was a P6 Pyr cell (Figure 5.10B). In

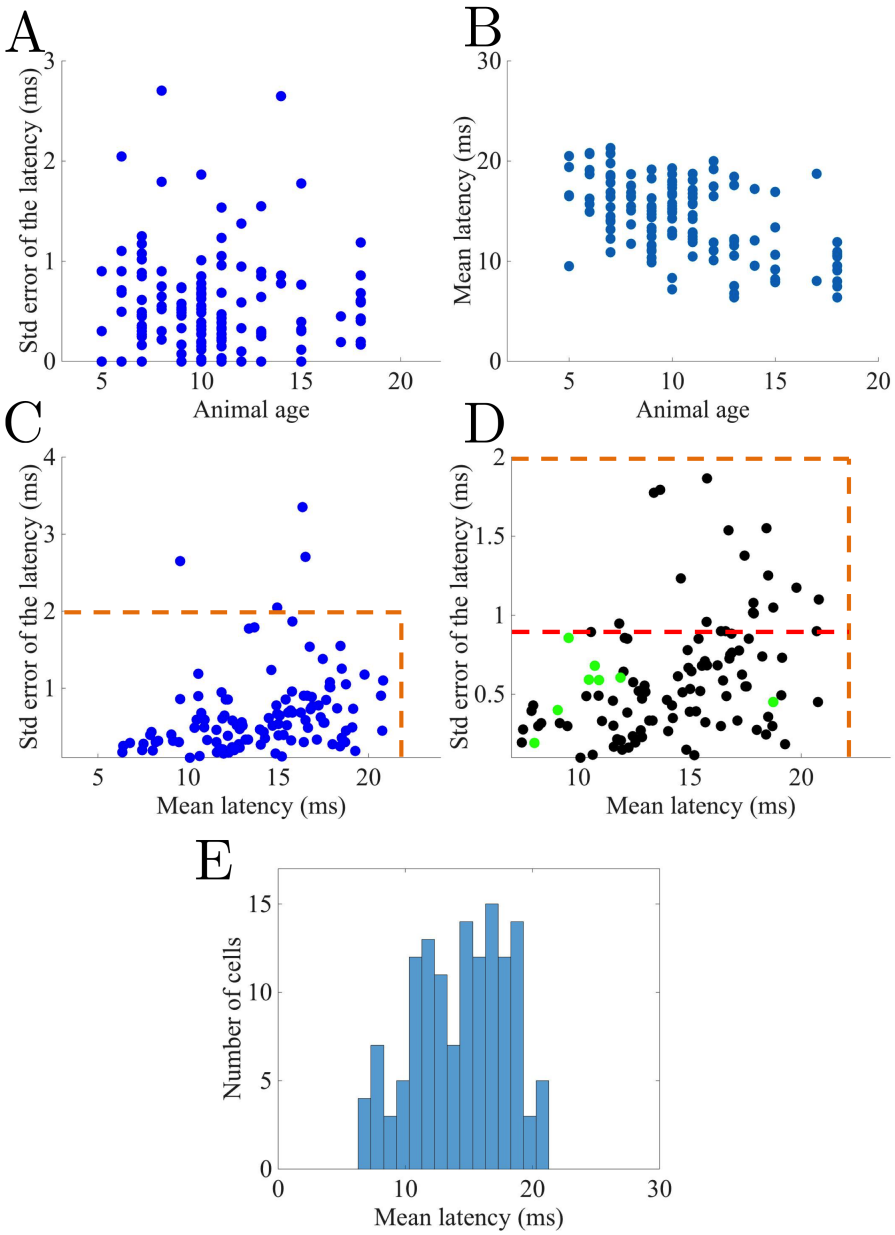


Figure 5.9: **The standard error of the latency of evoked responses plotted with respect to mean response latency. A)** Standard error of the evoked EPSC latency (jitter) with respect to animal age. **B)** Mean latency of evoked EPSC with respect to animal age. **C)** All recorded responses (blue). The orange dotted outline is enlarged in D. **D)** Evoked responses without TTX and 4-AP (black) and after the addition of TTX and 4-AP (green). Red dotted line represents the jitter threshold used to classify monosynaptic responses. **E)** Histogram of mean EPSC latency for all evoked responses. Data from n=22 animals

layer 5b of S1BF, monosynaptic inputs from the thalamus were first observed at postnatal day 9. These responses were recorded in fast-spiking and non-fast-spiking interneurons (Figure 5.10C). From P10 onwards, monosynaptic connections from the thalamus into layer 5b of S1BF were also observed in excitatory pyramidal neurons (Figure 5.10C). In the primary visual cortex, monosynaptic thalamic inputs were first observed in layer 5b at postnatal day 9. This first thalamic connection was observed in a FS IN (Figure 5.10D).

All of the recorded cells with monosynaptic input at this age in 5b were interneurons (both fast-spiking and non-fast-spiking). The first excitatory cell to receive monosynaptic thalamic input into layer 5b of the visual cortex was at age P12 (Figure 5.10D). In layer 4 of the primary visual cortex, only pyramidal cells were observed to receive monosynaptic thalamic input. From these data, it appears that for both V1 and S1, interneurons receive the first thalamic input in layer 5b, while in layer 4, excitatory cells are the first to receive thalamic input. V1 appears to receive input slightly later (P6 as compared to P5) than S1. Layer 5b receives input at the same time point in both S1 and V1.

Although the timing of thalamic innervation is similar between S1BF and V1, the percentage of connected cells in older (P9+) animals differed between the cortical regions and layers. Both L4 (10/15) and L5b (5/15) in V1 had a lower percentage of connected cells, compared to S1BF L4 (17/19) and L5b (10/11) (Figure 5.11B). The light-evoked amplitudes of connected cells also differed between S1BF and V1. For young mice (P5-P8), the mean amplitude of an evoked EPSC was higher than for V1, although not significantly so (Figure 5.11C). For older (P9+) animals, the mean amplitude of an evoked EPSC was significantly ($p<0.01$) greater in S1 L4 than for V1 L4 (Figure 5.11D).

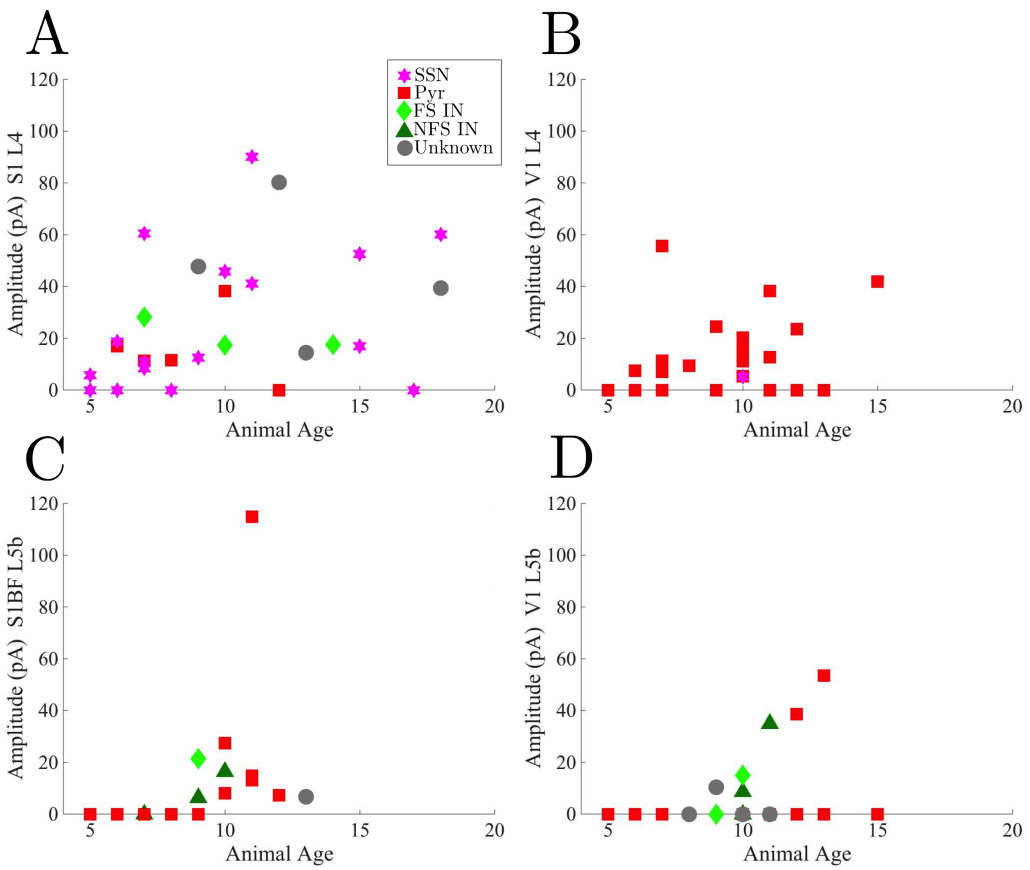


Figure 5.10: **Amplitude of evoked excitatory responses in S1BF and V1 after optogenetic stimulation of thalamic afferents with respect to age. A)** Evoked excitatory responses after optogenetic stimulation of thalamic afferents in S1BF layer 4. **B)** Evoked excitatory responses after optogenetic stimulation of thalamic afferents in V1 layer 4. **C)** Evoked excitatory responses after optogenetic stimulation of thalamic afferents in S1BF layer 5b. **D)** Evoked excitatory responses after optogenetic stimulation of thalamic afferents in V1 layer 5b. Cell subtype is shown as either SSN (magenta star), Pyramidal (red square), FS IN (bright green diamond), NFS IN (dark green triangle) or unknown cell morphology (grey circle). Data from n=22 animals

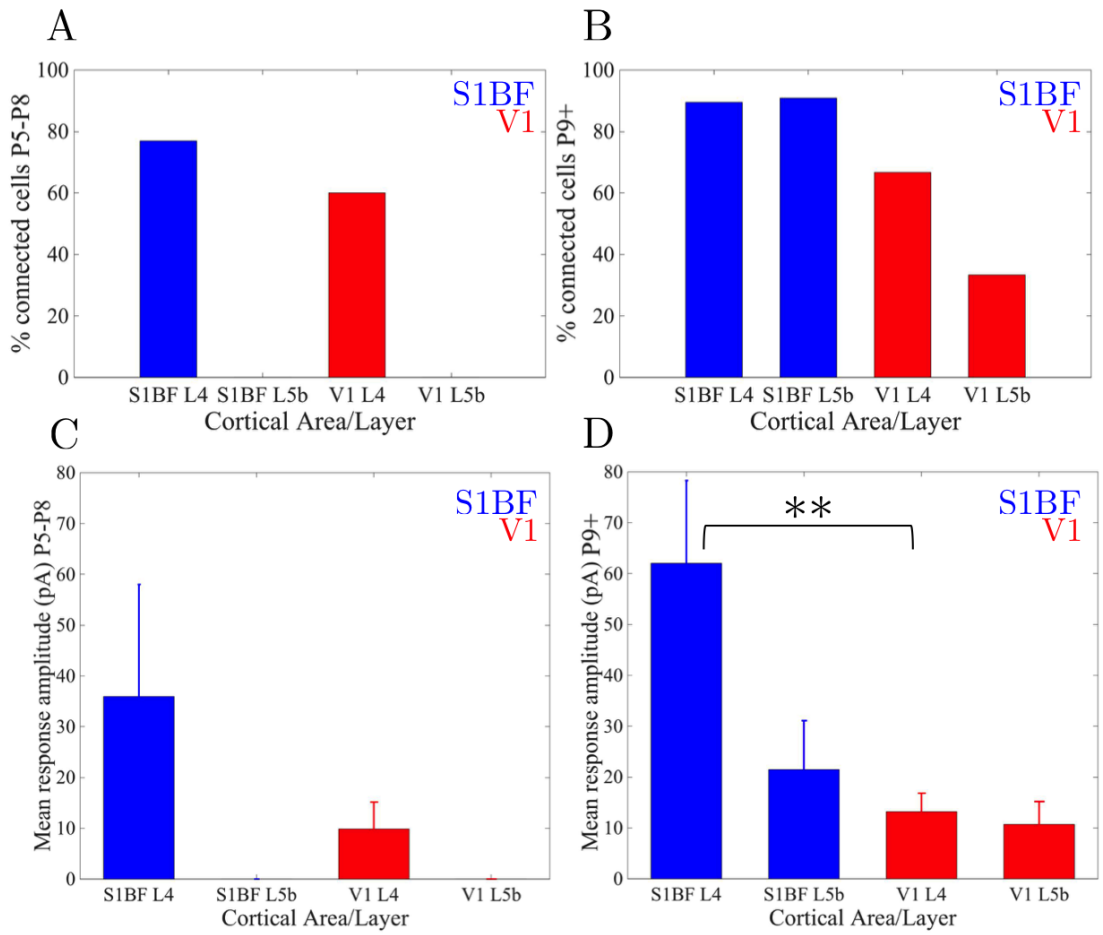


Figure 5.11: **The percentage of cells that appeared to receive monosynaptic input from the thalamus. A)** The percentage of cells for ages P5-P8 which appeared to receive monosynaptic input from the thalamus. n=13 for S1BF L4, n=7 for S1BF L5b, n=10 for V1 L4, n=6 for V1 L5b. **B)** The percentage of cells for ages P9+ which appeared to receive monosynaptic input from the thalamus. n=19 for S1BF L4, n=11 for S1BF L5b, n=15 for V1 L4, n=15 for V1 L5b. **C)** Mean and SEM for evoked response amplitudes for P5-P8 cells sample sizes=same as A) **D)** Mean and SEM for evoked response amplitudes for P9+ cells. Sample sizes are the same as in B). **=$p<0.01$ Statistical analysis used the two-sided Wilcoxon rank sum test for independent samples. Data from n=22 animals

5.3.1 Discussion

5.3.1.1 Lpar1-EGFP cell morphologies and distributions

The density and distribution of Lpar1-EGFP and SST+ve cells was found to be different between S1BF and V1 for both cortical layers and the subplate. In S1BF, significantly more Lpar1-EGFP cells in layers 5a and 5b were found than in V1. Additionally, the distribution of SST+ve cells across the layers shows that for V1, there are more SST+ve cells in layer 4 and subplate, while in S1BF, more SST+ve cells were found in L5b.

These differences in cell distribution point to a possible different role for SST+ve cells in V1 compared to S1BF. The reduced density of Lpar1-EGFP cells in layer 5b of the visual cortex points more specifically to a difference in interneuron circuit development. Lpar1-EGFP INs are involved in the L5b-L4 circuit in S1BF. Therefore, the reduced number found in L5b of the visual cortex suggests that the presence of a particular cell type might lead to the creation of the L5b-L4 transient connection.

The question that remains is, how do differences in these cell-types occur? There are three competing explanations for this. Firstly, that once young SST+ve interneurons have arrived in a cortical region, intrinsic factors within the region further specify the particular cell sub-type. Secondly, that intrinsic V1 factors cause Lpar1-EGFP cell apoptosis. Or, thirdly, that Lpar1-EGFP cells preferentially migrate into certain cortical regions. The third explanation relies on nuances of cell migration and, perhaps, expression of guidance cues in cortical areas, while the first two explanations attribute these differences solely to intrinsic cortical factors.

The 'progenitor specification model' and the 'progressive specification model' are two competing theories of how IN subtypes are specified (Wamsley & Fishell, 2017). SST+ve INs, which make up approximately 30% of all INs, are born in the medial ganglionic eminence (MGE) (Rudy et al., 2011) and as an interneuron group, are

already specified by temporal and spatial characteristics of their origin (Miyoshi, Butt, Takebayashi, & Fishell, 2007; Butt et al., 2005; Bandler, Mayer, & Fishell, 2017). There are, however, cell subtypes within the umbrella of 'SST+ve' and the exact mode of cell specification and differentiation is still unclear. (Tasic et al., 2016; Wamsley & Fishell, 2017).

In favour of the progenitor specification model, Mi et al. (2018) showed that single cell transcriptomics of both mature and embryonic interneurons found that nearly a dozen classes of interneuron could be identified shortly after their last mitosis (Mi et al., 2018). However, the role of the cortical environment, and particularly activity dependent transcription factors, has been well documented to influence interneuron cell morphology and synapse formation (Wamsley & Fishell, 2017; Chattopadhyaya et al., 2004; Dehorter et al., 2015; Tuncdemir et al., 2016). It is probable that the function of the final mature IN is a combination of both progenitor specification model and the progressive specification model in that an early genetic blueprint, specified at birth, interacts with the cortical environment to develop appropriate morphology and connections.

This process of specification for Lpar1-EGFP INs in V1 and S1BF is still unclear. In the Lpar1-EGFP mice, GFP expression is driven by a bacterial artificial chromosome (BAC) that is genomically integrated (Hoerder-Suabedissen & Molnár, 2012a). In this BAC, GFP has been inserted into the first codon of the *lpar1/edg2* gene. These mice show GFP expression in a subset of non-GABAergic subplate neurons as well as some GABAergic INs located primarily in cortical layers 5 and 6 (Hoerder-Suabedissen & Molnár, 2012a; Pedraza et al., 2014). From E15.5, GFP expression in Lpar1-GFP mice is observed in the subplate and marginal zone (MZ) with none observed in the cortical plate. By P6 GFP expression is no longer found in the MZ and GFP+ cells were observed in layers 2-6a (Hoerder-Suabedissen & Molnár, 2012a). These GFP+ L5b INs have been shown to be Lhx6+ which may

suggest that they originate from the Nkx2-1+ domain of the ventral telencephalon, the MGE, similar to other SST INs (Marques-Smith et al., 2016). When these Lpar1-EGFP cells become specified and if the two SST IN populations in V1 and S1BF would be classified as the same subtype is not yet clear.

The characterisation of SST+ Lpar-EGFP INs between S1BF and V1 showed that although intrinsic electrophysiological properties remained the same, Lpar1-EGFP cells in S1BF have a more extensive axonal arborisation. The lack of axon extending into superficial layers in V1 may provide an explanation for the lack of L4-L5b connection in V1. The differences in cell morphology between Lpar1-EGFP cells in S1 and V1 are possibly due to activity-dependent transcription factors. Activity-mediated morphology changes have been reported in many cortical neurons; for example, after P3, glutamatergic activity controls the development of both axons and dendrites in reelin (Re)-positive interneurons (García, Karayannis, & Fishell, 2011). For spiny stellates in the ferret, retinal input is required for axon retraction, and in mice, visual input is required for the maturation of perisomatic innervation (Chattopadhyaya et al., 2004). The activity-dependent expression of Etv1/Er81 has also been shown to modulate PV+ cell properties (Dehorter et al., 2015) and elevated expression of the activity-regulated transcription factor Satb1 causes SST INs to mature too quickly (Tuncdemir et al., 2016). In VIP INs, activity regulated Igf1 acts to increase inhibitory synapses onto these INs (Mardinly et al., 2016). Therefore, it is possible that activity also plays a role in morphology changes of Lpar1-EGFP INs.

If Lpar1-EGFP INs are specified before reaching the cortex, the two possible remaining explanations for the difference in cell distribution and number between V1 and S1BF are preferential migration or apoptosis. Multiple studies have shown that the cortex expresses chemoattractive guidance cues to migrating interneurons, which are required for these cells to reach the cortex (Hernández-Miranda, Parnave-

las, & Chiara, 2010; Flames et al., 2004; Pozas & Ibáñez, 2005). It is, therefore, plausible that long-range region-specific guidance cues exist to direct interneuron migration. Once reaching the cortex, interneurons migrate through multiple different zones, including the subventricular zone (SVZ), the intermediate zone (IZ), the subplate (SP) and the marginal zone (MZ) (Tanaka & Nakajima, 2012). It has been shown that perturbation of chemokine signalling results in early invasion of the cortical plate from the MZ and, as a consequence, disrupts laminar and regional IN distribution (López-Bendito et al., 2008; G. Li et al., 2008; Tanaka et al., 2010). It is possible that different cortical regions have intrinsically different chemokines and/or long range guidance cues that cause different IN distributions within these regions.

Recently, it has been published that the migration route of INs through the cortex also influences their morphology (Lim et al., 2018). SST+ve interneurons that migrated through the MZ developed into Martinotti cells with a prominent layer 1 axonal arborisation while INs migrating through the SVZ did not (Lim et al., 2018). Lpar1-EGFP INs have been shown to be Martinotti cells in S1BF (Marques-Smith et al., 2016). Perhaps these INs migrate preferentially through the MZ in S1BF and through the SVZ in V1, resulting in the more extensive axonal arborisation seen in S1BF.

During the first two postnatal weeks, there is a period of controlled interneuron cell death that peaks at P7 (Wamsley & Fishell, 2017; Southwell et al., 2012). In particular, interneuron numbers drop by about 30% between P5 and P10 (F. K. Wong et al., 2018). Survival of interneurons during this time depends on excitatory synaptic input from pyramidal cells and modulation of PTEN signalling (F. K. Wong et al., 2018). In mice deficient in GFRalpha1 signalling, discrete regions of the cortex, predominately in visual and frontal cortices, show complete loss of PV INs, indicating that IN survival can be specific to the cortical region (Canty et al., 2009). It

is possible that the fewer number of Lpar1-EGFP cells in V1, as opposed to S1BF, is as a result of programmed cell death, particularly if these cells lack the circuit connections established in S1BF. Further research is required to understand the underlying cause of interneuron type variation across cortical regions.

Once it was established that V1 and S1BF contained different distributions and numbers of Lpar1-EGFP SST+ve cells (a cell that both receives direct thalamic input and is part of the L5b-L4 circuit) it was hypothesised that S1BF and V1 might also show a different progression of thalamic innervation. The differences in subplate SST+ve IN and Lpar1-EGFP distributions between V1 and S1BF further suggest that thalamic innervation may develop differently between the two cortical areas. Therefore, the Olig3|Ai32 mouse was used to interrogate thalamic input into L4 and L5b of S1BF and V1 during an early developmental window (P5-P18).

5.3.1.2 Thalamocortical input

Regardless of stimulation length or intensity, all evoked EPSCs were abolished upon addition of TTX and 4-AP in animals younger than P17. It is well-known that thalamic afferents innervate the cortex and synapse onto cells well before P17 (López-Bendito & Molnár, 2003; Tuncdemir et al., 2016; Higashi et al., 2005, 2002). Thalamocortical axons reach layer 4 shortly after birth (Yang et al., 2018; López-Bendito et al., 2006; López-Bendito & Molnár, 2003) and from P2, peripheral stimulation is shown to influence cortical oscillations, indicating that these thalamocortical connections are functional. Therefore, the lack of EPSC in TTX-exposed younger cells is not thought to be indicative of an absence of monosynaptic input. The small number of cells which did respond after TTX/4-AP addition were useful in determining other parameters of an EPSC that could be used to classify responses in younger animals. The only parameter used to classify monosynaptic responses was latency jitter. This was because mean latency alone was found to be too variable.

Monosynaptic responses could vary anywhere from the expected 6-8 ms (P30-35, (Petreanu et al., 2007), P5-P21 (Tuncdemir et al., 2016)) to approximately 19 ms. Additionally, stimulation intensity and duration were observed to change the latency response of individual cells, further undermining mean latency as a parameter to classify monosynaptic events. The decrease in spike latency with increased laser power when using ChR2, although via viral injection, has also been reported previously in Petreanu et al. (2007). All evoked EPSCs in cells exposed to TTX and 4-AP had a latency jitter of less than 0.85 ms (Figure 5.9D). As a jitter of 0.85 ms was within the published range for monosynaptic responses (Petreanu et al., 2007) and included all TTX/4-AP EPSCs, this was used as a threshold to segregate all evoked EPSCs into either mono- or poly-synaptic. As age did not affect jitter, the same threshold for monosynaptic classification was deemed appropriate for all recordings.

The recordings of evoked monosynaptic EPSCs onto S1BF and V1 revealed that thalamic innervation occurs in L4 at roughly the same time point, with S1BF slightly earlier (P5) than V1 (P6). The timing of L5b innervation (P9) was the same for both cortical areas. Although the timing of the thalamic innervation was the same between S1BF and V1, the percentage of connected cells, the amplitude of evoked EPSCs, and the cell types receiving thalamic input were all different. Both the smaller number of connected cells and the smaller evoked EPSC amplitudes in V1 might be indicative of delayed maturation of thalamic input onto V1 as compared to S1BF. Thalamic input onto L5b occurs first in INs, both NFS and FS for V1 and S1BF. For S1BF L4, thalamic input was predominately observed in SSNs (11 cells), with three Pyr cells and three FS INs. In contrast, L4 of V1 showed thalamic innervation of almost exclusively pyramidal cells (13 cells). This reflects the different populations of excitatory cells between the two cortical areas, with SSNs abundant in S1BF, but absent in V1. Interestingly, no thalamic input onto FS INs in V1 L4 was observed. This could be attributed to the later critical period (P19-P32) of

V1 as compared to S1BF (Gordon & Stryker, 1996). The end of the critical period in V1, which occurs after the end of our recording window, is characterised by the maturation of GABAergic PV+ input into layer 4 (Hensch, 2005; Butt et al., 2017; Fagiolini et al., 2004). Additionally, sensory experience plays a permissive role in the developmental increase in GABAergic activity associated with the end of the critical period (Morales et al., 2002). Possibly, thalamic engagement of FS INs in V1 occurs at a later time, which is synchronised with GABAergic maturation and visual cortex critical period. The different populations of SST INs between S1BF and V1 could also influence the timing of thalamocortical input onto PV cells. Tuncdemir et al. (2016) reported that early SST networks in S1BF are required for the maturation of thalamic input onto PV INs. The increased numbers of Lpar1-EGFP SST INs and the presence the L5b-L4 circuit in S1BF may lead to earlier thalamic innervation of PV INs and, thereby, PV IN maturation and an earlier critical period.

It has previously been published that there is direct and dense thalamic input onto SST+ve NFS INs in L5b of S1BF during the first postnatal week (Tuncdemir et al., 2016; Marques-Smith et al., 2016). The density of thalamic input decreases with time (Tuncdemir et al., 2016) and in the adult mouse SST+ve L5b Martinotti cells receive no thalamic input (Naka & Adesnik, 2016; X.-y. Ji et al., 2015; Cruikshank, Urabe, Nurmikko, & Connors, 2010). Connections onto NFS INs in L5b were first observed in this data set at P9. As the cells in this data set were patched at random, it is possible that the cell type receiving thalamic input (Lpar1-EGFP NFS IN, which are a subset of SST+ve NFS INs) was not recorded, and therefore, this thalamic connection was missed. The nature of patching all cell-types, rather than targeted patching of NFS INs, is a limitation of this approach that may prevent the finer differences of thalamic L5b engagement between S1BF and V1 from being discovered.

Chapter 6

Discussion

6.1 Summary of contributions

In this thesis I have shown that thalamic input into the cortex has little effect on the developing L5b-L4 interneuron circuit studied. The results demonstrated that neonatal circuits differ considerably between two sensory regions and that this difference is also independent of sensory input. Finally, I also demonstrated that S1 and V1 differ not only in neonatal cortical circuits, but also in IN population distributions and thalamic input onto cortical cell types. These conclusions have been drawn from a multitude of experiments using LSPS and optogenetics in both S1BF and V1 through the first weeks of life.

More specifically, in Chapter 3, I demonstrated through the use of the Celsr3|Dlx5/6 mouse, that some transient cortical circuits, thought to be remodelled by sensory information (Marques-Smith et al., 2016), in fact develop independently of thalamic input. The proposed neonatal L5b-L4 circuit for both WT and Celsr3|Dlx5/6 S1BF is shown in Figure 6.1A and B. The use of the Celsr3|Dlx5/6 mouse as a model for early cortical development is a novel approach that allowed us to explore the contribution of thalamic connectivity to the refinement of early interneuron circuits.

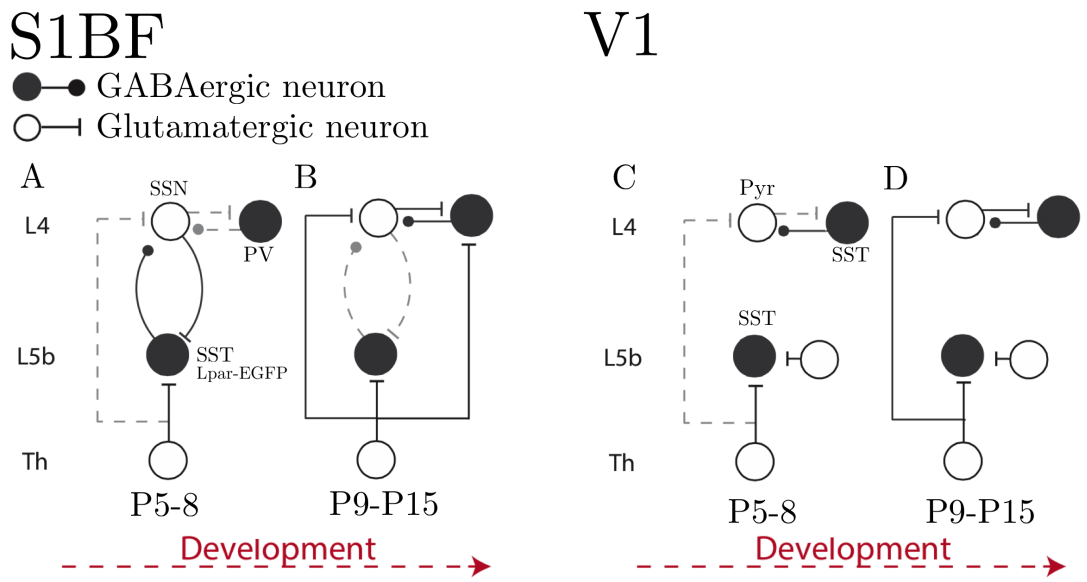


Figure 6.1: **Summary of early postnatal circuit differences between S1BF and V1. For both S1BF and V1, the WT and Celsr3|Dlx5/6 mice showed the same neonatal circuitry.**

In these mice L4 excitatory cells fail to remodel their apical dendrites to create the final stellate morphology. Moreover, no layer 4 neurons pattern into barrels. This indicates that while thalamic connections are not required for developing circuitry, fine tuning of mature cell morphology does appear to be modulated by activity. This is supported by numerous studies, outlined in the introduction, that show activity-dependent changes on the level of cell morphology and synapse formation. (García et al., 2015; Wamsley & Fishell, 2017; Chattopadhyaya et al., 2004; Hofer et al., 2009; Keck et al., 2008; Cheetham & Fox, 2011; Tuncdemir et al., 2016)

Once it had been confirmed that thalamic input was not required for the development of a connection that appeared to have a central role in later thalamic innervation of L4, it was hypothesised that this circuit might exist in all primary sensory areas. In chapter 4, I showed that this was not the case; no similar transient translaminar connection could be found in the visual cortex of mice. The neonatal

V1 circuit is illustrated in Figure 6.1C and D. The absence of a L5b-L4 circuit was confirmed in a number of optogenetic experiments, leading to the conclusion that early neonatal interneuron circuits differ between S1BF and V1. This difference is independent of any thalamic-driven activity and further suggests that some early circuit formation relies on intrinsic cortical factors and proceeds normally in the absence of thalamocortical connections. The neonatal circuit differences observed between S1BF and V1 are illustrated schematically in summary Figure 6.1

Chapter 5 further investigates the differences between S1BF and V1 which might underlie the circuit differences outlined in Chapters 3 and 4. It was shown that Lpar1-EGFP cell populations differ between S1BF and V1 with fewer Lpar1-EGFP INs in V1 L5b. The cause of the cell population differences is not clear and requires further investigation. It is possible that their reduced presence in V1 might account for the absence of the L5b-L4 connection, due to their central role in the L5b-L4 circuit. Not only were the cells' densities and distributions different between S1BF and V1, but Lpar1-EGFP cells in V1 lacked the extensive axonal arborisation into superficial layers that is seen in S1BF Lpar1-EGFP INs. This difference in morphology hints at different functions for this cell type across primary cortical regions and may be a factor in the lack of GABAergic input from these cells onto L4. Finally, Chapter 5 shows that thalamic input onto S1BF and V1 differs in connected cell type but not timing. The differences in cell type receiving direct thalamic innervation are partly explained by the known differences in excitatory cell populations between the two regions. Differences in thalamic innervation of Pv+ FS INs, however, may point to control of maturation of GABAergic circuits and the delayed critical period in V1, as compared to S1BF. This difference in thalamic input onto L4 INs during the second postnatal week is reflected in summary Figure 6.1. These expected differences in thalamic innervation between S1BF SST cells in L5b of S1BF and V1 were not observed. The lack of difference in thalamic innervation of

L5b could be explained by the methodology and likelihood of recording Lpar1-EGFP cells without targeted patching.

6.2 Implications

Given the extensive literature regarding the role of sensory input in remodelling and, in some cases redefining, cortical areas, it was expected that sensory information would also play a considerable role in remodelling the cortex at the level of early interneuron circuits (Pouchelon et al., 2014; Hensch, 2005; Sadato et al., 1996; Roe et al., 1990). Many studies point to thalamic input as a vital component of early circuit formation. From the instructive nature of retinal waves in ODC formation and the absence of barrels in sensory-deprived animals, to the peripherally driven early oscillations, activity appears central to early cortical development (H. Li et al., 2013; Erzurumlu & Gaspar, 2012; Feldman & Brecht, 2005; Gordon & Stryker, 1996; H.-P. Xu et al., 2015; Khazipov et al., 2004)

However, the results from Chapters 3-5 indicate that instead of thalamic-driven electrical information, it is intrinsic factors which play the largest role in the developing interneuron circuits. It is possible that early genetic factors between cortical regions create variation in interneuron populations that lead to differences in developing interneuron circuits. Specifically, it appears that differences in SST IN populations could underlie the neonatal circuit differences seen between S1BF and V1. How the differences in Lpar1-EGFP and, more broadly, the heterogeneity of IN populations between V1 and S1BF occurs is unknown.

As mentioned throughout this thesis, there are key differences in the early structure and function of S1BF and V1 which may underlie the observed neonatal circuit differences. These include differences in cell types, lamination, anatomy and activity.

Early spontaneous activity between S1BF and V1 is largely similar, consisting

of spindle bursts triggered by motor and retinal input and EGOs (Khazipov et al., 2004; Hanganu et al., 2007; Akhmetshina et al., 2016; Yang et al., 2009; Khazipov et al., 2004; Akhmetshina et al., 2016; Hanganu et al., 2006; Colonnese & Khazipov, 2010). However, the timing and quality of other spontaneous and evoked activity differs markedly. In S1BF, thalamic afferents reach the cortex before birth and innervate layer 4 at P0 (López-Bendito & Molnár, 2003; Lund & Mustari, 1977; Rakic, 1976; Shatz & Luskin, 1986). As soon as the thalamic afferents engage with the cortex, whisker information is able to be transmitted to the cortex. Although active whisking does not start until the second postnatal week, passive whisker stimulation is ongoing in the womb and throughout early life (Arakawa & Erzurumlu, 2015). In contrast, no visual information is available to the visual cortex *in utero* and while there is some level of visual information being transmitted through closed eyelids (Akerman et al., 2002; Krug et al., 2001) and retinal waves occur (Ackman et al., 2012; Galli & Maffei, 1988; Maffei & Galli-Resta, 1990; Sernagor & Grzywacz, 1999), the visual cortex does not get stimuli specific visual information until P12 in the mouse when the eyes begin to open (Feller & Scanziani, 2005; Crowley & Katz, 2000).

This temporal difference in stimulus relevant information is mirrored by the temporal differences observed in the critical period window for V1 (P19-P32) and S1BF (P3-P14) (Gordon & Stryker, 1996; Stern et al., 2001; Hensch, 2005; Rebsam et al., 2005). The timing of stimulus relevant sensory input could place different requirements on the neonatal sensory cortices during development. Because of the relatively early whisker-specific input in S1BF, it may be that this cortical area requires additional circuitry to guide correct thalamic integration at an earlier time point to V1. Although circuitry in other developing cortical areas was not mapped, it is possible that A1 neonatal circuitry is similar to V1. This is due to the later development of audition (critical period P10-P15 (Barkat, Polley, & Hensch, 2011))

which more closely resembles to timeline of V1 than S1. Mice first react to sounds at P10 (Ehret, 1976) and the external ear canals are closed until P8. It is not until P12 that the canals are fully opened and cochlear potentials appear first at P8 (Mikaelian & Ruben, 1965).

Although the neonatal circuit differences observed in S1BF and V1 could be necessitated by different temporal requirements, it is also possible that the L5b-L4 loop is unique to S1BF due to the spatial specificity of thalamic afferents connecting to individual barrels. In the somatosensory barrel field, whiskers map topographically onto the barrels and both the number and arrangement of whiskers and barrels is consistent from animal to animal (Van der Loos & Woolsey, 1973; Knutsen & Ahissar, 2009; Woolsey & Van der Loos, 1970). In the visual cortex, the development of ocular dominance columns and orientation columns appears to be governed by a self-organising process in which initial conditions are random (Swindale, 1996). Additionally, thalamic innervation of the target barrel has been shown to be very precise. The same level of precision and organisation of thalamic afferents is not seen in V1 (Agmon et al., 1995, 1993; Krug et al., 1998). These differences in organisation of thalamic input between the two cortical regions, coupled with the evidence that the L5b-L4 reciprocal loop plays a role in integration of thalamic input onto L4 in S1BF (Marques-Smith et al., 2016; Tuncdemir et al., 2016), suggests that the L5b-L4 circuit may perform an important role in thalamic integration in primary sensory cortices which require precise spatial connections.

The anatomy and structure of the cortical layers themselves is also an important point of difference between the V1 and S1BF. Although both cortices have the familiar 6 layers, the total width of V1 was seen to be markedly smaller than S1BF in the neonatal mouse, and the width of layer 4 in particular was observed to be narrower in V1 as compared to the barrel field of S1. The cell types which populate layer 4 are very different between S1BF and V1 in the mouse. Although spiny

stellate neurons can be readily observed in S1BF and participate in the L5b-L4 circuit (Marques-Smith et al., 2016), this cell type is absent in mouse V1.

Interestingly, SSNs are found in the visual cortices of other mammals which show ocular dominance columns (rather than the salt and pepper organisation of mouse V1). These animals include ferrets, cats and humans (Harris & Shepherd, 2015; Douglas & Martin, 2004; Peters & Kara, 1985; Nassi & Callaway, 2009; Ahmed, Anderson, Douglas, Martin, & Nelson, 1994; Mavroudis et al., 2012). It is possible that the formation of ocular dominance columns requires more complex neonatal circuitry which directs more precise and pre-determined thalamic integration. This may mean that along with SSNs, the L5b-4 circuit could be found in V1 of ferrets or cats.

As was discussed in Chapter 5, the density and distribution of Lpar1-EGFP SST INs was also different between S1BF and V1, particularly in L5b where these cells engage in the L5b-4 loop in S1BF. The fewer Lpar1-EGFP cells found in L5b could perhaps underlie the lack of GABAergic input from this cell type onto L4 in V1. Both the absence of SSNs in mouse V1 and the reduced number of L5b Lpar1-EGFP neurons highlights the differences in cell types within layers between primary sensory areas. These differences are likely to lead to differing neonatal circuitry and could result in presence of a L5b-L4 connection in S1 and its absence in V1.

This thesis has demonstrated that despite the evidence that sensory input guides changes in connectivity (such as those observed in ODC shifts during monocular deprivation), early IN circuit development is able to proceed largely unaffected in the complete absence of any thalamic input, spontaneous or evoked. It is the later maintenance of sensory cortical circuitry and fine tuning of cell morphology that require direction from sensory input.

These observations will hopefully lead to a re-evaluation of the importance of sensory activity in early circuit development and a renewed focus on the intrinsic

genetic differences between primary sensory regions. In particular, it would be of benefit to better understand the differences in cell subtypes between cortical areas, particularly interneurons, that may underlie neonatal circuit differences and thereby, emergent function.

6.3 Future work

The most immediate question is whether the L5b-L4 circuit is specific to whisker processing and if so, why? It would be of interest to map cortical circuitry in other primary sensory areas, for example, the primary auditory cortex (A1) to assess whether the L5b-L4 circuit is specific to S1BF alone.

Although spontaneous activity did not appear different between WT and Celsr3|Dlx5/6 animals, the recordings were limited to IPSCs in a single cell type. It would be of interest to look more comprehensively at early spontaneous activity in the Celsr3|Dlx5/6 mouse. Of particular interest would be the presence of spindle bursts and EGOs, reported to be partially driven by peripheral stimuli (Khazipov & Milh, 2017). Local inactivation of the VPM profoundly reduces spindle bursts, gamma oscillations and the majority of spontaneous events in S1BF (Yang et al., 2012). Therefore, it might be expected that spontaneous activity in the Celsr3|Dlx5/6 will be reduced and comparable between S1BF and V1.

It is believed that the input from SST and PV onto L4 exists in a see-saw like state and that extended 5b GABAergic input onto L4, in the case of ION nerve sectioning, compensates for the delayed maturation of PV cells in layer 4 (Marques-Smith et al., 2016). Tuncdemir et al. (2016) also demonstrated the requirement of SST networks for the maturation of thalamocortical input onto PV cells. Because the L5b-L4 circuit in Celsr3|Dlx5/6 animals is comparable to WT, it might, therefore, follow that maturation of PV cells is unaffected. However, thalamic input is thought

to play a permissive role in PV maturation around the end of the critical period (Daw et al., 2007; Morales et al., 2002; Hensch, 2005). In the visual cortex, timing of the critical period is controlled by inhibition from fast-spiking PV basket cells (Fagiolini et al., 2004). In S1BF, a subset of L4 PV INs orient strongly to the individual barrel (Koelbl et al., 2013) and whisker removal results in a reduction in perisomatic basket synaptic structures (Wamsley & Fishell, 2017; Chattopadhyaya et al., 2004). The activity-dependent expression of Etv1/Er81 has also been shown to modulate PV+ cell properties (Dehorter et al., 2015). It would, therefore, be of great interest to characterise the maturation of PV INs in Celsr3|Dlx5/6 mice in terms of both their electrophysiological properties and morphologies.

To expand on the differences found in Lpar1-EGFP IN populations between S1 and V1, it would be of interest to look into other SST+ve interneuron subtypes. Single-cell RNA sequencing in the adult mouse points to a number of marker genes that may segregate SST INs into interneuron subtypes and allow identification of these subtypes within the cortex (Tasic et al., 2016). It would be of great interest to investigate the presence and morphology of these different interneuron subgroups across cortical regions.

Subplate heterogeneity of both Lpar1-EGFP and SST INs in the subplate was evident between S1BF and V1. Further investigation of subplate heterogeneity between V1 and S1BF as well as subplate-specific circuits between these two regions would allow a better understanding of early regional differences within the cortex. Mapping and comparing earlier transient subplate circuits between cortical regions would also give a more complete picture of when areal circuit differences arise and what might be driving the later circuit development. Possibly, multiple early transient circuits such as barrel-specific subplate neurites and the L5b-L4 circuit are complementary to each other.

The question as to how cortical areas contain different interneuron populations

remains unanswered, with specification, migration and apoptosis possible candidates. To resolve this, two approaches could be taken. Firstly, one could look for the presence of cleaved caspase-3 (Southwell et al., 2012) in Lpar1-EGFP cells from the time point that they arrive in the developing cortex. Secondly, it would be possible using RNA-seq to look at the expression of guidance molecule receptors on migrating Lpar1-EGFP cells and the corresponding expression of chemoattractants in S1BF and V1. Possible candidates for cortical guidance molecules may be expression of isoforms of Neuregulin-1 within different cortical areas (Flames et al., 2004), the expression of glial cell-derived neurotrophic factor (GDNF) in the cortex and tangential migratory route (Pozas & Ibáñez, 2005), and expression of chemokines in the cortex (López-Bendito et al., 2008; G. Li et al., 2008; Tanaka et al., 2010). Additionally, it would be of interest to investigate which cortical zone Lpar1-EGFP neurons migrate through and if this differs between S1BF and V1.

Finally, the characterisation of thalamic input onto S1BF and V1 was limited by the ability to target specific cell types. Using the Lpar1-EGFP mouse line (Marques-Smith et al., 2016), combined with Olig3|Ai32 would allow more specific comparison of thalamic input relevant to the observed L5b-L4 circuit differences.

6.4 Concluding Remarks

In conclusion, this thesis has shown that cortical interneuron circuits can assemble, develop, and be dismantled independently of thalamic connectivity.

The data presented in the previous chapters characterises the differences in early interneuron circuits between two cortical regions and highlights the role of intrinsic factors rather than sensory input in the development of area-specific circuitry.

It is hoped that the data presented in this thesis will help advance the field of developmental neuroscience and encourage a renewed focus on the role of intrinsic

properties and cortical interneuron populations in instructing sensory-specific circuit development.

References

Ackman, J. B., Burbridge, T. J., & Crair, M. C. (2012). Retinal waves coordinate patterned activity throughout the developing visual system. *Nature*, *490*(7419), 219.

Agmon, A., & Connors, B. (1991). Thalamocortical responses of mouse somatosensory (barrel) cortexin vitro. *Neuroscience*, *41*(2-3), 365–379.

Agmon, A., Yang, L. T., Jones, E. G., & O'Dowd, D. K. (1995). Topological precision in the thalamic projection to neonatal mouse barrel cortex. *Journal of Neuroscience*, *15*(1), 549–561.

Agmon, A., Yang, L. T., O'Dowd, D. K., & Jones, E. G. (1993). Organized growth of thalamocortical axons from the deep tier of terminations into layer iv of developing mouse barrel cortex. *Journal of Neuroscience*, *13*(12), 5365–5382.

Ahmed, B., Anderson, J. C., Douglas, R. J., Martin, K. A., & Nelson, J. C. (1994). Polyneuronal innervation of spiny stellate neurons in cat visual cortex. *Journal of Comparative Neurology*, *341*(1), 39–49.

Akerman, C. J., & Cline, H. T. (2006). Depolarizing gabaergic conductances regulate the balance of excitation to inhibition in the developing retinotectal circuit in vivo. *Journal of Neuroscience*, *26*(19), 5117–5130.

Akerman, C. J., & Cline, H. T. (2007). Refining the roles of gabaergic signaling during neural circuit formation. *Trends in neurosciences*, *30*(8), 382–389.

Akerman, C. J., Smyth, D., & Thompson, I. D. (2002). Visual experience before eye-opening and the development of the retinogeniculate pathway. *Neuron*, *36*(5), 869–879.

Akhmetshina, D., Nasretdinov, A., Zakharov, A., Valeeva, G., & Khazipov, R. (2016). The nature of the sensory input to the neonatal rat barrel cortex. *Journal of Neuroscience*, *36*(38), 9922–9932.

Allendoerfer, K. L., & Shatz, C. J. (1994). The subplate, a transient neocortical structure: its role in the development of connections between thalamus and cortex. *Annual review of neuroscience*, *17*(1), 185–218.

Anastasiades, P. G., & Butt, S. J. (2012). A role for silent synapses in the development of the pathway from layer 2/3 to 5 pyramidal cells in the neocortex. *Journal of Neuroscience*, *32*(38), 13085–13099.

Anastasiades, P. G., Marques-Smith, A., & Butt, S. J. (2017). Studies of cortical connectivity using optical circuit mapping methods. *The Journal of physiology*.

Anastasiades, P. G., Marques-Smith, A., & Butt, S. J. (2018). Studies of cortical

connectivity using optical circuit mapping methods. *The Journal of physiology*, *596*(2), 145–162.

Anastasiades, P. G., Marques-Smith, A., Lyngholm, D., Lickiss, T., Raffiq, S., Kätzel, D., ... Butt, S. J. (2016). Gabaergic interneurons form transient layer-specific circuits in early postnatal neocortex. *Nature communications*, *7*, 10584.

Antonini, A., & Stryker, M. P. (1993). Rapid remodeling of axonal arbors in the visual cortex. *Science*, *260*(5115), 1819–1821.

Arakawa, H., & Erzurumlu, R. S. (2015). Role of whiskers in sensorimotor development of c57bl/6 mice. *Behavioural brain research*, *287*, 146–155.

Armstrong-James, M., Fox, K., & Das-Gupta, A. (1992). Flow of excitation within rat barrel cortex on striking a single vibrissa. *Journal of neurophysiology*, *68*(4), 1345–1358.

Bandler, R. C., Mayer, C., & Fishell, G. (2017). Cortical interneuron specification: the juncture of genes, time and geometry. *Current opinion in neurobiology*, *42*, 17–24.

Barkat, T. R., Polley, D. B., & Hensch, T. K. (2011). A critical period for auditory thalamocortical connectivity. *Nature neuroscience*, *14*(9), 1189.

Ben-Ari, Y. (2002). Excitatory actions of gaba during development: the nature of the nurture. *Nature Reviews Neuroscience*, *3*(9), 728.

Ben-Ari, Y., Cherubini, E., Corradetti, R., & Gaiarsa, J. (1989). Giant synaptic potentials in immature rat ca3 hippocampal neurones. *The Journal of physiology*, *416*(1), 303–325.

Ben-Ari, Y., Khalilov, I., Represa, A., & Gozlan, H. (2004). Interneurons set the tune of developing networks. *Trends in neurosciences*, *27*(7), 422–427.

Blakemore, C., & Cooper, G. F. (1970). Development of the brain depends on the visual environment. *Nature*, *228*(5270), 477.

Blankenship, A. G., & Feller, M. B. (2010). Mechanisms underlying spontaneous patterned activity in developing neural circuits. *Nature Reviews Neuroscience*, *11*(1), 18.

Boyden, E. S., Zhang, F., Bamberg, E., Nagel, G., & Deisseroth, K. (2005). Millisecond-timescale, genetically targeted optical control of neural activity. *Nature neuroscience*, *8*(9), 1263.

Brecht, M., & Sakmann, B. (2002). Whisker maps of neuronal subclasses of the rat ventral posterior medial thalamus, identified by whole-cell voltage recording and morphological reconstruction. *The Journal of Physiology*, *538*(2), 495–515.

Brill, J., Mattis, J., Deisseroth, K., & Huguenard, J. R. (2016). Lsps/optogenetics to improve synaptic connectivity mapping: unmasking the role of basket cell-mediated feedforward inhibition. *eNeuro*, *3*(4), ENEURO–0142.

Buonomano, D. V., & Merzenich, M. M. (1998). Cortical plasticity: from synapses to maps. *Annual review of neuroscience*, *21*(1), 149–186.

Butt, S. J., Fuccillo, M., Nery, S., Noctor, S., Kriegstein, A., Corbin, J. G., & Fishell, G. (2005). The temporal and spatial origins of cortical interneurons

predict their physiological subtype. *Neuron*, *48*(4), 591–604.

Butt, S. J., Stacey, J. A., Teramoto, Y., & Vagnoni, C. (2017). A role for gabaergic interneuron diversity in circuit development and plasticity of the neonatal cerebral cortex. *Current opinion in neurobiology*, *43*, 149–155.

Cajal, S. R. (1911). Histologie du syste me nerveux de i'homme et des verte be s. *Maloine (Paris)*, *2*, 891–942.

Callaway, E. M., & Borrell, V. (2011). Developmental sculpting of dendritic morphology of layer 4 neurons in visual cortex: influence of retinal input. *Journal of Neuroscience*, *31*(20), 7456–7470.

Canty, A. J., Dietze, J., Harvey, M., Enomoto, H., Milbrandt, J., & Ibáñez, C. F. (2009). Regionalized loss of parvalbumin interneurons in the cerebral cortex of mice with deficits in gfrα1 signaling. *Journal of Neuroscience*, *29*(34), 10695–10705.

Carić, D., & Price, D. J. (1999). Evidence that the lateral geniculate nucleus regulates the normal development of visual corticocortical projections in the cat. *Experimental neurology*, *156*(2), 353–362.

Catalano, S. M., Robertson, R. T., & Killackey, H. P. (1991). Early ingrowth of thalamocortical afferents to the neocortex of the prenatal rat. *Proceedings of the National Academy of Sciences*, *88*(8), 2999–3003.

Catania, K. C., & Henry, E. C. (2006). Touching on somatosensory specializations in mammals. *Current opinion in neurobiology*, *16*(4), 467–473.

Chattopadhyaya, B., Di Cristo, G., Higashiyama, H., Knott, G. W., Kuhlman, S. J., Welker, E., & Huang, Z. J. (2004). Experience and activity-dependent maturation of perisomatic gabaergic innervation in primary visual cortex during a postnatal critical period. *Journal of Neuroscience*, *24*(43), 9598–9611.

Cheetham, C. E., & Fox, K. (2011). The role of sensory experience in presynaptic development is cortical area specific. *The Journal of physiology*, *589*(23), 5691–5699.

Chiaia, N. L., Rhoades, R. W., Fish, S. E., & Killackey, H. P. (1991). Thalamic processing of vibrissal information in the rat: Ii. morphological and functional properties of medial ventral posterior nucleus and posterior nucleus neurons. *Journal of Comparative Neurology*, *314*(2), 217–236.

Chittajallu, R., & Isaac, J. T. (2010). Emergence of cortical inhibition by coordinated sensory-driven plasticity at distinct synaptic loci. *Nature neuroscience*, *13*(10), 1240.

Cho, J.-H., Deisseroth, K., & Bolshakov, V. Y. (2013). Synaptic encoding of fear extinction in mpfc-amygdala circuits. *Neuron*, *80*(6), 1491–1507.

Chou, S.-J., Babot, Z., Leingärtner, A., Studer, M., Nakagawa, Y., & O'Leary, D. D. (2013). Geniculocortical input drives genetic distinctions between primary and higher-order visual areas. *Science*, *340*(6137), 1239–1242.

Colonnese, M. T., Kaminska, A., Minlebaev, M., Milh, M., Bloem, B., Lescure, S., ... Khazipov, R. (2010). A conserved switch in sensory processing prepares developing neocortex for vision. *Neuron*, *67*(3), 480–498.

Colonnese, M. T., & Khazipov, R. (2010). Slow activity transients in infant rat

visual cortex: a spreading synchronous oscillation patterned by retinal waves. *Journal of Neuroscience*, *30*(12), 4325–4337.

Constantinople, C. M., & Bruno, R. M. (2013). Deep cortical layers are activated directly by thalamus. *Science*, *340*(6140), 1591–1594.

Cooke, S., Grant, G., McLauchlan, C., Lotto, R. B., & Price, D. J. (1999). Basic fibroblast growth factor promotes subplate cell survival in explant cultures of embryonic mouse cortex. *Neuroscience letters*, *271*(3), 143–146.

Crair, M. C., Gillespie, D. C., & Stryker, M. P. (1998). The role of visual experience in the development of columns in cat visual cortex. *Science*, *279*(5350), 566–570.

Crowley, J. C., & Katz, L. C. (1999). Development of ocular dominance columns in the absence of retinal input. *Nature neuroscience*, *2*(12), 1125.

Crowley, J. C., & Katz, L. C. (2000). Early development of ocular dominance columns. *Science*, *290*(5495), 1321–1324.

Cruikshank, S. J., Urabe, H., Nurmikko, A. V., & Connors, B. W. (2010). Pathway-specific feedforward circuits between thalamus and neocortex revealed by selective optical stimulation of axons. *Neuron*, *65*(2), 230–245.

Daw, M. I., Ashby, M. C., & Isaac, J. T. (2007). Coordinated developmental recruitment of latent fast spiking interneurons in layer iv barrel cortex. *Nature neuroscience*, *10*(4), 453–461.

Dehay, C., Giroud, P., Berland, M., Killackey, H., & Kennedy, H. (1996). Contribution of thalamic input to the specification of cytoarchitectonic cortical fields in the primate: effects of bilateral enucleation in the fetal monkey on the boundaries, dimensions, and gyrification of striate and extrastriate cortex. *Journal of Comparative Neurology*, *367*(1), 70–89.

Dehay, C., Savatier, P., Cortay, V., & Kennedy, H. (2001). Cell-cycle kinetics of neocortical precursors are influenced by embryonic thalamic axons. *Journal of Neuroscience*, *21*(1), 201–214.

Dehorter, N., Ciceri, G., Bartolini, G., Lim, L., del Pino, I., & Marín, O. (2015). Tuning of fast-spiking interneuron properties by an activity-dependent transcriptional switch. *Science*, *349*(6253), 1216–1220.

Dhruv, N. T. (2015). Rethinking canonical cortical circuits. *Nature neuroscience*, *18*(11), 1538.

Douglas, R. J., & Martin, K. A. (2004). Neuronal circuits of the neocortex. *Annu. Rev. Neurosci.*, *27*, 419–451.

Dupont, E., Hanganu, I. L., Kilb, W., Hirsch, S., & Luhmann, H. J. (2006). Rapid developmental switch in the mechanisms driving early cortical columnar networks. *Nature*, *439*(7072), 79.

Edgar, J. M., & Price, D. J. (2001). Radial migration in the cerebral cortex is enhanced by signals from thalamus. *European Journal of Neuroscience*, *13*(9), 1745–1754.

Ehret, G. (1976). Development of absolute auditory thresholds in the house mouse (mus musculus). *Journal of the American Audiology Society*, *1*(5), 179–184.

Erzurumlu, R. S., & Gaspar, P. (2012). Development and critical period plasticity

of the barrel cortex. *European Journal of Neuroscience*, *35*(10), 1540–1553.

Fagiolini, M., Fritschy, J.-M., Löw, K., Möhler, H., Rudolph, U., & Hensch, T. K. (2004). Specific gabaa circuits for visual cortical plasticity. *Science*, *303*(5664), 1681–1683.

Feldman, D. E., & Brecht, M. (2005). Map plasticity in somatosensory cortex. *Science*, *310*(5749), 810–815.

Feldmeyer, D., Egger, V., Lübke, J., & Sakmann, B. (1999). Reliable synaptic connections between pairs of excitatory layer 4 neurones within a single barrel of developing rat somatosensory cortex. *The Journal of Physiology*, *521*(1), 169–190.

Feller, M. B., & Scanziani, M. (2005). A precritical period for plasticity in visual cortex. *Current opinion in neurobiology*, *15*(1), 94–100.

Ferreira, T. A., Blackman, A. V., Oyrer, J., Jayabal, S., Chung, A. J., Watt, A. J., ... Van Meyel, D. J. (2014). Neuronal morphometry directly from bitmap images. *Nature methods*, *11*(10), 982.

Flames, N., Long, J. E., Garratt, A. N., Fischer, T. M., Gassmann, M., Birchmeier, C., ... Marın, O. (2004). Short-and long-range attraction of cortical gabaergic interneurons by neuregulin-1. *Neuron*, *44*(2), 251–261.

Fox, K. (1992). A critical period for experience-dependent synaptic plasticity in rat barrel cortex. *The Journal of neuroscience*, *12*(5), 1826–1838.

Fox, K. (2002). Anatomical pathways and molecular mechanisms for plasticity in the barrel cortex. *Neuroscience*, *111*(4), 799–814.

Frangeul, L., Kehayas, V., Sanchez-Mut, J. V., Fièvre, S., Krishna-K, K., Pouchelon, G., ... others (2017). Input-dependent regulation of excitability controls dendritic maturation in somatosensory thalamocortical neurons. *Nature communications*, *8*(1), 2015.

Fukuchi-Shimogori, T., & Grove, E. A. (2001). Neocortex patterning by the secreted signaling molecule fgf8. *Science*, *294*(5544), 1071–1074.

Gaillard, A., & Roger, M. (2000). Early commitment of embryonic neocortical cells to develop area-specific thalamic connections. *Cerebral Cortex*, *10*(5), 443–453.

Galli, L., & Maffei, L. (1988). Spontaneous impulse activity of rat retinal ganglion cells in prenatal life. *Science*, *242*(4875), 90–91.

Garaschuk, O., Linn, J., Eilers, J., & Konnerth, A. (2000). Large-scale oscillatory calcium waves in the immature cortex. *Nature neuroscience*, *3*(5), 452.

García, N. V. D. M., Karayannis, T., & Fishell, G. (2011). Neuronal activity is required for the development of specific cortical interneuron subtypes. *Nature*, *472*(7343), 351.

García, N. V. D. M., Priya, R., Tuncdemir, S. N., Fishell, G., & Karayannis, T. (2015). Sensory inputs control the integration of neurogliaform interneurons into cortical circuits. *Nature neuroscience*, *18*(3), 393.

Ge, S., Goh, E. L., Sailor, K. A., Kitabatake, Y., Ming, G.-l., & Song, H. (2006). Gaba regulates synaptic integration of newly generated neurons in the adult brain. *Nature*, *439*(7076), 589.

GENSAT Project at Rockefeller University. (2005). *Tg(lpar1-egfp)gx193gsat - mgi:4847204.* Retrieved 2018, from `http://www.informatics.jax.org/allele/MGI:4847204`

Ghosh, A., & Shatz, C. J. (1992). Involvement of subplate neurons in the formation of ocular dominance columns. *Science*, *255*(5050), 1441–1443.

Golshani, P., Gonçalves, J. T., Khoshkhoo, S., Mostany, R., Smirnakis, S., & Portera-Cailliau, C. (2009). Internally mediated developmental desynchronization of neocortical network activity. *Journal of Neuroscience*, *29*(35), 10890–10899.

Gordon, J. A., & Stryker, M. P. (1996). Experience-dependent plasticity of binocular responses in the primary visual cortex of the mouse. *Journal of Neuroscience*, *16*(10), 3274–3286.

Grant, E., Hoerder-Suabedissen, A., & Molnár, Z. (2016). The regulation of corticofugal fiber targeting by retinal inputs. *Cerebral Cortex*, *26*(3), 1336–1348.

Grubb, M. S., & Thompson, I. D. (2004). The influence of early experience on the development of sensory systems. *Current opinion in neurobiology*, *14*(4), 503–512.

Guan, W., Cao, J.-W., Liu, L.-Y., Zhao, Z.-H., Fu, Y., & Yu, Y.-C. (2017). Eye opening differentially modulates inhibitory synaptic transmission in the developing visual cortex. *eLife*, *6*.

Hagihara, K. M., Murakami, T., Yoshida, T., Tagawa, Y., & Ohki, K. (2015). Neuronal activity is not required for the initial formation and maturation of visual selectivity. *Nature neuroscience*, *18*(12), 1780.

Hanganu, I. L., Ben-Ari, Y., & Khazipov, R. (2006). Retinal waves trigger spindle bursts in the neonatal rat visual cortex. *Journal of Neuroscience*, *26*(25), 6728–6736.

Hanganu, I. L., Kilb, W., & Luhmann, H. J. (2001). Spontaneous synaptic activity of subplate neurons in neonatal rat somatosensory cortex. *Cerebral Cortex*, *11*(5), 400–410.

Hanganu, I. L., Kilb, W., & Luhmann, H. J. (2002). Functional synaptic projections onto subplate neurons in neonatal rat somatosensory cortex. *Journal of Neuroscience*, *22*(16), 7165–7176.

Hanganu, I. L., Okabe, A., Lessmann, V., & Luhmann, H. J. (2008). Cellular mechanisms of subplate-driven and cholinergic input-dependent network activity in the neonatal rat somatosensory cortex. *Cerebral Cortex*, *19*(1), 89–105.

Hanganu, I. L., Staiger, J. F., Ben-Ari, Y., & Khazipov, R. (2007). Cholinergic modulation of spindle bursts in the neonatal rat visual cortex in vivo. *Journal of Neuroscience*, *27*(21), 5694–5705.

Hanganu-Opatz, I. L. (2010). Between molecules and experience: role of early patterns of coordinated activity for the development of cortical maps and sensory abilities. *Brain research reviews*, *64*(1), 160–176.

Hannan, A. J., Blakemore, C., Katsnelson, A., Vitalis, T., Huber, K. M., Bear, M., ... Kind, P. C. (2001). Plc-β1, activated via mglurs, mediates activity-dependent differentiation in cerebral cortex. *Nature neuroscience*, *4*(3), 282.

Harb, K., Magrinelli, E., Nicolas, C. S., Lukianets, N., Frangeul, L., Pietri, M., ... others (2016). Area-specific development of distinct projection neuron subclasses is regulated by postnatal epigenetic modifications. *Elife*, *5*, e09531.

Harris, K. D., & Shepherd, G. M. (2015). The neocortical circuit: themes and variations. *Nature neuroscience*, *18*(2), 170.

Hensch, T. K. (2005). Critical period plasticity in local cortical circuits. *Nature Reviews Neuroscience*, *6*(11), 877–888.

Henze, D., & Buzsaki, G. (2001). Action potential threshold of hippocampal pyramidal cells in vivo is increased by recent spiking activity. *Neuroscience*, *105*(1), 121–130.

Hernández-Miranda, L. R., Parnavelas, J. G., & Chiara, F. (2010). Molecules and mechanisms involved in the generation and migration of cortical interneurons. *ASN neuro*, *2*(2), AN20090053.

Higashi, S., Hioki, K., Kurotani, T., Kasim, N., & Molnár, Z. (2005). Functional thalamocortical synapse reorganization from subplate to layer iv during postnatal development in the reeler-like mutant rat (shaking rat kawasaki). *Journal of Neuroscience*, *25*(6), 1395–1406.

Higashi, S., Molnár, Z., Kurotani, T., & Toyama, K. (2002). Prenatal development of neural excitation in rat thalamocortical projections studied by optical recording. *Neuroscience*, *115*(4), 1231–1246.

Hoerder-Suabedissen, A., Hayashi, S., Upton, L., Nolan, Z., Casas-Torremocha, D., Grant, E., ... others (2018). Subset of cortical layer 6b neurons selectively innervates higher order thalamic nuclei in mice. *Cerebral Cortex*, *28*(5), 1882–1897.

Hoerder-Suabedissen, A., Korrell, K. V., Hayashi, S., Jeans, A., Ramirez, D. M., Grant, E., ... Molnár, Z. (2018). Cell-specific loss of snap25 from cortical projection neurons allows normal development but causes subsequent neurodegeneration. *Cerebral Cortex*.

Hoerder-Suabedissen, A., & Molnár, Z. (2012a). Molecular diversity of early-born subplate neurons. *Cerebral cortex*, *23*(6), 1473–1483.

Hoerder-Suabedissen, A., & Molnár, Z. (2012b). Morphology of mouse subplate cells with identified projection targets changes with age. *Journal of Comparative Neurology*, *520*(1), 174–185.

Hoerder-Suabedissen, A., & Molnár, Z. (2015). Development, evolution and pathology of neocortical subplate neurons. *Nature Reviews Neuroscience*, *16*(3), 133.

Hoerder-Suabedissen, A., Wang, W. Z., Lee, S., Davies, K. E., Goffinet, A. M., Rakić, S., ... others (2008). Novel markers reveal subpopulations of subplate neurons in the murine cerebral cortex. *Cerebral Cortex*, *19*(8), 1738–1750.

Hofer, S. B., Mrsic-Flogel, T. D., Bonhoeffer, T., & Hübener, M. (2009). Experience leaves a lasting structural trace in cortical circuits. *Nature*, *457*(7227), 313–317.

Hubel, D. H., & Wiesel, T. N. (1962). Receptive fields, binocular interaction and functional architecture in the cat's visual cortex. *The Journal of physiology*,

160(1), 106.

Hubel, D. H., & Wiesel, T. N. (1970). The period of susceptibility to the physiological effects of unilateral eye closure in kittens. *The Journal of physiology*, *206*(2), 419–436.

Hubel, D. H., Wiesel, T. N., & LeVay, S. (1977). Plasticity of ocular dominance columns in monkey striate cortex. *Phil. Trans. R. Soc. Lond. B*, *278*(961), 377–409.

Huttenlocher, P. R., de Courten, C., Garey, L. J., & Van der Loos, H. (1982). Synaptogenesis in human visual cortexevidence for synapse elimination during normal development. *Neuroscience letters*, *33*(3), 247–252.

Iwasato, T., Datwani, A., Wolf, A. M., Nishiyama, H., Taguchi, Y., Tonegawa, S., ... Itohara, S. (2000). Cortex-restricted disruption of nmdar1 impairs neuronal patterns in the barrel cortex. *Nature*, *406*(6797), 726.

Jacob, V., Petreanu, L., Wright, N., Svoboda, K., & Fox, K. (2012). Regular spiking and intrinsic bursting pyramidal cells show orthogonal forms of experience-dependent plasticity in layer v of barrel cortex. *Neuron*, *73*(2), 391–404.

Ji, W., Gămănuţ, R., Bista, P., DSouza, R. D., Wang, Q., & Burkhalter, A. (2015). Modularity in the organization of mouse primary visual cortex. *Neuron*, *87*(3), 632–643.

Ji, X.-y., Zingg, B., Mesik, L., Xiao, Z., Zhang, L. I., & Tao, H. W. (2015). Thalamocortical innervation pattern in mouse auditory and visual cortex: laminar and cell-type specificity. *Cerebral Cortex*, *26*(6), 2612–2625.

Johnson, M. H. (2001). Functional brain development in humans. *Nature Reviews Neuroscience*, *2*(7), 475.

Kaas, J. H., Krubitzer, L. A., Chino, Y. M., Langston, A. L., Polley, E. H., & Blair, N. (1990). Reorganization of retinotopic cortical maps in adult mammals after lesions of the retina. *Science*, *248*(4952), 229.

Kahn, D. M., & Krubitzer, L. (2002). Massive cross-modal cortical plasticity and the emergence of a new cortical area in developmentally blind mammals. *Proceedings of the National Academy of Sciences*, *99*(17), 11429–11434.

Kanold, P. O. (2004). Transient microcircuits formed by subplate neurons and their role in functional development of thalamocortical connections. *Neuroreport*, *15*(14), 2149–2153.

Kanold, P. O., Kara, P., Reid, R. C., & Shatz, C. J. (2003). Role of subplate neurons in functional maturation of visual cortical columns. *Science*, *301*(5632), 521–525.

Kanold, P. O., & Luhmann, H. J. (2010). The subplate and early cortical circuits. *Annual review of neuroscience*, *33*, 23–48.

Katz, L. C., & Shatz, C. J. (1996). Synaptic activity and the construction of cortical circuits. *Science*, *274*(5290), 1133–1138.

Kätzel, D., Zemelman, B. V., Buetfering, C., Wölfel, M., & Miesenböck, G. (2011). The columnar and laminar organization of inhibitory connections to neocortical excitatory cells. *Nature neuroscience*, *14*(1), 100–107.

Keck, T., Mrsic-Flogel, T. D., Afonso, M. V., Eysel, U. T., Bonhoeffer, T., &

Hübener, M. (2008). Massive restructuring of neuronal circuits during functional reorganization of adult visual cortex. *Nature neuroscience*, *11*(10), 1162–1167.

Kerr, J. N., Greenberg, D., & Helmchen, F. (2005). Imaging input and output of neocortical networks in vivo. *Proceedings of the National Academy of Sciences*, *102*(39), 14063–14068.

Khazipov, R., & Milh, M. (2017). Early patterns of activity in the developing cortex: focus on the sensorimotor system. In *Seminars in cell & developmental biology.*

Khazipov, R., Sirota, A., Leinekugel, X., Holmes, G. L., Ben-Ari, Y., & Buzsáki, G. (2004). Early motor activity drives spindle bursts in the developing somatosensory cortex. *Nature*, *432*(7018), 758.

Kirischuk, S., Luhmann, H., & Kilb, W. (2014). Cajal–retzius cells: Update on structural and functional properties of these mystic neurons that bridged the 20th century. *Neuroscience*, *275*, 33–46.

Knutsen, P. M., & Ahissar, E. (2009). Orthogonal coding of object location. *Trends in neurosciences*, *32*(2), 101–109.

Ko, H., Cossell, L., Baragli, C., Antolik, J., Clopath, C., Hofer, S. B., & Mrsic-Flogel, T. D. (2013). The emergence of functional microcircuits in visual cortex. *Nature*, *496*(7443), 96–100.

Koelbl, C., Helmstaedter, M., Lübke, J., & Feldmeyer, D. (2013). A barrel-related interneuron in layer 4 of rat somatosensory cortex with a high intrabarrel connectivity. *Cerebral cortex*, *25*(3), 713–725.

Kostovic, I., & Rakic, P. (1980). Cytology and time of origin of interstitial neurons in the white matter in infant and adult human and monkey telencephalon. *Journal of neurocytology*, *9*(2), 219–242.

Kostovic, I., & Rakic, P. (1990). Developmental history of the transient subplate zone in the visual and somatosensory cortex of the macaque monkey and human brain. *Journal of Comparative Neurology*, *297*(3), 441–470.

Krug, K., Akerman, C. J., & Thompson, I. D. (2001). Responses of neurons in neonatal cortex and thalamus to patterned visual stimulation through the naturally closed lids. *Journal of neurophysiology*, *85*(4), 1436–1443.

Krug, K., Smith, A. L., & Thompson, I. D. (1998). The development of topography in the hamster geniculo-cortical projection. *Journal of Neuroscience*, *18*(15), 5766–5776.

Laing, R., Turecek, J., Takahata, T., & Olavarria, J. (2014). Identification of eye-specific domains and their relation to callosal connections in primary visual cortex of long evans rats. *Cerebral Cortex*, *25*(10), 3314–3329.

Landisman, C. E., & Connors, B. W. (2007). Vpm and pom nuclei of the rat somatosensory thalamus: intrinsic neuronal properties and corticothalamic feedback. *Cerebral cortex*, *17*(12), 2853–2865.

Lee, L.-J., Chen, W.-J., Chuang, Y.-W., & Wang, Y.-C. (2009). Neonatal whisker trimming causes long-lasting changes in structure and function of the somatosensory system. *Experimental neurology*, *219*(2), 524–532.

Le Vay, S., Wiesel, T. N., & Hubel, D. H. (1980). The development of ocular

dominance columns in normal and visually deprived monkeys. *Journal of Comparative Neurology*, *191*(1), 1–51.

Li, G., Adesnik, H., Li, J., Long, J., Nicoll, R. A., Rubenstein, J. L., & Pleasure, S. J. (2008). Regional distribution of cortical interneurons and development of inhibitory tone are regulated by cxcl12/cxcr4 signaling. *Journal of Neuroscience*, *28*(5), 1085–1098.

Li, H., Fertuzinhos, S., Mohns, E., Hnasko, T. S., Verhage, M., Edwards, R., ... Crair, M. C. (2013). Laminar and columnar development of barrel cortex relies on thalamocortical neurotransmission. *Neuron*, *79*(5), 970–986.

Lim, L., Pakan, J. M., Selten, M. M., Marques-Smith, A., Llorca, A., Bae, S. E., ... Marín, O. (2018). Optimization of interneuron function by direct coupling of cell migration and axonal targeting. *Nature neuroscience*, 1.

López-Bendito, G., Cautinat, A., Sánchez, J. A., Bielle, F., Flames, N., Garratt, A. N., ... others (2006). Tangential neuronal migration controls axon guidance: a role for neuregulin-1 in thalamocortical axon navigation. *Cell*, *125*(1), 127–142.

López-Bendito, G., & Molnár, Z. (2003). Thalamocortical development: how are we going to get there? *Nature Reviews Neuroscience*, *4*(4), 276.

López-Bendito, G., & Molnár, Z. (2003). Thalamocortical development: how are we going to get there? *Nature reviews. Neuroscience*, *4*(4), 276–289. doi: 10.1038/nrn1075

López-Bendito, G., Sánchez-Alcaniz, J. A., Pla, R., Borrell, V., Picó, E., Valdeolmillos, M., & Marín, O. (2008). Chemokine signaling controls intracortical migration and final distribution of gabaergic interneurons. *Journal of Neuroscience*, *28*(7), 1613–1624.

Luhmann, H. J., & Khazipov, R. (2018). Neuronal activity patterns in the developing barrel cortex. *Neuroscience*, *368*, 256–267.

Luhmann, H. J., Kilb, W., & Hanganu-Opatz, I. (2009). Subplate cells: amplifiers of neuronal activity in the developing cerebral cortex. *Frontiers in neuroanatomy*, *3*, 19.

Lund, R., & Mustari, M. (1977). Development of the geniculocortical pathway in rat. *Journal of Comparative Neurology*, *173*(2), 289–305.

Luskin, M., & Shatz, C. (1985). Studies of the earliest generated cells of the cat's visual cortex: cogeneration of subplate and marginal zones. *Journal of Neuroscience*, *5*(4), 1062–1075.

MacLean, J. N., Fenstermaker, V., Watson, B. O., & Yuste, R. (2006). A visual thalamocortical slice. *Nature methods*, *3*(2), 129.

Maffei, L., & Galli-Resta, L. (1990). Correlation in the discharges of neighboring rat retinal ganglion cells during prenatal life. *Proceedings of the National Academy of Sciences*, *87*(7), 2861–2864.

Malpeli, J. G. (1983). Activity of cells in area 17 of the cat in absence of input from layer a of lateral geniculate nucleus. *Journal of neurophysiology*, *49*(3), 595–610.

Mardinly, A., Spiegel, I., Patrizi, A., Centofante, E., Bazinet, J., Tzeng, C., ...

others (2016). Sensory experience regulates cortical inhibition by inducing igf1 in vip neurons. *Nature*, *531*(7594), 371.

Marin-Padilla, M. (1970). Prenatal and early postnatal ontogenesis of the human motor cortex: a golgi study. i. the sequential development of the cortical layers. *Brain Res*, *23*(2), 167–183.

Markram, H., Toledo-Rodriguez, M., Wang, Y., Gupta, A., Silberberg, G., & Wu, C. (2004). Interneurons of the neocortical inhibitory system. *Nature Reviews Neuroscience*, *5*(10), 793.

Marques-Smith, A. (2014). Using optical stimulation to study the developing thalamocortical circuit in mouse somatosensory cortex.

Marques-Smith, A., Lyngholm, D., Kaufmann, A.-K., Stacey, J. A., Hoerder-Suabedissen, A., Becker, E. B., ... Butt, S. J. (2016). A transient translaminar gabaergic interneuron circuit connects thalamocortical recipient layers in neonatal somatosensory cortex. *Neuron*, *89*(3), 536–549.

Mavroudis, I., Petrides, F., Manani, M., Theocharides, C., Ciobica, A., Padurariu, M., ... Baloyannis, S. (2012). Dendritic and spinal alterations of the spiny stellate cells of the human visual cortex during normal aging. *Folia neuropathologica*, *50*(3), 261–269.

Meng, X., Kao, J. P., & Kanold, P. O. (2014). Differential signaling to subplate neurons by spatially specific silent synapses in developing auditory cortex. *Journal of Neuroscience*, *34*(26), 8855–8864.

Mi, D., Li, Z., Lim, L., Li, M., Moissidis, M., Yang, Y., ... others (2018). Early emergence of cortical interneuron diversity in the mouse embryo. *Science*, *360*(6384), 81–85.

Miesenböck, G. (2011). Optogenetic control of cells and circuits. *Annual review of cell and developmental biology*, *27*, 731–758.

Mikaelian, D., & Ruben, R. (1965). Development of hearing in the normal cba-j mouse: correlation of physiological observations with behavioral responses and with cochlear anatomy. *Acta Oto-Laryngologica*, *59*(2-6), 451–461.

Minlebaev, M., Ben-Ari, Y., & Khazipov, R. (2007). Network mechanisms of spindle-burst oscillations in the neonatal rat barrel cortex in vivo. *Journal of Neurophysiology*, *97*(1), 692–700.

Minlebaev, M., Colonnese, M., Tsintsadze, T., Sirota, A., & Khazipov, R. (2011). Early gamma oscillations synchronize developing thalamus and cortex. *Science*, *334*(6053), 226–229.

Mitrukhina, O., Suchkov, D., Khazipov, R., & Minlebaev, M. (2014). Imprecise whisker map in the neonatal rat barrel cortex. *Cerebral cortex*, *25*(10), 3458–3467.

Miyashita-Lin, E. M., Hevner, R., Wassarman, K. M., Martinez, S., & Rubenstein, J. L. (1999). Early neocortical regionalization in the absence of thalamic innervation. *Science*, *285*(5429), 906–909.

Miyoshi, G., Butt, S. J., Takebayashi, H., & Fishell, G. (2007). Physiologically distinct temporal cohorts of cortical interneurons arise from telencephalic olig2-expressing precursors. *Journal of Neuroscience*, *27*(29), 7786–7798.

MMRRC - 031125-UCD. (2014). *Strain detail sheet.* Retrieved 2018, from `https://www.mmrrc.org/catalog/sds.php?mmrrc_id=31125`

Mo, A., Mukamel, E. A., Davis, F. P., Luo, C., Henry, G. L., Picard, S., ... others (2015). Epigenomic signatures of neuronal diversity in the mammalian brain. *Neuron*, *86*(6), 1369–1384.

Molnár, Z., Adams, R., & Blakemore, C. (1998). Mechanisms underlying the early establishment of thalamocortical connections in the rat. *Journal of Neuroscience*, *18*(15), 5723–5745.

Molnár, Z., & Blakemore, C. (1991). Lack of regional specificity for connections formed between thalamus and cortex in coculture. *Nature*, *351*(6326), 475.

Molnár, Z., Kurotani, T., Higashi, S., Yamamoto, N., & Toyama, K. (2003). Development of functional thalamocortical synapses studied with current source-density analysis in whole forebrain slices in the rat. *Brain research bulletin*, *60*(4), 355–371.

Molyneaux, B. J., Arlotta, P., Menezes, J. R., & Macklis, J. D. (2007). Neuronal subtype specification in the cerebral cortex. *Nature reviews neuroscience*, *8*(6), 427–437.

Mooney, R., Penn, A. A., Gallego, R., & Shatz, C. J. (1996). Thalamic relay of spontaneous retinal activity prior to vision. *Neuron*, *17*(5), 863–874.

Morales, B., Choi, S.-Y., & Kirkwood, A. (2002). Dark rearing alters the development of gabaergic transmission in visual cortex. *Journal of Neuroscience*, *22*(18), 8084–8090.

Moreno-Juan, V., Filipchuk, A., Antón-Bolanos, N., Mezzera, C., Gezelius, H., Andrés, B., ... others (2017). Prenatal thalamic waves regulate cortical area size prior to sensory processing. *Nature communications*, *8*, 14172.

Morishita, H., & Hensch, T. K. (2008). Critical period revisited: impact on vision. *Current opinion in neurobiology*, *18*(1), 101–107.

Mueller, A. L., Taube, J. S., & Schwartzkroin, P. A. (1984). Development of hyperpolarizing inhibitory postsynaptic potentials and hyperpolarizing response to gamma-aminobutyric acid in rabbit hippocampus studied in vitro. *Journal of Neuroscience*, *4*(3), 860–867.

Naka, A., & Adesnik, H. (2016). Inhibitory circuits in cortical layer 5. *Frontiers in neural circuits*, *10*, 35.

Nakayama, M., Nakajima, D., Nagase, T., Nomura, N., Seki, N., & Ohara, O. (1998). Identification of high-molecular-weight proteins with multiple egf-like motifs by motif-trap screening. *Genomics*, *51*(1), 27–34.

Nassi, J. J., & Callaway, E. M. (2009). Parallel processing strategies of the primate visual system. *Nature Reviews Neuroscience*, *10*(5), 360.

Ohtsuki, G., Nishiyama, M., Yoshida, T., Murakami, T., Histed, M., Lois, C., & Ohki, K. (2012). Similarity of visual selectivity among clonally related neurons in visual cortex. *Neuron*, *75*(1), 65–72.

Osheroff, H., & Hatten, M. E. (2009). Gene expression profiling of preplate neurons destined for the subplate: genes involved in transcription, axon extension, neurotransmitter regulation, steroid hormone signaling, and neuronal survival.

Cerebral Cortex, *19*(suppl_1), i126–i134.

Otsuka, T., & Kawaguchi, Y. (2009). Cortical inhibitory cell types differentially form intralaminar and interlaminar subnetworks with excitatory neurons. *Journal of Neuroscience*, *29*(34), 10533–10540.

Owens, D. F., Liu, X., & Kriegstein, A. R. (1999). Changing properties of gabaa receptor–mediated signaling during early neocortical development. *Journal of Neurophysiology*, *82*(2), 570–583.

OLeary, D. D., & Sahara, S. (2008). Genetic regulation of arealization of the neocortex. *Current opinion in neurobiology*, *18*(1), 90–100.

Pangratz-Fuehrer, S., & Hestrin, S. (2011). Synaptogenesis of electrical and gabaergic synapses of fast-spiking inhibitory neurons in the neocortex. *The Journal of Neuroscience*, *31*(30), 10767–10775.

Pedraza, M., Hoerder-Suabedissen, A., Albert-Maestro, M. A., Molnár, Z., & De Carlos, J. A. (2014). Extracortical origin of some murine subplate cell populations. *Proceedings of the National Academy of Sciences*, 201323816.

Peirson, S. N., Brown, L. A., Pothecary, C. A., Benson, L. A., & Fisk, A. S. (2018). Light and the laboratory mouse. *Journal of neuroscience methods*, *300*, 26–36.

Peters, A., & Kara, D. A. (1985). The neuronal composition of area 17 of rat visual cortex. 1. the pyramidal cells. *Journal of Comparative Neurology*, *234*(2), 218–241.

Petreanu, L., Huber, D., Sobczyk, A., & Svoboda, K. (2007). Channelrhodopsin-2–assisted circuit mapping of long-range callosal projections. *Nature neuroscience*, *10*(5), 663.

Picardo, M. A., Guigue, P., Bonifazi, P., Batista-Brito, R., Allene, C., Ribas, A., ... Cossart, R. (2011). Pioneer gaba cells comprise a subpopulation of hub neurons in the developing hippocampus. *Neuron*, *71*(4), 695–709.

Pinaudeau, C., Gaillard, A., & Roger, M. (2000). Stage of specification of the spinal cord and tectal projections from cortical grafts. *European Journal of Neuroscience*, *12*(7), 2486–2496.

Piñon, M. C., Jethwa, A., Jacobs, E., Campagnoni, A., & Molnár, Z. (2009). Dynamic integration of subplate neurons into the cortical barrel field circuitry during postnatal development in the golli-tau-egfp (gte) mouse. *The Journal of physiology*, *587*(9), 1903–1915.

Platkiewicz, J., & Brette, R. (2010). A threshold equation for action potential initiation. *PLoS computational biology*, *6*(7), e1000850.

Pluta, S., Naka, A., Veit, J., Telian, G., Yao, L., Hakim, R., ... Adesnik, H. (2015). A direct translaminar inhibitory circuit tunes cortical output. *Nature neuroscience*, *18*(11), 1631.

Pouchelon, G., Gambino, F., Bellone, C., Telley, L., Vitali, I., Lüscher, C., ... Jabaudon, D. (2014). Modality-specific thalamocortical inputs instruct the identity of postsynaptic l4 neurons. *Nature*.

Pozas, E., & Ibáñez, C. F. (2005). Gdnf and gfrα1 promote differentiation and tangential migration of cortical gabaergic neurons. *Neuron*, *45*(5), 701–713.

Price, D. J., Kennedy, H., Dehay, C., Zhou, L., Mercier, M., Jossin, Y., ... Molnár, Z. (2006). The development of cortical connections. *European Journal of Neuroscience*, *23*(4), 910–920.

Rakic, P. (1976). Prenatal genesis of connections subserving ocular dominance in the rhesus monkey. *Nature*, *261*(5560), 467.

Rakic, P., Suner, I., & Williams, R. W. (1991). A novel cytoarchitectonic area induced experimentally within the primate visual cortex. *Proceedings of the National Academy of Sciences*, *88*(6), 2083–2087.

Rash, B. G., & Grove, E. A. (2006). Area and layer patterning in the developing cerebral cortex. *Current opinion in neurobiology*, *16*(1), 25–34.

Rebsam, A., Seif, I., & Gaspar, P. (2005). Dissociating barrel development and lesion-induced plasticity in the mouse somatosensory cortex. *Journal of Neuroscience*, *25*(3), 706–710.

Rochefort, N. L., Garaschuk, O., Milos, R.-I., Narushima, M., Marandi, N., Pichler, B., ... Konnerth, A. (2009). Sparsification of neuronal activity in the visual cortex at eye-opening. *Proceedings of the National Academy of Sciences*, *106*(35), 15049–15054.

Rochefort, N. L., Narushima, M., Grienberger, C., Marandi, N., Hill, D. N., & Konnerth, A. (2011). Development of direction selectivity in mouse cortical neurons. *Neuron*, *71*(3), 425–432.

Roe, A. W., Pallas, S. L., Hahm, J.-O., & Sur, M. (1990). A map of visual space induced in primary auditory cortex. *Science*, *250*(4982), 818–820.

Roe, A. W., Pallas, S. L., Kwon, Y. H., & Sur, M. (1992). Visual projections routed to the auditory pathway in ferrets: receptive fields of visual neurons in primary auditory cortex. *Journal of Neuroscience*, *12*(9), 3651–3664.

Root, D. H., Mejias-Aponte, C. A., Zhang, S., Wang, H.-L., Hoffman, A. F., Lupica, C. R., & Morales, M. (2014). Single rodent mesohabenular axons release glutamate and gaba. *Nature neuroscience*, *17*(11), 1543.

Rudy, B., Fishell, G., Lee, S., & Hjerling-Leffler, J. (2011). Three groups of interneurons account for nearly 100% of neocortical gabaergic neurons. *Developmental neurobiology*, *71*(1), 45–61.

Sadato, N., Pascual-Leone, A., Grafman, J., Ibañez, V., Deiber, M.-P., Dold, G., & Hallett, M. (1996). Activation of the primary visual cortex by braille reading in blind subjects. *Nature*, *380*(6574), 526–528.

Schlaggar, B. L., & O'Leary, D. (1991). Potential of visual cortex to develop an array of functional units unique to somatosensory cortex. *Science*, *252*(5012), 1556–1560.

Sernagor, E., & Grzywacz, N. M. (1999). Spontaneous activity in developing turtle retinal ganglion cells: pharmacological studies. *Journal of Neuroscience*, *19*(10), 3874–3887.

Sharma, J., Angelucci, A., & Sur, M. (2000). Induction of visual orientation modules in auditory cortex. *Nature*, *404*(6780), 841–847.

Shatz, C. J., & Luskin, M. B. (1986). The relationship between the geniculocortical afferents and their cortical target cells during development of the cat's primary

visual cortex. *Journal of Neuroscience*, *6*(12), 3655–3668.

Shepherd, G. M. (2012). Circuit mapping by ultraviolet uncaging of glutamate. *Cold Spring Harbor Protocols*, *2012*(9), pdb–prot070664.

Shepherd, G. M., Pologruto, T. A., & Svoboda, K. (2003). Circuit analysis of experience-dependent plasticity in the developing rat barrel cortex. *Neuron*, *38*(2), 277–289.

Shoykhet, M., Land, P. W., & Simons, D. J. (2005). Whisker trimming begun at birth or on postnatal day 12 affects excitatory and inhibitory receptive fields of layer iv barrel neurons. *Journal of neurophysiology*, *94*(6), 3987–3995.

Simons, D. J., & Land, P. W. (1987). Early experience of tactile stimulation influences organization of somatic sensory cortex. *Nature*, *326*(6114), 694.

Sippy, T., & Yuste, R. (2013). Decorrelating action of inhibition in neocortical networks. *Journal of Neuroscience*, *33*(23), 9813–9830.

Southwell, D. G., Paredes, M. F., Galvao, R. P., Jones, D. L., Froemke, R. C., Sebe, J. Y., ... others (2012). Intrinsically determined cell death of developing cortical interneurons. *Nature*, *491*(7422), 109.

Steger, R., Ramos, R. L., Cao, R., Yang, Q., Chen, C.-C., Dominici, J., & Brumberg, J. C. (2013). Physiology and morphology of inverted pyramidal neurons in the rodent neocortex. *Neuroscience*, *248*, 165–179.

Stern, E. A., Maravall, M., & Svoboda, K. (2001). Rapid development and plasticity of layer 2/3 maps in rat barrel cortex in vivo. *Neuron*, *31*(2), 305–315.

Sun, Q.-Q., Huguenard, J. R., & Prince, D. A. (2006). Barrel cortex microcircuits: Thalamocortical feedforward inhibition in spiny stellate cells is mediated by a small number of fast-spiking interneurons. *Journal of Neuroscience*, *26*(4), 1219–1230.

Suzuki-Hirano, A., & Shimogori, T. (2009). The role of fgf8 in telencephalic and diencephalic patterning. In *Seminars in cell & developmental biology* (Vol. 20, pp. 719–725).

Swindale, N. (1996). The development of topography in the visual cortex: a review of models. *Network: Computation in neural systems*, *7*(2), 161–247.

Takeuchi, Y., Osaki, H., Yagasaki, Y., Katayama, Y., & Miyata, M. (2017). Afferent fiber remodeling in the somatosensory thalamus of mice as a neural basis of somatotopic reorganization in the brain and ectopic mechanical hypersensitivity after peripheral sensory nerve injury. *eNeuro*, *4*(2), ENEURO–0345.

Takeuchi, Y., Yamasaki, M., Nagumo, Y., Imoto, K., Watanabe, M., & Miyata, M. (2012). Rewiring of afferent fibers in the somatosensory thalamus of mice caused by peripheral sensory nerve transection. *Journal of Neuroscience*, *32*(20), 6917–6930.

Tanaka, D. H., Mikami, S., Nagasawa, T., Miyazaki, J.-i., Nakajima, K., & Murakami, F. (2010). Cxcr4 is required for proper regional and laminar distribution of cortical somatostatin-, calretinin-, and neuropeptide y-expressing gabaergic interneurons. *Cerebral Cortex*, *20*(12), 2810–2817.

Tanaka, D. H., & Nakajima, K. (2012). Migratory pathways of gabaergic interneurons when they enter the neocortex. *European Journal of Neuroscience*,

35(11), 1655–1660.

Tasic, B., Menon, V., Nguyen, T. N., Kim, T. K., Jarsky, T., Yao, Z., ... others (2016). Adult mouse cortical cell taxonomy revealed by single cell transcriptomics. *Nature neuroscience*, *19*(2), 335.

The Allen Institute. (2018). *The allen brain atlas.* Retrieved 2018, from `http://atlas.brain-map.org/`

The Jackson Laboratory - 007908. (2014). *Mouse strain datasheet - 007908.* Retrieved 2018, from `https://www.jax.org/strain/007908`

The Jackson Laboratory - 007909. (2014). *Mouse strain datasheet - 007909.* Retrieved 2018, from `https://www.jax.org/strain/007909`

The Jackson Laboratory - 012569. (2016). *Mouse strain datasheet - 012569.* Retrieved 2018, from `https://www.jax.org/strain/012569`

The Jackson Laboratory - 013044. (2014). *Mouse strain datasheet - 013044.* Retrieved 2018, from `https://www.jax.org/strain/013044`

Tissir, F., & Goffinet, A. M. (2003). Reelin and brain development. *Nature Reviews Neuroscience*, *4*(6), 496–505.

Tuncdemir, S. N., Wamsley, B., Stam, F. J., Osakada, F., Goulding, M., Callaway, E. M., ... Fishell, G. (2016). Early somatostatin interneuron connectivity mediates the maturation of deep layer cortical circuits. *Neuron*, *89*(3), 521–535.

Valverde, P. (1967). Apical dendritic spines of the visual cortex and light deprivation in the mouse. *Experimental Brain Research*, *3*(4), 337–352.

Van der Loos, H., & Woolsey, T. A. (1973). Somatosensory cortex: structural alterations following early injury to sense organs. *Science*, *179*(4071), 395–398.

van Rheede, J. J., Richards, B. A., & Akerman, C. J. (2015). Sensory-evoked spiking behavior emerges via an experience-dependent plasticity mechanism. *Neuron*, *87*(5), 1050–1062.

Viswanathan, S., Bandyopadhyay, S., Kao, J. P., & Kanold, P. O. (2012). Changing microcircuits in the subplate of the developing cortex. *Journal of Neuroscience*, *32*(5), 1589–1601.

Von Melchner, L., Pallas, S. L., & Sur, M. (2000). Visual behaviour mediated by retinal projections directed to the auditory pathway. *Nature*, *404*(6780), 871–876.

Vue, T. Y., Bluske, K., Alishahi, A., Yang, L. L., Koyano-Nakagawa, N., Novitch, B., & Nakagawa, Y. (2009). Sonic hedgehog signaling controls thalamic progenitor identity and nuclei specification in mice. *Journal of Neuroscience*, *29*(14), 4484–4497.

Wamsley, B., & Fishell, G. (2017). Genetic and activity-dependent mechanisms underlying interneuron diversity. *Nature Reviews Neuroscience*, *18*(5), 299.

Wang, W. Z., Hoerder-Suabedissen, A., Oeschger, F. M., Bayatti, N., Ip, B. K., Lindsay, S., ... others (2010). Subplate in the developing cortex of mouse and human. *Journal of anatomy*, *217*(4), 368–380.

Wess, J. M., Isaiah, A., Watkins, P. V., & Kanold, P. O. (2017). Subplate neurons

are the first cortical neurons to respond to sensory stimuli. *Proceedings of the National Academy of Sciences*, *114*(47), 12602–12607.

Wiesel, T. N., & Hubel, D. H. (1965). Extent of recovery from the effects of visual deprivation in kittens. *Journal of neurophysiology*, *28*(6), 1060–1072.

Wiesel, T. N., Hubel, D. H., et al. (1963). Single-cell responses in striate cortex of kittens deprived of vision in one eye. *J Neurophysiol*, *26*(6), 1003–1017.

Wilent, W. B., & Contreras, D. (2005). Stimulus-dependent changes in spike threshold enhance feature selectivity in rat barrel cortex neurons. *Journal of Neuroscience*, *25*(11), 2983–2991.

Wong, F. K., Bercsenyi, K., Sreenivasan, V., Portalés, A., Fernández-Otero, M., & Marín, O. (2018). Pyramidal cell regulation of interneuron survival sculpts cortical networks. *Nature*, *557*(7707), 668.

Wong, R. O. (1999). Retinal waves and visual system development. *Annual review of neuroscience*, *22*(1), 29–47.

Woolsey, T. A., & Van der Loos, H. (1970). The structural organization of layer iv in the somatosensory region (si) of mouse cerebral cortex: the description of a cortical field composed of discrete cytoarchitectonic units. *Brain research*, *17*(2), 205–242.

Xu, H., Furman, M., Mineur, Y. S., Chen, H., King, S. L., Zenisek, D., ... others (2011). An instructive role for patterned spontaneous retinal activity in mouse visual map development. *Neuron*, *70*(6), 1115–1127.

Xu, H.-P., Burbridge, T. J., Chen, M.-G., Ge, X., Zhang, Y., Zhou, Z. J., & Crair, M. C. (2015). Spatial pattern of spontaneous retinal waves instructs retinotopic map refinement more than activity frequency. *Developmental neurobiology*, *75*(6), 621–640.

Xu, X., & Callaway, E. M. (2009). Laminar specificity of functional input to distinct types of inhibitory cortical neurons. *Journal of Neuroscience*, *29*(1), 70–85.

Yakovlev, P. (1967). The myelogenetic cycles of regional maturation of the brain. *Regional development of the brain in early life*, 3–70.

Yamamoto, N., Higashi, S., & Toyama, K. (1997). Stop and branch behaviors of geniculocortical axons: a time-lapse study in organotypic cocultures. *Journal of Neuroscience*, *17*(10), 3653–3663.

Yamamoto, N., Kurotani, T., & Toyama, K. (1989). Neural connections between the lateral geniculate nucleus and visual cortex in vitro. *Science*, *245*(4914), 192–194.

Yamamoto, N., Yamada, K., Kurotani, T., & Toyama, K. (1992). Laminar specificity of extrinsic cortical connections studied in coculture preparations. *Neuron*, *9*(2), 217–228.

Yang, J.-W., An, S., Sun, J.-J., Reyes-Puerta, V., Kindler, J., Berger, T., ... Luhmann, H. J. (2012). Thalamic network oscillations synchronize ontogenetic columns in the newborn rat barrel cortex. *Cerebral Cortex*, *23*(6), 1299–1316.

Yang, J.-W., Hanganu-Opatz, I. L., Sun, J.-J., & Luhmann, H. J. (2009). Three patterns of oscillatory activity differentially synchronize developing neocortical networks in vivo. *Journal of Neuroscience*, *29*(28), 9011–9025.

Yang, J.-W., Kilb, W., Kirischuk, S., Unichenko, P., Stüttgen, M. C., & Luhmann, H. J. (2018). Development of the whisker-to-barrel cortex system. *Current opinion in neurobiology*, *53*, 29–34.

Zemelman, B. V., Nesnas, N., Lee, G. A., & Miesenböck, G. (2003). Photochemical gating of heterologous ion channels: remote control over genetically designated populations of neurons. *Proceedings of the National Academy of Sciences*, *100*(3), 1352–1357.

Zhang, F., Aravanis, A. M., Adamantidis, A., de Lecea, L., & Deisseroth, K. (2007). Circuit-breakers: optical technologies for probing neural signals and systems. *Nature Reviews Neuroscience*, *8*(8), 577.

Zhao, C., Kao, J. P., & Kanold, P. O. (2009). Functional excitatory microcircuits in neonatal cortex connect thalamus and layer 4. *Journal of Neuroscience*, *29*(49), 15479–15488.

Zhou, L., Bar, I., Achouri, Y., Campbell, K., De Backer, O., Hebert, J. M., ... others (2008). Early forebrain wiring: genetic dissection using conditional celsr3 mutant mice. *science*, *320*(5878), 946–949.

Zhou, L., Gall, D., Qu, Y., Prigogine, C., Cheron, G., Tissir, F., ... Goffinet, A. M. (2010). Maturation of neocortex isole in vivo in mice. *Journal of Neuroscience*, *30*(23), 7928–7939.

Appendix A

Abbreviations

4-AP	4-Aminopyridine
A1	Primary auditory cortex
ACSF	Artificial Cerebrospinal Fluid
AHP	Afterhyperpolarization
ATP	Adenosine Triphosphate
BAC	Bacterial Artificial Chromosome
ChR2	Channelrhodopsin-2
CR	Calretinin
DIC	Differential interference contrast
DNA	Deoxyribonucleic acid
EGO	Early gamma oscillations
EPSC	Excitatory post-synaptic current
EPSP	Excitatory post-synaptic potential
EYFP	Enhanced Yellow Fluorescent Protein
FGF	Fibroblast Growth Factor

FS	Fast-spiking
GABA	Gamma-Aminobutyric acid,
GDNF	Glial cell-derived neurotrophic factor
GFP	Green fluorescent protein
HDC	High divalent cation
IPSC	Inhibitory post-synaptic current
IPSP	Inhibitory post-synaptic potential
IN	Interneuron
ION	Infraorbital nerve
IZ	Intermediate Zone
L1,2/3,4,5a,5b,6	Layer 1, Layer 2/3 etc.
LGN	Lateral geniculate nucleus
LSPS	Laser scanning photo stimulation
MGE	Medial Ganglionic Eminence
mGluR5	metabotropic glutamate receptor 5
Mut	Mutant
MZ	Marginal Zone
NFS	Non-fastspiking
ODC	Ocular dominance column
P1, P2 etc	Postnatal day 1, postnatal day 2 etc.
P2X2	P2X purinoceptor 2
POM	Posterior medial nucleus
PV	Parvalbumin
Pyr	Pyramidal
RFP	Red fluorescent protein
RMP	Resting Membrane potential
RT	Room temperature
S1	Primary somatosensory cortex
S1BF	Somatosensory barrel field
SP	Subplate
SSN	Spiny stellate neuron
SST	Somatostatin
SVZ	Subventricular Zone
TC	Thalamocortical
TTX	Tetrodotoxin
V1	Primary visual cortex
VIP	Vasoactive Intestinal Polypeptide
VPM	Ventral posteromedial nucleus
WT	Wildtype